COMPARISON OF SEVERAL NUMERICAL METHODS FOR SOLVING THE EULER EQUATIONS FOR COMPRESSIBLE AERODYNAMIC FLOWS

by

Dan Stanescu

Department of Mechanical Engineering
McGill University
Montreal, Quebec, Canada
August 1994

A thesis submitted to the Faculty of Graduate Studies and Research
in partial fulfillment of the requirements for the degree of
Master of Engineering

ISBN 0-612-05479-9

Canada

COMPUTATIONAL METHODS FOR COMPRESSIBLE AERODYNAMIC FLOWS

ABSTRACT

Two explicit time-integration schemes based on a finite-volume approach for the solution of the Euler equations are developed and used in the study of compressible flows. The starting point is a comparison of the performance of three widely used methods (i.e., Jameson's, MacCormack's and Godunov's) in several rather difficult test problems, characterized by the existence of flow discontinuities or strong nonlinearities. This indicates that the best solutions for such flows are obtained when the numerical method is closely related to the physical behaviour of the fluid, as is the case with Godunov's method, in contrast with the other two methods, which need a special treatment of the discontinuities, and are very prone to numerically induced oscillations. Therefore, a first scheme, which improves the way Jameson's method computes the flux-node variables in that it treats in a more realistic manner the physics of signal propagation in both subsonic and supersonic flow, is developed. The numerical experiments with this scheme suggest that it converges more rapidly and does not need the dissipation terms, thus leading to computer efficiency and a gain in accuracy. The second method is a linear hybrid, in conservative form, between MacCormack's and Godunov's methods, which is shown to keep the best features of both the methods: second order accuracy in smooth regions of the flow and lack of oscillations near discontinuities, where it behaves locally like a first-order monotone scheme.

SOMMAIRE

Deux méthodes pour l'intégration numérique explicite en temps des équations Euler, utilisant l'approche des volumes finis, sont développées et utilisées pour l'étude des écoulements des fluides compressibles. Le point de départ est une comparaison des solutions obtenues avec trois méthodes classiques (Jameson, MacCormack et Godunov) pour des problèmes relativement difficiles, caractérisés par l'existence des discontinuités ou des grandes nonlinéairités. Ceci indique que les meilleures solutions pour ces écoulements sont obtenues quand la méthode numérique reproduit les caractéristiques physiques de l'écoulement du fluide, comme par exemple la méthode développée par Godunov, par contrast avec les deux autres méthodes qui nécessitent un traitement spécial des discontinuités et sont susceptibles d'engendrer des oscillations numériques. En conséquence, une première méthode qui améliore la modalité dont le flux numérique est calculé dans la méthode de Jameson, en traitant d'une manière plus réaliste la propagation physique des perturbations dans les régimes subsonique et supersonique, est mise au point. Les expériments numériques avec cette méthode prouvent sa convergence plus rapide sans avoir besoin des termes de dissipation, ce qui apporte un temps de calcul diminué ainsi qu'une plus grande précision. La deuxième méthode est une méthode hybride, en forme conservative, entre les méthodes de MacCormack et Godunov, qui garde les meilleures caractéristiques de ces deux méthodes: précison globale de deuxième ordre et manque des oscillations auprès des discontinuités, où elle emprunte un comportement monotone.

ACKNOWLEDGEMENTS

The author would like to thank Prof. D. Mateescu for guiding his first steps in a fascinating field and making all this possible.

During the course of the graduate studies at McGill University, of a great benefit have also been the discussions with Prof. G. G. Bach, which provided a great stimulus and helped to clarify many issues.

Many thanks also to my colleagues Seyed Razavi and Pierre Nasrallah for their suggestions regarding the numerical test cases.

Table of Contents

List of Figures

List of Tables

Nomenclature

A	cell area; area
A	flux/state vector Jacobian matrix
c	speed of sound
c	airfoil chord
C	artificial viscosity constant, Lapidus formulation
CFL	Courant-Friederichs-Levy number (or Courant number)
d	adaptive dissipation term
D	adaptive dissipation operator
E	total specific energy
f	state vector
F	x-axis component of the flux vector
$\mathcal{F}$	function relating the flux vector to the primitive variables
g	vector related to the pressure forces
G	y-axis component of the flux vector
h	duct height
H	stagnation enthalpy
$\vec{i}$	x-axis unit vector
$Imax$	total number of cells on the x-axis
$\vec{j}$	y-axis unit vector
$Jmax$	total number of cells on the y-axis
$k^{(2)}$	constant for second-order dissipation
$k^{(4)}$	constant for fourth-order dissipation
$\dot{m}$	mass flux

$\vec{n}$	normal unit vector
p	pressure
P	pressure-term vector in quasi one-dimensional flow
q	normal velocity component flux through a cell side
Q	flux terms algebraic operator
$\vec{Q}$	total flux vector with components F and G
$\vec{r}$	position vector
s	length along a cell boundary
S	cross-sectional area of the duct
t	time
$\vec{t}$	tangential unit vector
u	x-axis component of the velocity
U_s	velocity of an unsteady shock wave front
v	y-axis component of the velocity
$\vec{V}$	velocity
V_n	normal velocity component
V_t	tangential velocity component
w	characteristic variable
γ	specific heats ratio
$\epsilon^{(2)}$	coefficient for second-order adaptive dissipation
$\epsilon^{(4)}$	coefficient for fourth-order adaptive dissipation
θ_{in}	flow angle at inflow boundary
θ	numerical switch for hybrid method flux computation
λ	eigenvalue for quasi-linear Euler equations
ν	numerical switch for adaptive dissipation
ρ	density
υ	control volume
χ	numerical constant for hybrid method switch computation
ϑ	specific volume

Subscripts

ex	outflow/exit values
i,j	cell indices
$i+½$	cell interface index
in	inflow values
L	left state for the Riemann problem
pr	predicted values
ref	reference variables
R	right state for the Riemann problem
0	stagnation parameters

Superscripts

n	time step
$\overline{n+1}$	intermediate time step in MacCormack's method
T	vector transpose
*	intermediate state in a Riemann problem solution

Chapter 1

INTRODUCTION

Over the last 35 years, a great emphasis has been laid upon the development of numerical methods for solving the equations of fluid flow, which can yield realistic simulations of flows about aircraft configurations and thus save much of the costs otherwise implied by tunnel testing and experiments. The Navier-Stokes equations, which take into account the full viscous behaviour of the fluid, are of course able to accurately represent the flow phenomena. However, even with today's supercomputers, their solution for real aircraft configurations is very difficult, and various simpler models are used. One of these models is the boundary layer concept introduced by Prandtl, which takes into account the viscous effects only within a thin layer in the vicinity of the body, while outside this layer the flow is considered inviscid. For the large Reynolds numbers encountered in aircraft flight, where the viscous forces are very small as compared to the inertial forces, this approximation proves satisfactory and provides a basis for a simpler approach to the problem.

In the inviscid flow outside the boundary layer, the motion of the fluid is described either by the potential flow theory or by the Euler equations. The potential flow theory allowed the first useful predictions for flows about real aircrafts in the transonic range, starting with the solutions to the transonic small-perturbations equation of the potential (the pioneering work has been done by Murman and Cole [29], followed by Bailey and Ballhaus [2] in the U.S.A. and Albone, Hall and Joyce [1] in Great Britain, who extended the method for three-dimensional flows) and

following with solutions to the full potential equation (methods of Garabedian and Korn [9] and Jameson [15]). It proved however unreliable when the flow discontinuities (shocks) are not weak, because it doesn't ensure the conservation of the normal momentum. It is now generally agreed that potential flow assumption may be used as far as the Mach number in front of the shock wave is lower than 1.25.

The Euler equations, as a limiting case of the Navier-Stokes equations in the absence of viscosity, admit a correct representation of strong shocks, taking account of the rotational effects. Thus, outside the viscous layer, they provide a more realistic solution for the flow, especially for the transonic and supersonic flows, when shocks develop at various locations on the aircraft. The use of the Euler equations is made easier by the fact that for unsteady flows they are hyperbolic partial differential equations, although for steady flows they are of elliptic type for locally subsonic and hyperbolic type for locally supersonic flow. This makes possible the use of the same method, time integration, for any kind of flow, subsonic, transonic, or supersonic. Furthermore, steady and unsteady flows allow the same basic tehnique to be applied: in unsteady flows the equations are integrated in time starting from real initial conditions, while in steady flows the initial conditions are assumed and the equations are integrated in virtual time until the steady state is attained.

Of course, Euler equations solutions are more demanding on computer time than the potential flow solution. Therefore, their use is justified only in the presence of flow discontinuities, and hence, a correct representation of these discontinuities is a main issue for Euler methods. Two different approaches have been developed towards this goal. The first one is shock fitting: the shock is explicitly accounted for in the numerical scheme, its position is updated at every time step, and the correct Rankine-Hugoniot relations are applied across it. The flow is thus divided in smooth regions, within which any numerical method can be applied, connected by correct

discontinuous jumps. The explicit fitting of shocks results in complicated computer codes and increase in computer time, although the results obtained by this method are relatively accurate. This approach has been widely used by several researchers, in principal Moretti [7], [43], [28] and Zanetti and Colasurdo [42]. They use the Euler equations in characteristic form and follow the position of the shock by marking the grid lines that it crosses. It is to be emphasized here that these methods succeeded in solving very complicated flows, as those about ablated bodies (see [43]) where shock-capturing methods like MacCormack or Lax-Wendroff tended to fail, and which could be simulated up to that date only by Godunov's method, which will be presented further.

The second approach, and the one used in this work, is shock capturing. This was originally suggested by von Neuman and Richtmyer [41] and is based on a comparison with real fluid flows: in these, we may believe that there are no dicontinuities, but very thin regions of severe variation. Inclusion of terms modeling viscosity ("artificial viscosity") in the Euler equations makes the solution behave in a similar manner, the discontinuity is smeared over a certain region which is negligible, but still resolvable on a practical computational mesh.

Considerable work in this area has been done by Lax. In a paper [20] that had a great influence on the evolution of computational fluid dynamics, he shows that the use of the Euler equations in conservative variables (or conservation) form leads to sufficiently accurate representations of discontinuities. In a subsequent paper [21], Lax and Wendroff define the conservative differencing schemes, and show that the use of conservative variables and of a conservative differencing scheme consistent with the equations can guarantee that the discontinuities are correctly solved for and they move with the correct speed. The scheme devised by Lax and Wendroff has been widely used afterwards, and various variations have appeared later, many of

them generated by the need of a simpler method to treat the nonlinearity in the Euler equations.

MacCormack's method [22], [23], can be regarded as a particular variation of the Lax-Wendroff method. It uses the same shock-capturing approach, generally treating discontinuities by the means of artificial viscosity, although variants using shock-fitting also exist ([23]). It is more efficient and easier to program than the original Lax-Wendroff method because it does not need the explicit computation of the Jacobians in the Euler equations. It was extensively studied and many variants have been proposed, both implicit and explicit, with or without time splitting. The variant used in this study is a finite-volume explicit method without time splitting, and uses an artificial viscosity of the type introduced by Lapidus [19] in order to prevent numerical instabilities and oscillations near discontinuities.

Jameson [18] introduced another numerical method which is equivalent to central differencing in space, and uses a Runge-Kutta method for time integration. Because central differencing is not stable, this method incorporates a carefully designed dissipation operator which allows odd and even point coupling and suppresses oscillations near shocks. This method has also been very well developed, and adapted to multiple grid techniques [16], triangular meshes [17], and unsteady flows [40]. It has been effectively used for flow simulation around real aircraft configurations by several companies, being very efficient in terms of computer time, and allowing vectorizable algorithms for parallel processing. It was chosen as the second method for the comparison in the present study.

MacCormack's and Jameson's methods are different ways of using the Taylor series expansions for all the terms in the differential equations. This is based upon the assumption that the distribution of the variables is continuous; at a discontinuity the expansions are not valid, hence the solution is forcibly smoothed by the use of

additional means. Godunov [10], opened the way to a more realistic treatment of the problem: he builds the full solution to the hydrodynamic equations by piecing together a great number of discontinuous, nonlinear solutions which are valid even at discontinuities. His method belongs to the same class of shock capturing methods, the discontinuous solutions being linked in a conservative difference scheme. The main element of Godunov's method is a Riemann-problem study, for which he describes an iterative solver.

Another aspect that Godunov [10] emphasized was that of monotonicity. He showed that a desirable quality of the solution obtained by a finite difference scheme would be that, given an initial solution which is a monotone function, the solution obtained by time integration is also monotone. Such algorithms are necessarily first-order accurate if they are expressed in simple linear-combination form, as shown in [10] and [32], so being the case with Godunov's initial method also.

Following the same approach as Godunov's method, i.e. the use of Riemann solvers and of monotonicity preserving schemes, a great number of methods for flows with strong discontinuities have been developed, some of the most successful ones being the MUSCL schemes of Van Leer [39], the piecewise parabolic method (PPM) of Woodward and Colella [6], and the later essentially non oscillatory (ENO) schemes developed initially by Harten, Engquist, Osher and Chakravarthy [13], with recent extensions in finite-volume formulation for two dimensions by Casper and Atkins [3], [4]. Results obtained with these methods are clearly superior, for complicated flows, to those obtained by ordinary methods. All these methods are basically extensions to a higher degree of accuracy of Godunov's method.

A different way to obtain higher order accuracy was initiated by Harten and Zwas [14], [12]. They used a special way to couple together a higher order method, very accurate in smooth regions but oscillating near discontinuities, with a first order

method which guarantees a monotone solution near discontinuities. The two methods can be chosen from the wide range of existing ones, the result being known as a hybrid method.

The first objective of the present work is the comparison of the performance of the three methods developed by MacCormack ([22], [23]), Jameson ([18]) and Godunov ([10]) presented above for a variety of fluid flow problems. For each method, a quasi-one-dimensional and a bidimensional code have been created, on a personal computer. Problems, which have been studied by other authors also, have been chosen in order to assess the accuracy of these methods. The results are compared and the main conclusions drawn from this comparison represent the basis for subsequent developments.

The second objective is to develop improved time integration schemes which can be regarded as extensions of these methods, while still bringing about an improvement in the performance. A first one is similar to Jameson's method, but uses a weighted average of the cell node variables for the computation of fluxes. This flux computation is so constructed that it takes into account, in a simple but effective manner, the physics of signal propagation (in locally subsonic flows, two signals propagate in the flow direction, while in locally supersonic flows information comes only from upstream). This represents an extension of the two-stage method developed by Mateescu and Lauzon [27], with a more efficient implementation for multi-dimensional flows. The scheme so constructed is tested and shown to be less prone to oscillations and to converge faster. It is also stable in the absence of dissipation, as is shown in a quasi-one-dimensional case, although for practical computations in two dimensions a certain amount of dissipation may be needed in order to avoid marginal stability.

The second method is a hybrid between MacCormack's and Godunov's methods. The hybrid improves overall accuracy by raising to second order in smooth regions, hence the mesh to be used can be coarser, which can result in a better computer efficiency. For the great majority of mesh points, only the second order method is applied; in the neighborhood of discontinuities, a mathematically constructed switch detects oscillations and the first order flux computation by Godunov's method is activated. For these points, of course, the computational time grows; however, since the number of discontinuities in real fluid flow is limited, this extra computer time is not exhaustive, and results in a more exact representation of shocks than with the use of the artificial viscosity.

Chapter 2

BASIC EQUATIONS

This chapter presents the numerical approach used in the analysis of compressible flows. The Euler equations in differential and integral form, their finite-volume discretization, together with the physical boundary conditions, which completely define a flow problem, are discussed.

2.1 Problem formulation

For the numerical study of a flow problem, the region of interest of the flow must be delimited to form a finite computational domain. The boundaries of this computational domain can be actual, solid-wall boundaries, associated with the bodies around (or through) which the flow takes place, and artificial boundaries, introduced because the domain can not be extended to infinity.

Once the computational domain has been established, the numerical solution supposes four main steps:

1) Spatial discretization of the computational domain in a finite number of components (generation of a mesh).
2) Discretization of the partial differential equations of motion.
3) Numerical implementation of the boundary conditions.

4) Solution of the discretized equations, subjected to these boundary conditions.

2.2 The Euler equations

The integral form of the Euler equations can be derived by applying Reynold's Transport Theorem to a control volume υ bounded by the surface $\partial\upsilon$ for each of the three equations of conservation of mass, momentum and energy ([25]), and can be expressed as

$$\frac{\partial}{\partial t}\int_{\upsilon} f(\vec{r},t)\,d\upsilon + \int_{\partial\upsilon} f(\vec{r},t)[\vec{n}(\vec{r})\cdot\vec{V}(\vec{r},t)]\,dA + \int_{\partial\upsilon} g(\vec{r},t)\,dA = 0 \qquad (2.1)$$

where the function $f(\vec{r},t)$ is a vector of flow variables describing the fluid state, $\vec{n}(\vec{r})$ is the local normal unit vector to the surface $\partial\upsilon$, $\vec{V}(\vec{r},t)$ is the local fluid velocity and $g(\vec{r},t)$ is a vector related to the pressure forces. The other variables have been denoted by the usual notation, t being the time and $d\upsilon$ and dA the elements of volume and area, respectively. In a vectorial formulation, f and g have three components corresponding to the three conserved variables: mass, momentum and energy, i.e.

$$f(\vec{r},t) = \begin{bmatrix} \rho(\vec{r},t) \\ \rho(\vec{r},t)\,\vec{V}(\vec{r},t) \\ \rho(\vec{r},t)E(\vec{r},t) \end{bmatrix} \qquad (2.2)$$

$$g(\vec{r},t) = \begin{bmatrix} 0 \\ p(\vec{r},t)\vec{n}(\vec{r}) \\ p(\vec{r},t)[\vec{n}(\vec{r},t)\cdot\vec{V}(\vec{r},t)] \end{bmatrix} \qquad (2.3)$$

In equations (2.2), (2.3), ρ is the density, E is the total specific energy, and p is the pressure, related to the other variables through the equation of state,

$$p=(\gamma-1)\rho(E-\frac{V^2}{2}) \tag{2.4}$$

γ being the specific heats ratio.

Using (2.1), (2.2) and (2.3), one can express the Euler equations for the two-dimensional flow case as:

$$\frac{\partial}{\partial t}\int_A f dA+\int_{\partial A}(\vec{i}F+\vec{j}G)\cdot\vec{n}ds=0 \tag{2.5}$$

the control volume being in this case replaced by the control area A, with ∂A the frontier of this area and ds the element of length along the frontier. The function f is the state vector, and F and G are the x- and the y-component flux vectors, which are vector-valued functions of four components. They are given by:

$$f=\begin{bmatrix}\rho\\ \rho u\\ \rho v\\ \rho E\end{bmatrix},\ F=\begin{bmatrix}\rho u\\ \rho u^2+p\\ \rho uv\\ (\rho E+p)u\end{bmatrix},\ G=\begin{bmatrix}\rho v\\ \rho uv\\ \rho v^2+p\\ (\rho E+p)v\end{bmatrix} \tag{2.6}$$

In equation (2.6), u and v are the components of the velocity along the x- and y-axis respectively.

For the case of a quasi one-dimensional flow in a duct of variable cross-sectional area $S(x)$, the Euler equations can be written in integral form as

$$\frac{\partial}{\partial t}\int_A f dA+\int_{\partial A}(\vec{i}F)\cdot\vec{n}ds=\int_A P dA \tag{2.7}$$

in this case the variation of the control area being $dA(x)=S(x)\cdot dx$. The new state and flux vectors have three components:

$$f=\begin{bmatrix}\rho\\ \rho u\\ \rho E\end{bmatrix},\ F=\begin{bmatrix}\rho u\\ \rho u^2+p\\ (\rho E+p)u\end{bmatrix},\ P=\begin{bmatrix}0\\ \frac{p}{S}\frac{dS}{dx}\\ 0\end{bmatrix} \tag{2.8}$$

The differential, strong conservation law, form of the Euler equations can be obtained directly from (2.5) and (2.7) by applying Gauss' theorems. The corresponding form for two-dimensional flows is:

$$\frac{\partial f}{\partial t} + \frac{\partial F}{\partial x} + \frac{\partial G}{\partial y} = 0 \tag{2.9}$$

where f, F, and G are the same as in (2.6).

For quasi one-dimensional flows, the equations become:

$$\frac{\partial (fS)}{\partial t} + \frac{\partial (FS)}{\partial x} = PS \tag{2.10}$$

f, F and P being the same as in (2.8).

2.3 Finite-volume discretization

2.3.1 Quasi one-dimensional flows

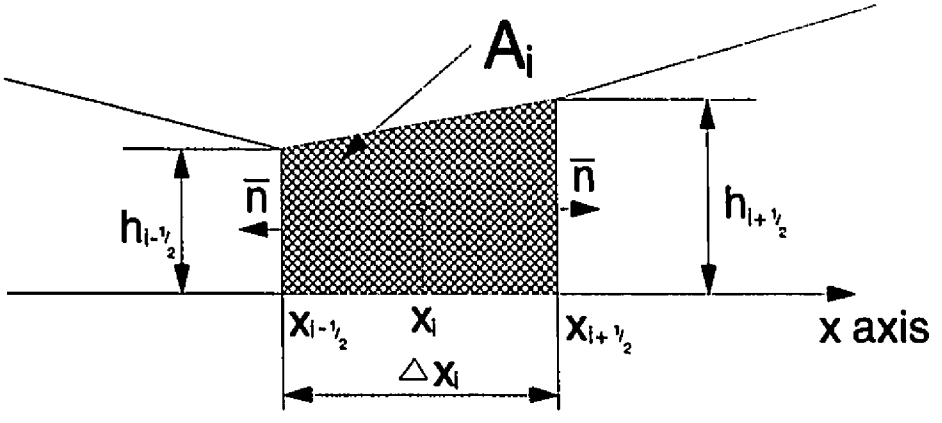

Fig. 2.1

To obtain the discretized finite-volume formulation of the Euler equations for a quasi one-dimensional flow, consider a duct with an axially variable area $S(x)=h(x)\cdot 1=h(x)$, where $h(x)$ represents the height of the duct, which has an unitary

width. The computational domain is divided in a finite number *Imax* of quadrilateral cells of area A_i , $i=1, Imax$, and the equation (2.7) is discretized for the control area A_i as can be seen in Fig. 2.1.

The first integral in (2.7) can be written as

$$\frac{\partial}{\partial t}\int_{A_i} f dA = \frac{\partial}{\partial t}(\bar{f}_i A_i) = A_i \frac{\partial \bar{f}_i}{\partial t} \tag{2.11}$$

where $\bar{f}_i$ is an average value for the cell, assigned to the geometrical center of the cell, x_i.

The second integral becomes:

$$\int_{\partial A_i} (\vec{i}F)\cdot\vec{n}dl = F_{i+1/2}h_{i+1/2} - F_{i-1/2}h_{i-1/2} \tag{2.12}$$

while the third one can be written as:

$$\int_{A_i} PdA = \int_{x_{i-1/2}}^{x_{i+1/2}} \begin{bmatrix} 0 \\ \frac{p}{h}\frac{dh}{dx} \\ 0 \end{bmatrix} h dx = \int_{x_{i-1/2}}^{x_{i+1/2}} \begin{bmatrix} 0 \\ pdh \\ 0 \end{bmatrix} = \begin{bmatrix} 0 \\ \bar{p}_i \\ 0 \end{bmatrix} (h_{i+1/2} - h_{i-1/2}) \tag{2.13}$$

the tilde over p_i denoting also an average value of the pressure for the cell *i*.

Equations (2.11), (2.12) and (2.13) give:

$$\frac{\partial \bar{f}_i}{\partial t} = -\frac{1}{A_i}(F_{i+1/2}h_{i+1/2} - F_{i-1/2}h_{i-1/2}) + \frac{1}{A_i}\begin{bmatrix} 0 \\ \bar{p}_i \\ 0 \end{bmatrix}(h_{i+1/2} - h_{i-1/2}) \tag{2.14}$$

Using for the time derivative a discretization of the form

$$\frac{\partial \bar{f}_i}{\partial t} = \frac{\bar{f}_i^{n+1} - \bar{f}_i^{n}}{\Delta t} \tag{2.15}$$

and dropping the tilde for the average value, one obtains:

$$f_i^{n+1} = f_i^n - \frac{\Delta t}{A_i}(F_{i+1/2}h_{i+1/2} - F_{i-1/2}h_{i-1/2}) + \frac{\Delta t}{A_i}\begin{bmatrix} 0 \\ p_i \\ 0 \end{bmatrix}(h_{i+1/2} - h_{i-1/2}) \tag{2.16}$$

where the superscript n is used to denote $f_i(t_n)$, the time being discretized as $t_{n+1}=t_n+\Delta t$, with t_0 the initial time moment.

As a particular case, for the one-dimensional flows, when $h(x)$=constant, the Euler equations become:

$$f_i^{n+1} = f_i^n - \frac{\Delta t}{\Delta x_i}(F_{i+1/2} - F_{i-1/2}) \tag{2.17}$$

2.3.2 Two-dimensional flows

The two-dimensional finite-volume discretized form of the Euler equations can be obtained directly from (2.5). Expressing again the first integral in terms of the average value for the cell, f_{ij}, following the notation in equation (2.6) and Fig. 2.2, the equations can be written:

$$A_{ij}\frac{\partial f_{ij}}{\partial t} = -Q_{ij} \tag{2.18}$$

where Q_{ij} is the sum of the fluxes corresponding to the four sides of the cell *(i,j)*:

$$Q_{ij} = (\vec{\mathrm{Q}}\cdot\vec{n}\Delta s)_{i+1/2,j} + (\vec{\mathrm{Q}}\cdot\vec{n}\Delta s)_{i-1/2,j} + (\vec{\mathrm{Q}}\cdot\vec{n}\Delta s)_{i,j+1/2} + (\vec{\mathrm{Q}}\cdot\vec{n}\Delta s)_{i,j-1/2} \tag{2.19}$$

in which the subscripts $(i\pm 1/2, j)$ and $(i, j\pm 1/2)$ are used to define the four sides of the cell, of length $\Delta s_{i\pm 1/2,j}$ and $\Delta s_{i,j\pm 1/2}$, and:

$$\vec{\mathrm{Q}} = \vec{i}F + \vec{j}G \tag{2.20}$$

is the total flux vector.

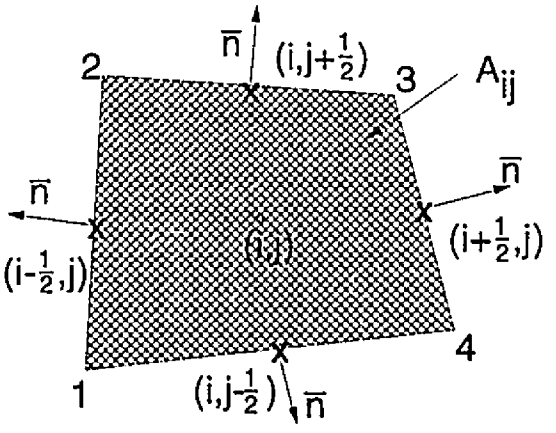

Fig. 2.2

For example, for the side $(i+½,j)$, the flux becomes:

$$(\bar{Q}\cdot\bar{n}s)_{i+½,j}=(F\Delta y)_{i+½,j}-(G\Delta x)_{i+½,j} \tag{2.21}$$

or, in terms of flow variables:

$$(\bar{Q}\cdot\bar{n}\Delta s)_{i+½,j}=\begin{bmatrix}\rho q\\ \rho qu+p(y_3-y_4)\\ \rho qv-p(x_3-x_4)\\ (\rho E+p)q\end{bmatrix} \tag{2.22}$$

where ρ, u, v, p and E are appropriate values for the corresponding variables on the side $(i+½,j)$, which are approximated differently according to the method used, and

$$q=V_n\cdot\Delta s_{i+½,j}=u\cdot\Delta y_{i+½,j}-v\cdot\Delta x_{i+½,j}=u(y_3-y_4)-v(x_3-x_4) \tag{2.23}$$

represents the flux of the velocity component normal to the side $(i+½,j)$, denoted by V_n, through this side of length $\Delta s_{i+½,j}$.

2.4 Boundary conditions

In order for a given flow problem to be completely defined, the system of the Euler equations has to be supplemented by the appropriate boundary conditions, as well as by the initial conditions for the flow variables. The problem to be solved can be fully described as an initial value problem, i.e. solving the system of partial differential equations:

$$\frac{\partial f}{\partial t}+\frac{\partial F}{\partial x}+\frac{\partial G}{\partial y}=0 \tag{2.24}$$

within the computational domain, with initial conditions:

$$f(x,y,t_0)=f_0(x,y) \tag{2.25}$$

subjected to the corresponding boundary conditions at the inflow, outflow and solid wall boundaries.

The inflow and outflow boundaries are treated according to the theory of characteristics, as described in Appendix A. A set of boundary variables can be prescribed at each boundary, depending upon the local character of the flow; these variables are usually the ones that can be easily detemined by experiment (for example, the pressure at a subsonic outflow boundary) and constitute physical boundary conditions. The other variables are computed from the solution within the domain (numerical boundary conditions). The exact way in which inflow/outflow boundary conditions are treated can be found in Chapter 4.

In two-dimensional flows, boundary conditions must also be specified on the solid walls. The boundary condition which is suited for the Euler equations (inviscid fluid) is the impermeability (or flow tangency) condition:

$$\vec{V}\cdot\vec{n}=0 \tag{2.26}$$

which implies that there is no flux of fluid flow through the surface. For finite-volume discretizations with flow variables defined at the center of the cell, this means that

one only needs a pressure evaluation at the solid boundary, as will be shown in Section 4.2 on numerical boundary conditions.

2.5 Nondimensionalization

For numerical computations, in order to have all variables at about the same magnitude around unity, and thus minimize the rounding-off errors, the equations are used in nondimensional form. The choice of the nondimensional parameters is such that the resulting equations are formally identical to the dimensional ones. The nondimensional time, space and flow variables, denoted by the superscript "*", are defined by:

$$t^* = \frac{t \cdot V_{ref}}{L_{ref}} \quad , \quad A^* = \frac{A}{(L_{ref})^2} \quad , \quad x^* = \frac{x}{L_{ref}}$$
$$y^* = \frac{y}{L_{ref}} \quad , \quad u^* = \frac{u}{V_{ref}} \quad , \quad v^* = \frac{v}{V_{ref}} \qquad (2.27)$$
$$\rho^* = \frac{\rho}{\rho_{ref}} \quad , \quad p^* = \frac{p}{\rho_{ref}(V_{ref})^2} \quad , \quad E^* = \frac{E}{(V_{ref})^2}$$

The subscript "*ref*" denotes reference variables which have to be chosen according to the flow character. For the present study, the reference variables used are:

i) $V_{ref} = a_0$ (stagnation speed of sound).

ii) $\rho_{ref} = \rho_0$ (stagnation density).

iii) $L_{ref} = (\Delta x)_{average}$ (average step on x).

The Euler equations written in nondimensional variables remain identical to (2.5), (2.7) for the integral form, respectively (2.9), (2.10) for the differential form. The discretized equations in nondimensional form are also identical to (2.16), (2.17), (2.18). Therefore, all subsequent analysis will be done in terms of the nondimensional variables, disregarding the superscript "*".

2.6 Convergence criterion

In the case of steady state flows, the integration in virtual time must be stopped when the distribution of the flow variables becomes, within a certain degree of accuracy, stationary; this translates also into satisfying, to a certain precision, the equations of motion. Different convergence criteria can therefore be established to this regard. According to the advice given by Roe (see [33], page 73), in this study, convergence has been considered when the difference between all the components of the state vector at two successive time steps satisfies:

$$| f^{n+1} - f^{n} | \leq \epsilon \tag{2.28}$$

for all the cells of the discretization. The quantity ϵ was usually taken as 10^{-4}.

Chapter 3

CLASSICAL TIME INTEGRATION METHODS

This chapter describes the explicit time integration methods developed by Godunov, MacCormack and Jameson, based on a finite-volume discretization. The basic conservation forms of the discretized equations are (2.14) for one-dimensional flows, respectively (2.18) for two-dimensional flows, which are valid for all the methods to be described in this study. The differences between the methods come from the way the flux variables F and G are computed at the cell interfaces, and from the discretization of the time derivative.

3.1 Godunov's method

3.1.1 The Riemann problem

The Riemann problem is the initial value problem defined by the partial differential equation

$$\frac{\partial f}{\partial t} + \frac{\partial F}{\partial x} = 0 \tag{3.1}$$

with the particular initial conditions:

$$f(x, t_0=0) = \begin{cases} f_L, & x<0 \\ f_R, & x \geq 0 \end{cases} \tag{3.2}$$

where the system of equations (3.1) is supposed to be hyperbolic, that is all the eigenvalues of the Jacobian

$$A(f) = \frac{\partial F}{\partial f} \tag{3.3}$$

are real and distinct. The independent variables are the time t, and the space coordinate x; in the case of the Euler equations, the dependent variables f and F are the state and flux vectors for one-dimensional flows, respectively, given by (2.8). Because the state vector is a function of the flow variables ρ, u, and p, the flux vector is also a function of the same variables, and hence a function of the state vector, and it is convenient to denote it by:

$$F = \Psi(f) \tag{3.4}$$

For the Euler equations of fluid dynamics, the Riemann problem has a solution which is known from the generalization of the flow in a shock tube (see [35] for example). The solution is represented by 3 waves moving from the initial discontinuity at $x=0$ with different speeds: a rarefaction wave, a contact discontinuity (slip line) and a shock wave, as represented in Fig. 3.1; the rarefaction is not a simple wave, but a fan of waves whose extension between the head and the tail waves depends on the initial data (3.2).

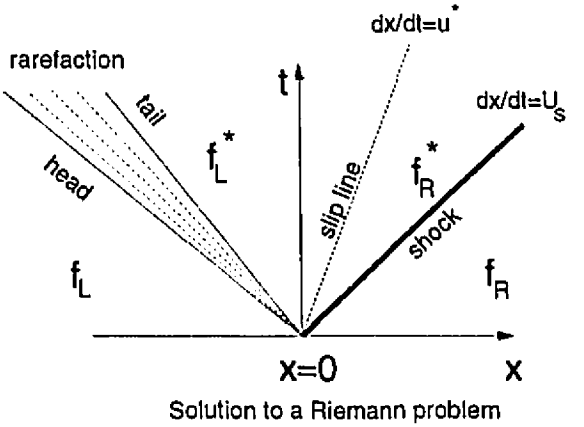

Fig. 3.1

If the initial data (3.2) is known, there is an analytical solution for this Riemann problem, i.e. we can find $f(x,t)$ for any $t>t_0$. This solution, which implies an iterative process, is due to S. K. Codunov, and will be presented briefly in this chapter.

The shock wave propagates with the speed U_s from the initial discontinuity at $x=0$ into the region with lower pressure, supposed to lie at the right $(x>0)$ in Fig. 3.1. Before the shock, the fluid remains in the same initial state $f_R = [\rho_R, \rho_R u_R, \rho_R E_R]^T$ while behind the shock the fluid is compressed and accelerated, such that the state behind the shock will be $f_R^* = [\rho_R^*, \rho_R^* u_R^*, \rho_R^* E_R^*]^T$. The expansion fan propagates into the region of higher pressure (to the left in Fig. 3.1) such that after the tail expansion wave the state of the fluid will be $f_L^* = [\rho_L^*, \rho_L^* u_L^*, \rho_L^* E_L^*]^T$, while before the head expansion wave the fluid is not perturbed, the state being the initial left state $f_L = [\rho_L, \rho_L u_L, \rho_L E_L]^T$. The fluid initially at $x<0$ is separated from the fluid initially at $x>0$ by a contact discontinuity. Across this discontinuity, the velocity of the fluid u and the pressure p are continuous, $u_L^* = u_R^* = u^*$ and $p_L^* = p_R^* = p^*$ respectively, but the density can be discontinuous, $\rho_L^* \neq \rho_R^*$.

To compute the solution, one first evaluates the pressure at the contact discontinuity p^*. Using the momentum equation, the absolute value of the mass flux $|\dot{m}_R|$ swept across the right wave (which can be either a shock or a rarefaction) can be expressed (see Appendix B, eq. B.19) as:

$$|\dot{m}_R| = \frac{|p_R - p^*|}{|u_R - u^*|} \tag{3.5}$$

This mass flux can be expressed as a function of the ratio of the two pressures p^* and p_R for either case of a shock or an expansion (eq. B.43 and B.44):

$$|\dot{m}_R| = \sqrt{p_R \rho_R} \cdot \Phi\left(\frac{p^*}{p_R}\right) \tag{3.6}$$

where the unified expression for Φ is:

$$\Phi(w) = \begin{cases} \sqrt{\dfrac{\gamma+1}{2} w + \dfrac{\gamma-1}{2}} & , \ w \geq 1 \quad \text{(compression)} \\ \dfrac{\gamma-1}{2\sqrt{\gamma}} \cdot \dfrac{1-w}{1-w^{\frac{\gamma-1}{2\gamma}}} & , \ w \leq 1 \quad \text{(expansion)} \end{cases} \tag{3.7}$$

The same expression can be established for the left wave:

$$|\dot{m}_L| = \frac{|p_L - p^*|}{|u_L - u^*|} = \sqrt{p_L \rho_L} \cdot \Phi\left(\frac{p^*}{p_L}\right) \tag{3.8}$$

with $\Phi(w)$ given by the same equation (3.7).

Once $|\dot{m}_L|$ and $|\dot{m}_R|$ are known, p^* can be computed from the following relation established by eliminating u^* between (3.5) and (3.8), with due account paid to the fact that across a rarefaction the mass flux has a negative value:

$$p^* = \frac{u_L - u_R + \dfrac{p_R}{|\dot{m}_R|} + \dfrac{p_L}{|\dot{m}_L|}}{\dfrac{1}{|\dot{m}_R|} + \dfrac{1}{|\dot{m}_L|}} \tag{3.9}$$

Using these formulae, the following iterative procedure due mainly to Godunov (slight improvements have been brought by Chorin [5]) can be defined to find p^* if the left and right states (ρ_L, u_L, p_L) and (ρ_R, u_R, p_R) respectively are known:

i) Construct a starting value for the pressure at the contact discontinuity, p^*, for example:

$$p_{i\,0}^{\cdot} = \frac{p_R + p_L}{2} \tag{3.10}$$

ii) Compute $\dot{m}_R$, $\dot{m}_L$ using the value $p_i^{\cdot}$ for the pressure $p^{\cdot}$ in (3.6) and (3.8)

iii) Compute a new value for the pressure $p^{\cdot}$, $\bar{p}_i^{\cdot}$, i>0, with relation (3.9)

iv) Check for convergence using a certain convergence criterion, for example:

$$\left|\bar{p}_i^{\cdot} - p_{i-1}^{\cdot}\right| \leq \epsilon \tag{3.11}$$

v) If convergence has not been obtained yet, repeat from step ii), with $p_i^{\cdot} = \bar{p}_i^{\cdot}$.

This procedure does converge in practical computations unless one is in the presence of a very strong rarefaction, in which case negative values for the pressure are lightly to be obtained, and the above iterative process is slightly modified. The modification used in the present study is due to Chorin [5]; namely, if convergence is not obtained after L iterations, the value obtained at step iii) is replaced by:

$$\bar{p}_i^{\cdot} = \alpha \max\left(\epsilon_p, p_{i-1}^{\cdot}\right) + (1-\alpha)\, p_i^{\cdot} \tag{3.12}$$

with $\alpha=\alpha_1=½$, and ϵ_p an admissible truncation error for the pressure, taken for the present work as $\epsilon_p = 10^{-6}$. The value of L is set to $L=20$, and the equation (3.12) is modified if convergence has not been reached in kL iterations by setting:

$$\alpha = \alpha_k = \frac{\alpha_{k-1}}{2} \tag{3.13}$$

For the test cases used, this modification was not needed at any point; the process i)-v) generally converged in 2-4 steps.

If the value of the pressure at the contact discontinuity $p^{\cdot}$ has been found and $|\dot{m}_R|$, $|\dot{m}_L|$ determined accordingly from (3.6), (3.8), the velocity $u^{\cdot}$ can be readily computed using:

$$u^* = \frac{p_L - p_R + |\dot{m}_R| u_R + |\dot{m}_L| u_L}{|\dot{m}_R| + |\dot{m}_L|} \tag{3.14}$$

relation obtained from (3.5) and (3.8) by eliminating this time the pressure p^*.

The complete solution $f_P = [\rho_P, \rho_P u_P, \rho_P E_P]^T$ at a point $P(x_P, t_P)$ — x_P and t_P being the space and time coordinates of P in the time-space diagram in Fig. 3.1 — is determined by situating the point P in one of the five regions of the diagram according to the following possible cases:

• If P is situated to the right of the slip line $(x_P > u^* t_P)$ and the right wave is a shock, the velocity of the shock, U_s is found from the continuity equation (B.13):

$$U_s = \frac{\rho_R u_R - \rho_R^* u^*}{\rho_R - \rho_R^*} \tag{3.15}$$

Then, if P is situated to the right of the shock $(x_P > U_s t_P)$:

i) $(\rho_P, u_P, p_P) = (\rho_R, u_R, p_R)$

If P is to the left of the shock, then

ii) $(\rho_P, u_P, p_P) = (\rho_R^*, u^*, p^*)$

where ρ_R^* can also be found using the continuity equation in the form (B.17):

$$\rho_R^* = -\frac{\dot{m}_R}{U_s - u^*} \tag{3.16}$$

• If P is situated to the left of the slip line $(x_P < u^* t_P)$ and the left wave is a rarefaction, one evaluates first the speeds of the head and tail waves of the rarefaction. The head wave moves with speed $\frac{dx}{dt} = u_L - c_L$, while the tail wave moves with speed $\frac{dx}{dt} = u^* - c_L^*$, where c_L^* can be computed by considering the Riemann invariant w_{2_L} propagated from the left of the rarefaction along the right-running characteristic C_2 (see Appendix A):

$$w_{2_L} = \frac{2c_L^*}{\gamma - 1} + u^* = \frac{2c_L}{\gamma - 1} + u_L \tag{3.17}$$

Then, if P lies to the left of the rarefaction, $x_P < (u_L - c_L)t_P$, the solution is:

iii) $(\rho_P, u_P, p_P) = (\rho_L, u_L, p_L)$

If P lies to the right, $x_P > (u^* - c_L^*)t_P$, then:

iv) $(\rho_P, u_P, p_P) = (\rho_L^*, u^*, p^*)$

where ρ_L^* can be obtained from the isentropic law:

$$\frac{p_L}{\rho_L^\gamma} = \frac{p^*}{(\rho_L^*)^\gamma} \tag{3.18}$$

v) If P lies between the head and the tail waves of the rarefaction, $(u_L - c_L)t_P < x_P < (u^* - c_L^*)t_P$, then the solution is found as follows:

- obtain ρ_L^* by the isentropic law (3.18);
- equate the slope of the characteristic through P with that of the line through P and the origin to get:

$$u_P - c_P = \frac{x_P}{t_P} \tag{3.19}$$

c_P being the speed of sound at point P;

- use the Riemann invariant to obtain:

$$W_{2_P} = W_{2_L} \Leftrightarrow \frac{2c_P}{\gamma - 1} + u_P = \frac{2c_L}{\gamma - 1} + u_L \tag{3.20}$$

Solving for c_P,

$$c_P = c_L + \frac{\gamma - 1}{2}(u_L - u_P) \tag{3.21}$$

Inserting this expression into (3.19) and solving for u_P:

$$u_P = \frac{2}{\gamma + 1}\left(\frac{x_P}{t_P} + c_L + \frac{\gamma - 1}{2}u_L\right) \tag{3.22}$$

Equation (3.22) gives the velocity at point P in terms of known variables; then one can find c_P from (3.21) and the density is obtained from the isentropic law and the definition of the speed of sound:

$$\rho_P = \left(\frac{c_P^2}{\gamma p_L \rho_L^{-\gamma}} \right)^{\frac{1}{\gamma-1}} \tag{3.23}$$

If, on the contrary, the right wave is a rarefaction and the left one a shock, the five possible positions for point P are mirror images of the preceding ones, with the Riemann invariant w_{2_L} replaced by:

$$w_{3_R} = \frac{2c_R}{\gamma - 1} - u_R \tag{3.24}$$

and the treatment is similar.

Because the solution of the Riemann problem at a certain point P depends only on the left and right initial states $f_L = [\rho_L, \rho_L u_L, \rho_L E_L]^T$ and $f_R = [\rho_R, \rho_R u_R, \rho_R E_R]^T$ and on the coordinates of the point (x_P, t_P), it can be denoted by:

$$f_P = [\rho_P, \rho_P u_P, \rho_P E_P]^T = \varphi^{Rm}(x_P, t_P; f_L, f_R).$$

where φ^{Rm} is a vector-valued function of its variables. This solution represents the building stone of Godunov's method.

3.1.2 One-dimensional flows

For one-dimensional flows, Godunov's method for time integration can be expressed in the form given by equation 2.17, where the fluxes are computed from:

$$F_{i+\frac{1}{2}} = F_{i+\frac{1}{2}}^{n+\frac{1}{2}} = \Psi\left(\varphi^{Rm}(0, \frac{\Delta t}{2}; f_i^n, f_{i1}^n) \right) \tag{3.25}$$

Relation (3.25) states that the flux at the interface $x_{i+\frac{1}{2}}$ between the cells i and $i+1$ is computed as the solution, at time $t_{n+\frac{1}{2}} = t_n + \Delta t/2$, of the Riemann problem

obtained by considering the two cells separated by an imaginary diaphragm which is "broken" at time t_n.

For stability of the solution, the computation of a flux at a certain cell interface should not be influenced by waves propagating from neighboring interfaces. Since the wave speeds are $u \pm c$, this stability condition translates into the current *CFL* condition:

$$CFL \leq 1 \tag{3.26 a}$$

or, in terms of the time step:

$$\Delta t \leq \frac{\Delta x}{\max_i(|u_i| + c_i)} \tag{3.26 b}$$

3.1.3 Two-dimensional flows

For a two-dimensional flow, there is no corresponding equivalent to the analytical one-dimensional Riemann problem solver. Therefore, when treating two-dimensional flows, the problem is split into two one-dimensional problems, treated under the basic assumption that waves pertaining to these two "separate" one-dimensional flows do not interact.

For a given cell *(i,j)* the computation of the flux on each side is done using the normal and tangential components of the velocity at that side. The two cells neighboring on the chosen side are supposed to interact giving birth to a one-dimensional Riemann problem in the normal component of the velocity only, while the tangential velocity component is preserved.

For example, referring to Fig. 2.2 and equation (2.22), for the side $(i+\frac{1}{2},j)$, the initial conditions for the corresponding one-dimensional Riemann problem are:

$$f(x,t_0) = \begin{cases} f_L = [\rho_L, \rho_L V_{n_L}, \rho_L E_L]^T , & x<0 \\ f_R = [\rho_R, \rho_R V_{n_R}, \rho_R E_R]^T , & x \geq 0 \end{cases} \tag{3.27}$$

where subscript L refers to cell (i,j), subscript R to cell $(i+1,j)$, and V_n is the respective velocity component normal to side $(i+½,j)$ computed from:

$$V_{n_R} = u_R \frac{\Delta y}{\Delta s} - v_R \frac{\Delta x}{\Delta s} \tag{3.28}$$

and a similar relation for the left side, Δs being the length of the side $(i+½,j)$:

$$\Delta s = \sqrt{(\Delta x)^2 + (\Delta y)^2} \tag{3.29 a}$$

$$\Delta x = x_3 - x_4 \quad , \quad \Delta y = y_3 - y_4 \tag{3.29 b}$$

The values of the flow variables on the side $(i+½,j)$ are obtained by solving the Riemann problem:

$$\begin{bmatrix} \rho \\ \rho V_n \\ \rho\left(\frac{1}{\gamma-1}\frac{p}{\rho} + \frac{V_n^2}{2}\right) \end{bmatrix} = \varphi^{Rm}\left(0, \frac{\Delta t}{2}; f_L, f_R\right) \tag{3.30}$$

To find the cartesian components of the velocity needed in (2.22), the tangential component on the side $(i+½,j)$, denoted by V_t, is also needed. It is found as follows: first, the tangential components to the left (cell (i,j)) and to the right (cell $(i+1,j)$) are computed:

$$V_{t_L} = -u_L \frac{\Delta x}{\Delta s} - v_L \frac{\Delta y}{\Delta s} \tag{3.31}$$

and similarly for the right cell. The solution V_t at the interface is taken to be V_{t_L} if the interface $(i+½,j)$ is left of the slip line, respectively V_{t_R} if the interface is right of the slip line. The Cartesian components u and v are then computed by projection of the velocity vector:

$$\vec{V} = V_n \cdot \vec{n} + V_t \cdot \vec{t} = u \cdot \vec{i} + v \cdot \vec{j} \tag{3.32}$$

which yields:

$$u = V_n \frac{\Delta y}{\Delta l} - V_t \frac{\Delta x}{\Delta l}$$
$$v = -V_n \frac{\Delta x}{\Delta l} - V_t \frac{\Delta y}{\Delta l} \tag{3.33}$$

Finally, the computed values: ρ, V_n, p, u, v, together with the energy E obtained from the equation of state are used in (2.22), (2.23) to compute the fluxes on side $(i+\frac{1}{2}, j)$, and the process is repeated for all four sides of the cell with corresponding initial values for the Riemann problem.

For stability, the two-dimensional scheme requires that the time step Δt satisfy the Courant-Friederichs-Levy condition:

$$\Delta t \leq \frac{\Delta t_x \cdot \Delta t_y}{\Delta t_x + \Delta t_y} \tag{3.34}$$

where Δt_x and Δt_y are the time steps that would guarantee stability for the split one-dimensional schemes:

$$\Delta t_x = \min_{ij} \frac{\Delta x_{ij}}{(|u_{ij}| + c_{ij})} \tag{3.35 a}$$

$$\Delta t_y = \min_{ij} \frac{\Delta y_{ij}}{(|v_{ij}| + c_{ij})} \tag{3.35 b}$$

$$\Delta x_{ij} = x_{i+1,j} - x_{ij} \quad , \quad \Delta y_{ij} = y_{i,j+1} - y_{ij} \tag{3.35 c}$$

3.2 MacCormack's method

3.2.1 Quasi one-dimensional flows

MacCormack's method is a two-step, predictor-corrector method, in which the two steps use different directions for the computation of the derivatives in the Euler equations. In finite-volume formulation, it can be expressed as:

- predictor step (corresponding to backward differencing)

$$f_i^{\overline{n+1}} = f_i^n - \frac{\Delta t}{A_i}\left(F_i^n h_{i+1/2} - F_{i-1}^n h_{i-1/2}\right) + \frac{\Delta t}{A_i}\begin{bmatrix} 0 \\ p_i^n \\ 0 \end{bmatrix}\left(h_{i+1/2} - h_{i-1/2}\right) \qquad (3.36\text{ a})$$

- corrector step (corresponding to forward differencing)

$$f_i^{n+1} = \frac{1}{2}\left[f_i^n + f_i^{\overline{n+1}} - \frac{\Delta t}{A_i}\left(F_{i+1}^{\overline{n+1}} h_{i+1/2} - F_i^{\overline{n+1}} h_{i-1/2}\right) + \frac{\Delta t}{A_i}\begin{bmatrix} 0 \\ p_i^{\overline{n+1}} \\ 0 \end{bmatrix}\left(h_{i+1/2} - h_{i-1/2}\right)\right] \qquad (3.36\text{ b})$$

The order backward-forward chosen above is not the only possible one. Other variants use forward-backward schemes, or even schemes reversing the order at each time step: forward-backward at, say, odd time steps, followed by backward-forward at even time steps.

Relations (3.36) can formally be expressed in the conservative form (2.16) using the notation:

$$F_{i+1/2} = \frac{F_{i+1}^{\overline{n+1}} + F_i^n}{2} \quad , \quad F_{i-1/2} = \frac{F_i^{\overline{n+1}} + F_{i-1}^n}{2} \quad , \quad p_i = \frac{p_i^{\overline{n+1}} + p_i^n}{2} \qquad (3.37)$$

One may notice that the intermediate time step $\overline{n+1}$ does not appear explicitly in the conservative difference scheme (2.16) but only in the expressions of the fluxes (3.37).

For stability, this scheme requires the same *CFL* number condition given by (3.26).

3.2.2 Two-dimensional schemes

The variant used in this study is a non-split backward-forward scheme for which the two steps are defined by:

- predictor step (backward)

$$\overline{f_{ij}^{n+1}} = f_{ij}^{n} - \frac{\Delta t}{A_{ij}} Q_{ij}^{n} \tag{3.38}$$

- corrector step (forward)

$$f_{ij}^{n+1} = \frac{1}{2}\left[f_{ij}^{n} + \overline{f_{ij}^{n+1}} - \frac{\Delta t}{A_{ij}} \overline{Q_{ij}^{n+1}} \right] \tag{3.39}$$

where the fluxes in the two steps are computed differently according to:

$$Q_{ij}^{n} = \vec{Q}_{ij}^{\,n} \cdot (\vec{n}\Delta s)_{i+1/2,j} + \vec{Q}_{i-1,j}^{\,n} \cdot (\vec{n}\Delta s)_{i-1/2,j} + \vec{Q}_{ij}^{\,n} \cdot (\vec{n}\Delta s)_{i,j+1/2} + \vec{Q}_{i,j-1}^{\,n} \cdot (\vec{n}\Delta s)_{i,j-1/2} \tag{3.40}$$

$$\overline{Q_{ij}^{n+1}} = \vec{Q}_{i+1,j}^{\,\overline{n+1}} \cdot (\vec{n}\Delta s)_{i+1/2,j} + \vec{Q}_{ij}^{\,\overline{n+1}} \cdot (\vec{n}\Delta s)_{i-1/2,j} + \vec{Q}_{i,j+1}^{\,\overline{n+1}} \cdot (\vec{n}\Delta s)_{i,j+1/2} + \vec{Q}_{ij}^{\,\overline{n+1}} \cdot (\vec{n}\Delta s)_{i,j-1/2} \tag{3.41}$$

For example, a typical term appearing in the computation of the fluxes is:

$$\vec{Q}_{ij}^{\,n} \cdot (\vec{n}\Delta s)_{i+1/2,j} = \begin{bmatrix} \rho_{ij}^{n} q_{ij}^{n} \\ \rho_{ij}^{n} q_{ij}^{n} u_{ij}^{n} + p_{ij}^{n} \Delta y_{i+1/2,j} \\ \rho_{ij}^{n} q_{ij}^{n} v_{ij}^{n} - p_{ij}^{n} \Delta x_{i+1/2,j} \\ (\rho_{ij}^{n} E_{ij}^{n} + p_{ij}^{n}) q_{ij}^{n} \end{bmatrix} \tag{3.42}$$

where the velocity flux is defined by:

$$q_{ij}^{n} = u_{ij}^{n}\Delta y_{i+1/2,j} - v_{ij}^{n}\Delta x_{i+1/2,j} \tag{3.43}$$

The maximum time step $\Delta t = t_{n+1} - t_n$ can be evaluated [25] from the Courant number stability condition:

$$\Delta t \leq \min_{ij} \frac{1}{\frac{|u_{ij}|}{\Delta x} + \frac{|v_{ij}|}{\Delta y} + c_{ij}\sqrt{\frac{1}{(\Delta x)^2} + \frac{1}{(\Delta y)^2}}} \tag{3.44}$$

3.2.3 Artificial viscosity

Although MacCormack's scheme has certain dissipative properties, when the flow field contains discontinuities this implicit dissipation is generally not enough to maintain stability. Therefore, the scheme is augmented by the addition of an explicit artifical viscosity. For the present study, the formulation introduced by Lapidus [19] has been used, in which terms describing diffusion of mass, momentum and energy are added to the respective equations. Only the modification required in the two-dimensional flows will be presented, for the quasi one-dimensional flows the extension being straightforward.

The values f_{ij}^{n+1} calculated from (3.39) are replaced by the new ones $f_{ij}^{``n+1}$ obtained by smoothing first in the x direction and then in the y direction according to the following relations:

- for the x direction:

$$f_{ij}^{`n+1} = f_{ij}^{n+1} + \frac{\Delta t}{A_{ij}} C\cdot\Delta`\left[|\Delta` u_{i+1,j}^{n+1}|\cdot\Delta`(f_{i+1,j}^{n+1})\right] \tag{3.45}$$

- for the y direction:

$$f_{ij}^{n+1} = f_{ij}^{n+1} + \frac{\Delta t}{A_{ij}} C \cdot \Delta'' \left| |\Delta'' v_{ij-1}^{n+1}| \cdot \Delta'' (f_{ij-1}^{n+1}) \right| \tag{3.46}$$

where the difference operators are defined as:

$$\Delta' u_{ij} = u_{ij} - u_{i-1,j} \quad , \quad \Delta'' u_{ij} = u_{ij} - u_{ij-1} \tag{3.47}$$

and C is a constant of order unity. Its value must be adapted to each flow case, therefore it will be indicated in the section on numerical results.

Equations (3.45), (3.46) are equivalent to adding to the Euler equations a diffusion term of the type:

$$C \cdot \left\{ (\Delta x)^3 \cdot \frac{\partial}{\partial x} \left[\left| \frac{\partial u}{\partial x} \right| \frac{\partial f}{\partial x} \right] + (\Delta y)^3 \cdot \frac{\partial}{\partial y} \left[\left| \frac{\partial v}{\partial y} \right| \frac{\partial f}{\partial y} \right] \right\} \quad .$$

Being of the third order, this term does not affect the truncation error of the difference equation, as is underlined by Lapidus in [19].

3.3 Jameson's method

This scheme uses a Runge-Kutta method for advancing the solution in time and central differences for the estimation of the flux values. The Runge-Kutta method can be chosen from the wide variety of existing ones; in this study, the most frequently encountered four-stage method is used.

The fundamental feature of Jameson's method is that it keeps the spatial operator separate from the time-marching operator. Thus, if a steady state solution is looked for, it does not depend on the value of the time step used for integration,

whereas in MacCormack's method, for example, it can be shown that the second-order term $\frac{\partial^2 f}{\partial t^2}$ depends on the spatial differencing operations. This allows the use of a local time step based on the maximum value for the local Courant number to accelerate convergence without altering the steady state solution (see [18]).

3.3.1 Quasi one-dimensional flows

For convenience, equation (2.14) is recast in the form:

$$\frac{\partial f_i}{\partial t} = -\tilde{Q}_i(f) \tag{3.48}$$

where $\tilde{Q}_i(f)$ is the total flux operator for quasi one-dimensional flows, defined as:

$$\tilde{Q}_i(f) = \frac{1}{A_i}\left(F_{i+1/2}h_{i+1/2} - F_{i-1/2}h_{i-1/2}\right) - \frac{1}{A_i}\begin{bmatrix}0\\ p_i\\ 0\end{bmatrix}\left(h_{i+1/2} - h_{i-1/2}\right) - D_i(f) \tag{3.49}$$

The fluxes at an interface are obtained through an averaging process equivalent to central differencing if the area of the duct is constant. In this study, the average value of the flow variables in the two cells neighboring the interface has been used, as defined by the equation:

$$w_{i\pm 1/2} = \frac{1}{2}\left(w_i + w_{i\pm 1}\right) \tag{3.50}$$

where w is either ρ, u or p.

In (3.49), $D_i(f)$ is the artificial dissipation operator, introduced in order to make the spatial operator stable by preventing odd and even point decoupling which is characteristic to central differencing, and to avoid oscillations near discontinuities. These two goals are accomplished by the use of the second and fourth order differences, with coefficients which depend on the local change in static pressure,

being expressed in conservation law form as:

$$D_i(f) = d_{i+\frac{1}{2}} f - d_{i-\frac{1}{2}} f \tag{3.51}$$

where the terms on the right hand side have the form:

$$d_{i+\frac{1}{2}} f = \frac{1}{\Delta t}\{\epsilon^{(2)}_{i+\frac{1}{2}}(f_{i+1} - f_i) - \epsilon^{(4)}_{i+\frac{1}{2}}(f_{i+2} - 3f_{i+1} + 3f_i - f_{i-1})\} \tag{3.52}$$

The coefficients $\epsilon^{(2)}_{i+\frac{1}{2}}$ and $\epsilon^{(4)}_{i+\frac{1}{2}}$ are defined from:

$$\epsilon^{(2)}_{i+\frac{1}{2}} = k^{(2)} \max(\nu_{i+1}, \nu_i) \tag{3.53}$$

and:

$$\epsilon^{(4)}_{i+\frac{1}{2}} = \max\{0, (k^{(4)} - \epsilon^{(2)}_{i+\frac{1}{2}})\} \tag{3.54}$$

where ν_i is a switch based on the normalized second order difference of pressure:

$$\nu_i = \frac{|p_{i+1} - 2p_i + p_{i-1}|}{|p_{i+1} + 2p_i + p_{i-1}|} \tag{3.55}$$

and $k^{(2)}$, $k^{(4)}$ are arbitrary constants with typical values of *1/4* and *1/256* respectively.

The fourth order difference terms, with coefficient $\epsilon^{(4)}$, are important in smooth regions of the flow, calculations made without them failing to converge to a completely steady state; instead, after having reached a state close to the steady one, they oscillate indefinetely about it with a low amplitude. Near the shocks, however, they have been found to introduce overshoots, therefore they are switched off by subtracting $\epsilon^{(2)}$ from $k^{(4)}$ in equation (3.54).

Equation (3.48) is integrated in time using a four step Runge-Kutta scheme:

$$f_i^{(0)} = f_i^n \tag{3.56 a}$$

$$f_i^{(1)} = f_i^{(0)} - \frac{\Delta t}{2}\tilde{Q}_i(f^{(0)}) \tag{3.56 b}$$

$$f_i^{(2)} = f_i^{(0)} - \frac{\Delta t}{2}\tilde{Q}_i(f^{(1)}) \tag{3.56 c}$$

$$f_i^{(3)} = f_i^{(0)} - \Delta t\,\tilde{Q}_i(f^{(2)}) \tag{3.56 d}$$

$$f_i^{(4)} = f_i^{(0)} - \frac{\Delta t}{6}\left[\tilde{Q}_i(f^{(0)}) + 2\tilde{Q}_i(f^{(1)}) + 2\tilde{Q}_i(f^{(2)}) + \tilde{Q}_i(f^{(3)})\right] \tag{3.56 e}$$

$$f_i^{n+1} = f_i^{(4)} \tag{3.56 f}$$

The time-stepping method defined by (3.56) has the above-mentioned advantage of being independent of the time step, because at the steady state $\tilde{Q}_i(f) = 0$, so that $f^{(1)} = f^{(0)}$ and so forth up to $f^{n+1} = f^n$.

However, the dissipative terms are relatively expensive in terms of computer time. In order to avoid their evaluation for each of the four stages of the Runge-Kutta process (3.56), Jameson suggests that their evaluation be made only in the first stage, after which their value is frozen. Using the notation:

$$\tilde{Q}_i(f) = Q_i(f) - D_i(f) \tag{3.57}$$

where $Q_i(f)$ is only the flux operator:

$$Q_i(f) = \frac{1}{A_i}\left(F_{i+1/2}\,h_{i+1/2} - F_{i-1/2}\,h_{i-1/2}\right) - \frac{1}{A_i}\begin{bmatrix}0\\ p_i\\ 0\end{bmatrix}\left(h_{i+1/2} - h_{i-1/2}\right) \tag{3.58}$$

the above simplification results in the following set of equations to be used instead of (3.56):

$$f_i^{(0)} = f_i^n \tag{3.59 a}$$

$$f_i^{(1)} = f_i^{(0)} - \frac{\Delta t}{2} Q_i(f^{(0)}) + \frac{\Delta t}{2} D_i(f^{(0)}) \tag{3.59 b}$$

$$f_i^{(2)} = f_i^{(0)} - \frac{\Delta t}{2} Q_i(f^{(1)}) + \frac{\Delta t}{2} D_i(f^{(0)}) \tag{3.59 c}$$

$$f_i^{(3)} = f_i^{(0)} - \Delta t Q_i(f^{(2)}) + \Delta t D_i(f^{(0)}) \tag{3.59 d}$$

$$f_i^{(4)} = f_i^{(0)} - \frac{\Delta t}{6}\left[Q_i(f^{(0)}) + 2\,Q_i(f^{(1)}) + 2\,Q_i(f^{(2)}) + Q_i(f^{(3)}) \right] + \Delta t D_i(f^{(0)}) \tag{3.59 e}$$

$$f_i^{n+1} = f_i^{(4)} \tag{3.59 f}$$

If relations (3.59) are used instead of (3.56), the steady state solution is no longer independent of the time step.

When applied to the linear wave equation, this scheme is stable under the Courant number condition:

$$CFL \leq 2\sqrt{2} \tag{3.60}$$

3.3.2 Two-dimensonal flows

The two-dimensional discretization can be obtained if equation (2.18) is supplemented by the dissipation terms and recast into the form:

$$A_{ij}\frac{\partial f_{ij}}{\partial t} = -Q_{ij}(f) + D_{ij}(f) = -\tilde{Q}_{ij}(f) \tag{3.61}$$

Then, the Runge-Kutta process for the two-dimensional version of the scheme can be expressed by the following set of equations:

$$f_{ij}^{(0)} = f_{ij}^{n} \tag{3.62 a}$$

$$f_{ij}^{(1)} = f_{ij}^{(0)} - \frac{\Delta t}{2A_{ij}} \tilde{Q}_i(f^{(0)}) \tag{3.62 b}$$

$$f_{ij}^{(2)} = f_{ij}^{(0)} - \frac{\Delta t}{2A_{ij}} \tilde{Q}_i(f^{(1)}) \tag{3.62 c}$$

$$f_{ij}^{(3)} = f_{ij}^{(0)} - \Delta t \tilde{Q}_i(f^{(2)}) \tag{3.62 d}$$

$$f_{ij}^{(4)} = f_{ij}^{(0)} - \frac{\Delta t}{6}\left[\tilde{Q}_i(f^{(0)}) + 2\tilde{Q}_i(f^{(1)}) + 2\tilde{Q}_i(f^{(2)}) + \tilde{Q}_i(f^{(3)}) \right] \tag{3.62 e}$$

$$f_{ij}^{n+1} = f_{ij}^{(4)} \tag{3.62 f}$$

The flux term at the cell interfaces, $Q_{ij}(f)$, is given by (2.19), F and G being computed using average values for the flow variables between the values in the two neighboring cells. For example, between cells *(i+1,j)* and *(i,j)*, flow variables are taken to be:

$$w_{i+1/2,j} = \frac{w_{ij} + w_{i+1,j}}{2} \quad , \quad w_{i+1/2,j} = \frac{w_{ij} + w_{i+1,j}}{2} \tag{3.63}$$

where w is either ρ, u, v, or p.

The dissipation operator contains terms pertaining to the two coordinate directions:

$$D_{ij}(f) = D_x(f) + D_y(f) \tag{3.64}$$

given by:

$$D_x(f) = d_{i+1/2,j}f - d_{i-1/2,j}f \quad , \quad D_y(f) = d_{i,j+1/2}f - d_{i,j-1/2}f \tag{3.65}$$

where the right hand side terms have a form similar to (3.52), for example:

$$d_{i+1/2,j}f = \frac{1}{\Delta t}\{\epsilon^{(2)}_{i+1/2,j}(f_{i+1,j} - f_{ij}) - \epsilon^{(4)}_{i+1/2,j}(f_{i+2,j} - 3f_{i+1,j} + 3f_{ij} - f_{i-1,j})\} \tag{3.66}$$

the coefficients being computed in a manner similar to the quasi one-dimensional case (eqs. 3.53-3.55).

Finally, for steady state computations, one can also freeze the dissipation at the first stage (3.62 b) of the Runge-Kutta process, resulting in equations similar to (3.59). This improves the computer efficiency, without impediments on the convergence process. The stability condition, in terms of the *CFL* number, can be expressed in the same form (3.60).

Chapter 4

NUMERICAL BOUNDARY CONDITIONS

The finite-volume methods used to solve the Euler equations require the specification of all the flux terms on the cell interfaces which lie on the boundary of the computational domain. This is in contrast with the physics of the problem because in reality a certain flow regime is established when only a certain combination of flow parameters is specified on a boundary, not all of them. This can best be illustrated for the case of a steady quasi one-dimensional flow in a duct. Supposing the flow comes from an infinite tank where two flow parameters are known, for example the stagnation pressure p_0 and the stagnation speed of sound c_0, and the exit pressure from the duct, p_{ex}, is given, then the flow regime in the duct is fully determined. However, the numerical scheme needs, for the computation of the fluxes, three combinations of independent flow variables at each boundary. For the unknown variables (e.g. ρ_{ex}, u_{ex}), the only possibility which occurs, in accord with the theory of characteristics, is to use the information from the interior of the computational domain to update their values. The modality by which the boundary variables are updated is called a numerical boundary-condition procedure.

In the case of two-dimensional flows, a boundary-condition procedure must also be applied for the solid wall boundaries. This chapter describes the classical boundary procedures used in the present study as well as the basic implementation features for each method. To simplify the presentation, only the two-dimensional case is developed; the quasi one-dimensional case results immediately, by discarding the

y-axis equation and components.

4.1 Inflow and outflow boundaries

The inflow and outflow boundary-condition procedures must obey the rules imposed by the theory of characteristics applied to the partial differential equations of the flow (see Appendix A). For the two-dimensional Euler equations, at a subsonic inflow there are three incoming characteristics, and one outgoing characteristic. Therefore three boundary conditions must be specified at a subsonic inflow, and one is determined by the solution inside the domain. At a supersonic inflow, all four conditions must be specified from upstream.

At a subsonic outflow, three characteristics leave the domain while only one enters the domain, corresponding to the information supplied to the system from the surrounding world. Therefore, only one boundary condition can be imposed from downstream (usually the pressure) while three boundary values are determined from inside. At a supersonic outflow, all four characteristics leave the domain, hence the four variables are determined from the interior.

4.1.1 Subsonic inflow boundary

For all the methods used in this study, the inflow boundary-condition procedure is identical, in order to have a meaningful comparison between the methods. The three quantities imposed from upstream are:

- stagnation pressure, p_0.
- flow direction, $\tan\theta_{in} = \frac{v_{in}}{u_{in}}$.
- stagnation enthalpy, H.

The flow parameters on the boundary are updated according to the following scheme:

i) Evaluate pressure at inflow, p_{in}, using an extrapolation from the interior of the domain.

ii) Compute ρ_{in} using the isentropic law:

$$\rho_{in} = \rho_0 \left(\frac{p_{in}}{p_0} \right)^{\frac{1}{\gamma}} \tag{4.1}$$

iii) Compute velocity magnitude:

$$V_{in} = \sqrt{u_{in}^2 + v_{in}^2} = \sqrt{2\left(H - \frac{\gamma}{\gamma - 1} \frac{p_{in}}{\rho_{in}} \right)} \tag{4.2}$$

iv) Compute velocity components,

$$v_{in} = V_{in} \sin\theta_{in} \quad , \quad u_{in} = V_{in} \cos\theta_{in} \tag{4.3}$$

The implementation was different only for step i). For Godunov and Jameson methods, supposing the inflow boundary lies on a line x=constant and the first two cells have the same length Δx, p_{in} can be extrapolated as:

$$p_{in_j} = 1.5\, p_{1j}^n - 0.5\, p_{2j}^n \tag{4.4}$$

For MacCormack's method, at the predictor step (backward) the inflow pressure is given by:

$$p_{in_j} = 2\, p_{1j}^n - p_{2j}^n \tag{4.5 a}$$

while at the corrector step (forward):

$$p_{in_j} = p_{1j}^{\overline{n+1}} \qquad (4.5\ b)$$

4.1.2 Subsonic outflow boundary

For Godunov's method, the boundary procedure uses a fictitious cell denoted by the indices *(Imax+1, j)* where the flow parameters are taken to be:

$$\rho_{Imax+1,j} = \rho_{Imax,j} \quad , \quad u_{Imax+1,j} = u_{Imax,j} \quad , \quad v_{Imax+1,j} = v_{Imax,j} \quad , \quad p_{Imax+1,j} = p_{ex} \qquad (4.6)$$

The fluxes on the outflow interface are then computed using the solution to the Riemann problem:

$$F_{Imax+\frac{1}{2},j} = \Psi\left(\varphi^{Rm}\left(0, \frac{\Delta t}{2}; f_{Imax}, f_{Imax+1}\right)\right) \qquad (4.7)$$

For the methods of MacCormack and Jameson, a nonreflecting type boundary condition developed by Rudy and Strikwerda [34] for steady state flows was used. The incoming characteristic variable for the one-dimensional problem is $p - \bar{\rho}\,\bar{c}u$, the bar denoting linearized quantities. A boundary condition which would eliminate the incoming waves would therefore be:

$$\frac{\partial p}{\partial t} - \rho c \frac{\partial u}{\partial t} = 0 \qquad (4.8)$$

but this does not impose $p = p_{ex}$. To ensure that both conditions are satisfied, a linear combination of them gives:

$$\frac{\partial p}{\partial t} - \rho c \frac{\partial u}{\partial t} + \alpha(p - p_{ex}) = 0 \qquad (4.9)$$

where α is a numerical parameter without any physical meaning (taken as 0.8 in actual computations). Equation (4.9) artificially constructs a value for the exit pressure p which attenuates the waves coming from the exterior of the domain, and becomes equal to p_{ex} when the steady state is reached.

The following boundary procedure can be constructed starting from this equation:

i) Extrapolate u, v, E at the outflow boundary, giving u_{ex}^n, v_{ex}^n, E_{ex}^n.

ii) Using the values p_{ex}^{n-1}, ρ_{ex}^{n-1}, u_{ex}^{n-1}, c_{ex}^{n-1} from the previous time step, compute the new value for the pressure from the discretized form of equation (4.9):

$$p_{ex}^n = \frac{p_{ex}^{n-1} + \alpha \cdot \Delta t \cdot \rho_{ex}^{n-1} \cdot c_{ex}^{n-1} (u_{ex}^n - u_{ex}^{n-1})}{1 + \alpha \cdot \Delta t} \tag{4.10}$$

iii) Use the energy equation to compute ρ_{ex}^n:

$$\rho_{ex}^n = \frac{p_{ex}^n}{(\gamma - 1)\left(E_{ex}^n - \frac{(u_{ex}^n)^2 + (v_{ex}^n)^2}{2} \right)} \tag{4.11}$$

iv) Compute the outflow fluxes using the values ρ_{ex}^n, u_{ex}^n, v_{ex}^n, p_{ex}^n in equation (2.22).

The use of a nonreflecting boundary procedure of this kind results in a decrease of the number of time iterations required to reach a steady state.

4.1.3 Supersonic inflow boundary

At a supersonic inflow, all parameters are specified through the use of the stagnation pressure p_0, stagnation speed of sound c_0, flow direction θ_{in}, and inflow Mach number M_{in}. The inflow pressure is given by:

$$p_{in} = \frac{p_0}{\left(1 + \frac{\gamma - 1}{2} M_{in}^2\right)^{\frac{\gamma}{\gamma - 1}}} \tag{4.12}$$

whereas the density is:

$$\rho_{in} = \frac{\rho_0}{\left(1 + \frac{\gamma - 1}{2} M_{in}^2\right)^{\frac{1}{\gamma - 1}}} = \frac{\gamma \frac{p_0}{c_0^2}}{\left(1 + \frac{\gamma - 1}{2} M_{in}^2\right)^{\frac{1}{\gamma - 1}}} \tag{4.13}$$

The velocity magnitude can be expressed as:

$$V_{in} = M_{in} c_{in} = M_{in} \sqrt{\gamma \frac{p_{in}}{\rho_{in}}} \tag{4.14}$$

which gives for the x- and y-components:

$$u_{in} = \cos\theta_{in} \cdot M_{in} \sqrt{\gamma \frac{p_{in}}{\rho_{in}}} \quad , \qquad v_{in} = \sin\theta_{in} \cdot M_{in} \sqrt{\gamma \frac{p_{in}}{\rho_{in}}} \tag{4.15}$$

The values obtained for ρ_{in}, u_{in}, v_{in}, p_{in} are used in (2.22) to compute the inflow fluxes.

4.1.4 Supersonic outflow boundary

For this type of boundary, all flow variables ρ_{ex}, u_{ex}, v_{ex}, p_{ex} are extrapolated from within the computational domain. In the case of the Godunov and Jameson methods, supposing the last two cells have the same length $\Delta x_{Imax} = \Delta x_{Imax-1}$, the extrapolation formula to obtain $\rho_{ex} = \rho_{Imax+½}$, for example, takes the form:

$$\rho_{ex,j} = \rho_{Imax+1/2,j} = 1.5 \cdot \rho_{Imax,j} - 0.5 \cdot \rho_{Imax-1,j} \qquad (4.16)$$

and similarly for the other variables.

In MacCormack's method, taking into consideration the directions of differentiation in the two steps, outflow values for ρ_{ex} are obtained as follows:

- predictor step (backward):

$$\rho^{n}_{ex,j} = \rho^{n}_{Imax,j} \qquad (4.17\ a)$$

- corrector step (forward):

$$\rho^{\overline{n+1}}_{ex,j} = \rho^{\overline{n+1}}_{Imax+1/2,j} = 2 \cdot \rho^{\overline{n+1}}_{Imax,j} - \rho^{\overline{n+1}}_{Imax-1,j} \qquad (4.17\ b)$$

Similar extrapolation formulae are used for the other variables.

4.2 Solid wall boundaries

At a solid wall, the tangency condition $\vec{V} \cdot \vec{n} = 0$ (2.27), or the equivalent $V_n = 0$ implies that only the pressure is needed for the evaluation of the fluxes. Indeed, one has (see 2.22):

$$(\vec{Q} \cdot \vec{n}s) = \begin{bmatrix} \rho q \\ \rho q u + p\Delta y \\ \rho q v - p\Delta x \\ (\rho E + p) q \end{bmatrix} \qquad (4.18)$$

where $q = V_n \cdot \Delta s = 0$.

This implies that, at a solid boundary:

$$(\bar{Q}\cdot\bar{n}s) = \begin{bmatrix} 0 \\ p\Delta y \\ -p\Delta x \\ 0 \end{bmatrix} \tag{4.19}$$

Hence, for finite-volume methods with the state defined at the center of the cell, only the pressure is needed at a solid boundary.

4.2.1 The image cell method

For Godunov's scheme, the flow tangency condition (2.27) can be implemented in a way which is consistent with the computation of the fluxes inside the computational domain. Since a solid wall is a streamline of the flow, it can be artificially obtained by considering a mirror-image state on the other side of the wall, with the same values for the flow parameters, except for the normal velocity component which changes sign.

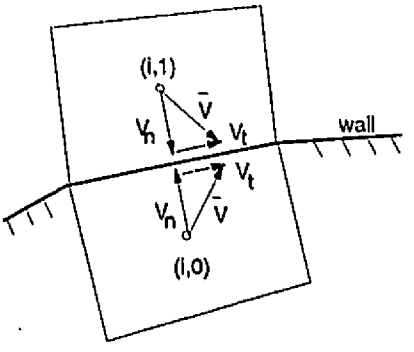

Fig. 4.1

Consider the lower boundary *(j=1)*, and cell *(i,1)* with flow parameters ρ_{i1}, $V_{n_{i1}}$, $V_{t_{i1}}$, p_{i1} inside the computational domain. To compute fluxes on the boundary *(i,½)*, an image cell is created, in a position which is symmetric to that of cell *(i,1)* relative to the boundary (see Fig. 4.1). The flow parameters in this cell, denoted by *(i,0)*, are taken to be:

$$\begin{aligned} \rho_{i,0} &= \rho_{i,1} \quad ; \qquad V_{n_{i,0}} = -V_{n_{i,1}} \\ p_{i,0} &= p_{i,1} \quad ; \qquad V_{t_{i,0}} = V_{t_{i,1}} \end{aligned} \tag{4.20}$$

The normal velocity components in the two neighboring cells being equal but of opposite sign ensure that the normal velocity at the wall is $V_{n_{i,1/2}} = 0$; thus, the wall is a streamline as it was desired.

The fluxes on the boundary are then computed using the value of the pressure $p_{i,1/2}$ calculated from the solution to the Riemann problem with initial states $f_{i,1} = [\rho_{i,1}, \rho_{i,1} V_{n_{i,1}}, \rho_{i,1} E_{i,1}]^T$ and $f_{i,0} = [\rho_{i,0}, \rho_{i,0} V_{n_{i,0}}, \rho_{i,0} E_{i,0}]^T$:

$$f_{i,1/2} = \varphi^{Rm}(0, \frac{\Delta t}{2}; f_{i,1}, f_{i,0}) \tag{4.21}$$

A completely similar approach is used at the upper wall $j=Jmax$.

4.2.2 The predictor-corrector characteristics method

In the basic paper describing his method [18], Jameson suggests either the use of the normal momentum equation or the extrapolation from the interior of the domain in order to compute the pressure at a solid wall boundary.

For nonorthogonal meshes, as those used in this study, the normal momentum equation, which requires derivatives normal to the wall, is difficult to use and can lead to errors (see again [18]). On the other hand, a simple extrapolation procedure did not allow a sufficiently accurate evaluation of the pressure at the boundary, especially when relatively coarse grids were used. Therefore, a more accurate boundary procedure based on the analysis of the characteristics of the Euler equations in a reference frame normal to the boundary has been implemented with

satisfactory results.

The eigenvalues λ and the corresponding characteristic variables w in this reference frame are (see Appendix A, eq. A.38):

$$\lambda = \begin{bmatrix} V_n \\ V_n \\ V_n + c \\ V_n - c \end{bmatrix} = \begin{bmatrix} \lambda_1 \\ \lambda_2 \\ \lambda_3 \\ \lambda_4 \end{bmatrix} \quad , \quad W = \begin{bmatrix} \rho - \frac{p}{\bar{c}^2} \\ V_t \\ V_n + \frac{p}{\bar{\rho}\,\bar{c}} \\ -V_n + \frac{p}{\bar{\rho}\,\bar{c}} \end{bmatrix} = \begin{bmatrix} w_1 \\ w_2 \\ w_3 \\ w_4 \end{bmatrix} \tag{4.22}$$

where bar quantities are linearized state quantities, taken as those at the previous step.

Since at a solid wall V_n must vanish, λ_4 should be a negative value, which corresponds to a wave propagating from the boundary inside the computational domain. This means one is allowed to impose one boundary condition, corresponding to w_4, while the information pertaining to the other three characteristic variables must come from the interior. Let subscript "*pr*" denote predicted values for the flow variables, which are obtained by extrapolation from the interior of the domain; the predicted value for the normal velocity V_n at the wall will not be in general equal to zero. Then the following relations can be written:

- for w_1:

$$\rho_{pr} - \frac{p_{pr}}{\bar{c}^2} = \rho - \frac{p}{\bar{c}^2} \tag{4.23 a}$$

- for w_2:

$$V_{t_{pr}} = V_t \tag{4.23 b}$$

- for w_3:

$$V_{n_{pr}} + \frac{p_{pr}}{\bar{\rho}\bar{c}} = V_n + \frac{p}{\bar{\rho}\bar{c}} \tag{4.23 c}$$

- for w_4, the boundary condition:

$$V_n = 0 \tag{4.23 d}$$

These equations result in the following values for the boundary parameters:

$$\begin{aligned} V_n &= 0 \quad , \qquad \rho = \rho_{pr} + V_{n_{pr}} \frac{\bar{\rho}}{\bar{c}} \\ V_t &= V_{t_{pr}} \, , \qquad p = p_{pr} + V_{n_{pr}} \bar{\rho}\bar{c} \end{aligned} \tag{4.24}$$

and the only flow variable needed to be computed from (4.24) is the pressure.

The resulting boundary procedure can be summarized as follows:

i) Compute the predicted values for the pressure p_{pr} and the normal velocity $V_{n_{pr}}$ using an extrapolation from inside the domain.

ii) Correct the value of the pressure according to (4.24), which ensures that $V_n=0$.

iii) Use the value obtained for the pressure, p, to compute the boundary fluxes in equation (4.19).

Chapter 5

NEWLY DEVELOPED METHODS

This chapter describes the basic ideas which have led to improvements of the methods described in Chapter 3, as well as their numerical implementation. For the first method presented, the starting point was Jameson's Runge-Kutta time-integration scheme. A two-stage method which updates separately the flux and the cell-node variables was developed by Mateescu and Lauzon [27]; this method takes into account the physically permissible directions of perturbation propagation and was shown to provide a better accuracy of the solution. However, it is rather difficult to implement for multi-dimensional flows. Therefore, an easier way to take account of the physics of the problem has been looked for ([26]), resulting in the α-method to be described.

The second method that has been developed uses the concept of linear hybrid methods, introduced by Harten and Zwas [12], [14]. In their work, the first-order method used for hybridization is a general, strongly diffusive, finite-difference scheme, which does not take into consideration the permissible directions of signal propagation. Using a more physical method, such as that developed by Godunov, is succeptible to give better results, especially for very complicated flow patterns.

5.1 The biased flux method (α-method)

5.1.1 Theoretical considerations

In Jameson's method, fluxes at an interface are computed using an average of the values corresponding to the two neighboring cells (see equations 3.50 and 3.63). This represents of course an approximation which would only be exact if the flow variables varied linearly, a case which is not likely to occur in real flows.

Furthermore, for the computation of the flux vector, relation (3.50) uses on an equal basis the information from the two cells. However, in supersonic flows, no information comes from downwind, while in subsonic flows the information should come from both downwind and upwind, but on an unequal basis. Many flux-splitting schemes which take into consideration these effects are already in use. The flux-splitting is however expensive in terms of computer time.

The present method suggests a different way to compute the fluxes, which can easily be implemented in an existing computer code based on Jameson's method, improving the performance. It is based on a more realistic approach to the physics of the flow.

Consider a subsonic quasi one-dimensional flow in a nozzle. The flow is supposed to come from an infinite tank with stagnation conditions; the information specified at the exit of the duct is usually the pressure, p_{ex}. This information is "transmitted" to the whole flow in the duct, such that at the entrance of the duct the flow regime that occurs depends on p_{ex}. Therefore, when working with primitive variables, the pressure is a good choice for the information which propagates upstream (corresponding to the characteristic variable w_3 in Appendix A).

The same choice is suggested by the specific form of the flux vectors, given by equations (2.6) and (2.8). According to the flux splitting techniques, the one-dimensional flux vector can be written:

$$F = \begin{bmatrix} \rho u \\ \rho u^2 + p \\ \rho H u \end{bmatrix} = u \begin{bmatrix} \rho \\ \rho u \\ \rho H \end{bmatrix} + \begin{bmatrix} 0 \\ p \\ 0 \end{bmatrix} = F^u + F^p \tag{5.1}$$

The first component, F^u, corresponds to a convection with the velocity u of the respective scalar quantities. The second term, F^p, represents the contribution of the pressure to the flux, which can be considered separately.

The aspects discussed above are taken into consideration by replacing equation (3.63), in the case of a two-dimensional flow, by:

$$F_{i+1/2,j} = \begin{bmatrix} \rho_{i+1/2,j} u_{i+1/2,j} \\ \rho_{i+1/2,j} u^2_{i+1/2,j} + p_{i+1/2,j} \\ \rho_{i+1/2,j} u_{i+1/2,j} v_{i+1/2,j} \\ \rho_{i+1/2,j} u_{i+1/2,j} H_{i+1/2,j} \end{bmatrix} = \mathcal{F}(\rho_{i+1/2,j}, u_{i+1/2,j}, v_{i+1/2,j}, p_{i+1/2,j}) \tag{5.2}$$

where the flow variables at the cell interface are computed from a weighted average:

$$\begin{aligned} \rho_{i+1/2,j} &= \alpha^{\rho}_{x_i} \cdot \rho_{ij} + (1 - \alpha^{\rho}_{x_i}) \cdot \rho_{i+1,j} \quad , \quad u_{i+1/2,j} = \alpha^{u}_{x_i} \cdot u_{ij} + (1 - \alpha^{u}_{x_i}) \cdot u_{i+1,j} \\ v_{i+1/2,j} &= \alpha^{v}_{x_i} \cdot v_{ij} + (1 - \alpha^{v}_{x_i}) \cdot v_{i+1,j} \quad , \quad p_{i+1/2,j} = \alpha^{p}_{x_i} \cdot p_{ij} + (1 - \alpha^{p}_{x_i}) \cdot p_{i+1,j} \end{aligned} \tag{5.3}$$

The superscript notation implies that the weights α can be chosen differently for different flow variables, while the subscript indicates that a different value can be used for the x- and y-direction fluxes. Further, the values of the weights depend mainly on the local character of the flow in the cell situated upstream (cell (i,j) in eq. 5.3). In particular, for subsonic flows, the weight for the pressure α^p is chosen to be

smaller than 0.5, while for the other flow variables α^u, α^v, α^ρ are greater than 0.5. In subsonic flows, this simulates an upwind propagation of the outflow pressure signal, while all other information propagates downwind. The optimal values for the weights have been determined by numerical experiments, as will be discussed further.

5.1.2 Quasi one-dimensional flow

In this case, the flux vector is computed with the one-dimensional correspondent of formula (5.2):

$$F_{i+\frac{1}{2}} = \mathcal{F}(\rho_{i+\frac{1}{2}}, u_{i+\frac{1}{2}}, p_{i+\frac{1}{2}}) \tag{5.4}$$

where the flow variables are obtained by interpolations of the form:

$$\rho_{i+\frac{1}{2}} = \alpha_i^\rho \cdot \rho_{i+1} + (1-\alpha_i^\rho)\cdot \rho_{i} \tag{5.5}$$

and similarly for the other variables. The weights are chosen as:

$$\begin{aligned} &\alpha_i^\rho = \alpha_i^u = \alpha_i^p = \alpha_1 > 0.5 \ , \quad \text{for } u_i > c_i \ \text{ (supersonic flow)} \\ &\alpha_i^\rho = \alpha_i^u = \alpha_2 > 0.5 \ ; \ \alpha_i^p = \alpha_3 < 0.5 \ , \quad \text{for } u_i < c_i \ \text{ (subsonic flow)} \end{aligned} \tag{5.6}$$

In locally supersonic flows, numerical experiments indicate that an optimal value for the coefficient α_1 exists, lying between 0.75 and 0.8, depending on the flow. A value of 1 would correspond to a first-order upwind scheme, with a resulting first-order accuracy. Results of several tests with various values for α_1 can be summarized as follows:

i) For values of α_1 between 0.5 and the optimal value, the iterations converge in less time steps, as the value of α_1 increases, with practically the same accuracy.

ii) After the optimal value, a further increase in the value of α_1 brings about a loss in the accuracy of the computed results, as compared to the analytical isentropic flow solution.

These effects can be followed in Table 5.1, for the case of a supersonic flow in a quasi one-dimensional duct of area $A(x) = 0.2 + 0.1x$, $x \in [0,1]$ and entrance Mach number $M_{in}=1.4$, discretized in 60 cells. The initial distribution of flow variables has been chosen to be the same over the whole length of the duct, equal to that in the entrance section; the RMS error in the Mach number distribution is calculated using the exact analytic solution. As suggested by these results, the value $\alpha_1=0.775$ has been used in all quasi one-dimensional locally supersonic flows reported subsequently in this study, unless otherwise specified.

Table 5.1

α_1	0.6	0.7	0.775	0.8	0.9	0.5 (Jameson)
Number of time steps*	112	107	99	99	96	127
RMS error in Mach no.	$1.12 \cdot 10^{-4}$	$1.13 \cdot 10^{-4}$	$1.13 \cdot 10^{-4}$	$1.13 \cdot 10^{-4}$	$1.20 \cdot 10^{-4}$	$1.12 \cdot 10^{-4}$

* for convergence to 10^{-4} in all three equations.

For a locally subsonic flow, the appropriate values for α_2, α_3 have also been determined by numerical experiment. While the optimal choice is dependent of the flow, it has been found through a large number of tests that the best range lies between $0.23 \div 0.3$ for α_3 and $0.7 \div 0.775$ for α_2. The great majority of the computations failed to converge if α_2 were increased more than 0.78, or if α_3 were

decreased more than 0.2. However, the optimal values were always very close to these limits. A good choice, which worked for all the flows treated in this work, was:

$$\alpha_2=0.75 \; ; \; \alpha_3=0.25$$

Examples of the variation of the accuracy and required number of iterations for the case of a steady subsonic flow in a duct of area $A(x) = 0.3 - 0.1x$, $x \in [0,1]$, and exit pressure $p_{ex}=0.658p_0$ are given in Table 5.2. Again, the RMS error is calculated using the exact analytic solution.

Table 5.2

Flux averaging method	$\alpha_2=0.6$ $\alpha_3=0.3$ No dissipation	$\alpha_2=0.75$ $\alpha_3=0.25$ No dissipation	Jameson No dissipation	Jameson With dissipation
Number of time steps *	327	303	Did not converge	323
RMS error in Mach number	$6.95 \cdot 10^{-4}$	$5.04 \cdot 10^{-4}$	–	$7.24 \cdot 10^{-4}$

* for convergence to 10^{-4} in all three equations.

A very important advantage of this method can be seen from Table 5.2: convergence is obtained without the use of the artificial dissipation, if the flow field does not contain shocks. This leads to a greater computational efficiency, since the dissipation terms are about as expensive to compute as the flux terms; as will be shown, it also improves the accuracy of the results.

A typical convergence history for this method, displaying the evolution of the RMS variation in density between two successive time steps, is shown in Fig. 5.1.

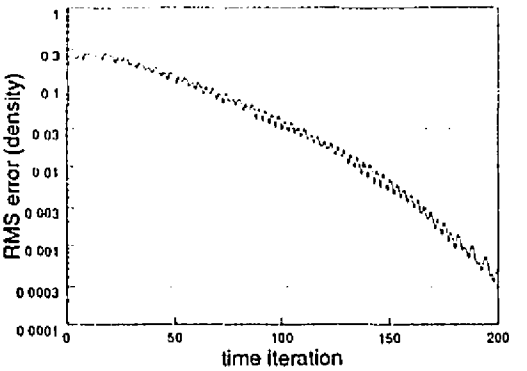

Fig. 5.1 - Convergence history for subsonic quasi one-dimensional duct flow, α-method.

5.1.3 Two-dimensional flow

In this case, the x- and y-direction fluxes are computed from:

$$\begin{aligned} F_{i+\frac{1}{2}j} &= \mathcal{F}\left(\rho_{i+\frac{1}{2}j}, u_{i+\frac{1}{2}j}, v_{i+\frac{1}{2}j}, p_{i+\frac{1}{2}j}\right) \\ F_{ij+\frac{1}{2}} &= \mathcal{F}\left(\rho_{ij+\frac{1}{2}}, u_{ij+\frac{1}{2}}, v_{ij+\frac{1}{2}}, p_{ij+\frac{1}{2}}\right) \end{aligned} \tag{5.7}$$

The interpolation formulae take the form:

$$\begin{aligned} \rho_{i+\frac{1}{2}j} &= \alpha^{\rho}_{x_i} \cdot \rho_{ij} + \left(1-\alpha^{\rho}_{x_i}\right) \cdot \rho_{i+1j} \\ \rho_{ij+\frac{1}{2}} &= \alpha^{\rho}_{y_i} \cdot \rho_{ij} + \left(1-\alpha^{\rho}_{y_i}\right) \cdot \rho_{ij+1} \end{aligned} \tag{5.8}$$

and similarly for the other variables.

The weights are chosen according to the local character of the flow:

$$\begin{aligned}
\alpha^{p}_{x_i} = \alpha^{u}_{x_i} = \alpha^{v}_{x_i} \quad \alpha^{p}_{x_i} = \alpha_1 > 0.5 \ , \quad & \text{for } u_{ij} > c_{ij} \\
\alpha^{p}_{x_i} = \alpha^{u}_{x_i} = \alpha^{v}_{x_i} = \alpha_2 > 0.5 \ , \ \alpha^{p}_{x_i} = \alpha_3 < 0.5 \ , \quad & \text{for } u_{ij} < c_{ij} \\
\alpha^{p}_{y_i} = \alpha^{u}_{y_i} = \alpha^{v}_{y_i} = \alpha^{p}_{y_i} = \alpha_1 > 0.5 \ , \quad & \text{for } v_{ij} > c_{ij} \\
\alpha^{p}_{y_i} = \alpha^{u}_{y_i} = \alpha^{v}_{y_i} = \alpha^{p}_{y_i} = 0.5 \ , \quad & \text{for } v_{ij} < c_{ij}
\end{aligned} \tag{5.9}$$

In the above relations the direction of the flow has been assimilated to the x-axis, since in aerodynamic flows the velocities along the y-axis are relatively small. Hence, the entire upwinding effect has been related to u. A supersonic flow along the y-axis is not likely to occur, hence on this axis the centered differences are generally used.

5.2 The hybrid method MacCormack-Godunov

The hybrid method is built according to the principles set out in [12], [14]. Consider a r-th order accurate scheme, $r \geq 2$, for the solution of a nonlinear system of conservation laws:

$$\frac{\partial f}{\partial t} + \frac{\partial F}{\partial x} = 0 \tag{5.10}$$

In conservation form, the scheme can be expressed in the form of an operator, L_r, acting on f_i, as (see also eq. 2.17):

$$(L_r f)_i = f_i^{n+1} = f_i^n - \sigma (F^{r,n}_{i+1/2} - F^{r,n}_{i-1/2}) \tag{5.11}$$

Here, σ stands for $\frac{\Delta t}{\Delta x}$, and $F^{r,n}$ is the numerical flux computed with the r-th order scheme at time step n.

Similarly, a first-order accurate sheme is defined by the operator:

$$(L_1 f)_i = f_i^{n+1} = f_i^n - \sigma(F_{i+1/2}^{1,n} - F_{i-1/2}^{1,n}) \tag{5.12}$$

A first-order monotone scheme will ensure a nonoscillatory behavior near discontinuities.

A hybrid scheme is defined in the same conservation form as:

$$(Lf)_i = f_i^{n+1} = f_i^n - \sigma(F_{i+1/2}^{n} - F_{i-1/2}^{n}) \tag{5.13}$$

where the numerical flux is computed as a blending of the first- and r-th order accurate fluxes:

$$F_{i+1/2}^n = \theta_{i+1/2}^n F_{i+1/2}^{1,n} + (1 - \theta_{i+1/2}^n) F_{i+1/2}^{r,n} \tag{5.14}$$

The parameter θ is a scalar quantity (a switch) which satisfies $0 \le \theta_{i+1/2}^n \le 1$, and it is constructed such that at discontinuities $\theta \approx 1$; therefore, close to discontinuities, the hybrid scheme (5.13) behaves basically as the nonoscillatory first-order scheme (5.12). In the smooth regions of the flow, $\theta \approx 0((\Delta x)^{r-1})$, such that r-th order accuracy is obtained via the (L_r) operator in such regions.

5.2.1 One-dimensional flow

The first step is to write MacCormack's method in conservation form as:

$$(L_{MC} f)_i = f_i^{n+1} = f_i^n - \sigma(F_{i+1/2}^{MC,n} - F_{i-1/2}^{MC,n}) \tag{5.15}$$

where (see also eq. 3.37):

$$F_{i+\frac{1}{2}}^{MC,n} = \frac{F_i^n + F_{i+1}^{n+1}}{2}, \quad F_{i+\frac{1}{2}}^{MC,n} = \frac{F_{i+1}^n + F_i^{n+1}}{2} \tag{5.16}$$

The hybrid method can be therefore expressed as:

$$(Lf)_i = f_i^{n+1} = f_i^n - \sigma(F_{i+\frac{1}{2}}^n - F_{i-\frac{1}{2}}^n) \tag{5.17}$$

where:

$$F_{i\pm\frac{1}{2}}^n = \theta_{i\pm\frac{1}{2}}^n F_{i\pm\frac{1}{2}}^{G,n} + (1-\theta_{i\pm\frac{1}{2}}^n) F_{i\pm\frac{1}{2}}^{MC,n} \tag{5.18}$$

In (5.18), $F^{G,n}$ denotes the flux computed by Godunov's method, given by (3.25).

The switch θ must detect the discontinuities. Since the density is the only primitive flow variable which is discontinuous both at shocks and at contact discontinuities, it can be used to construct an appropriate expression for θ. In the present study two forms have been used for this switch. The first one is:

$$\theta_{i+\frac{1}{2}} = \chi \left(\frac{|\rho_{i+1} - \rho_i|}{\max_i |\rho_{i+1} - \rho_i|} \right)^m \tag{5.19}$$

(see also [14]). Here χ is a positive constant (taken as 1 in the actual computations) and m is an exponent which must satisfy $m \geq 1$ because θ is supposed to be of order $0(\Delta x)$ in the smooth regions of the flow.

The second form used for θ is suggested in [12]:

$$\theta_{i+\frac{1}{2}} = \max(\bar{\theta}_i, \bar{\theta}_{i+1}) \tag{5.20}$$

with the quantity $\bar{\theta}_i$ defined from:

$$\bar{\theta}_i = \begin{cases} \left| \dfrac{|\Delta_{i+\frac{1}{2}}\rho| - |\Delta_{i-\frac{1}{2}}\rho|}{|\Delta_{i+\frac{1}{2}}\rho| + |\Delta_{i-\frac{1}{2}}\rho|} \right|^m, & \text{for } |\Delta_{i+\frac{1}{2}}\rho| + |\Delta_{i-\frac{1}{2}}\rho| > \epsilon_\rho \\ 0, & \text{for } |\Delta_{i+\frac{1}{2}}\rho| + |\Delta_{i-\frac{1}{2}}\rho| < \epsilon_\rho \end{cases} \tag{5.21}$$

In (5.21), ϵ_ρ is a suitably chosen measure of insignificant variation in ρ, m satisfies $m \geq 1$, such that the solution behaves like the second-order scheme in smooth regions (m=4 has been taken in actual computations), and $\Delta_{i+\frac{1}{2}}\rho = \rho_{i+1} - \rho_i$.

The switch defined by (5.20), (5.21) is a very sensible way to detect discontinuities. It is more expensive computationally than the form (5.19), but offers the advantage that when its value becomes θ=0, the first order fluxes need not be computed. For most flows, the results obtained with the two forms are identical. The form that has been used will be indicated for each numerical example.

For stability, the hybrid scheme must satisfy the most restrictive of the stability conditions of the constitutive schemes. Since both MacCormack's and Godunov's schemes have the *CFL* number at the stability bound equal to 1, this results in:

$$CFL \leq 1 \tag{5.22}$$

as the stability condition for the present hybrid method.

5.2.2 Two-dimensional flow

For a two-dimensional flow, a switch must be used for each direction. For example, for the side $(i+\frac{1}{2},j)$, the flux becomes (see eq. 2.21):

$$(\bar{Q}\cdot\vec{n}s)_{i+\frac{1}{2},j} = \{[\theta^x F^{G_+}(1-\theta^x)F^{MC}](\Delta y)\}_{i+\frac{1}{2},j} - \\ -\{[\theta^x G^{G_+}(1-\theta^x)G^{MC}](\Delta x)\}_{i+\frac{1}{2},j} \tag{5.23}$$

while for the side $(i,j+\frac{1}{2})$, the flux is:

$$(\bar{Q}\cdot\vec{n}s)_{i,j+\frac{1}{2}} = \{[\theta^y F^{G_+}(1-\theta^y)F^{MC}](\Delta y)\}_{i,j+\frac{1}{2}} - \\ -\{[\theta^y G^{G_+}(1-\theta^y)G^{MC}](\Delta x)\}_{i,j+\frac{1}{2}} \tag{5.24}$$

The two switches θ^x and θ^y take into consideration the variation of the flow parameters on the respective axes. For example, using the form defined by (5.19), they are given by:

$$\theta^x_{i+\frac{1}{2},j} = \chi\left(\frac{|\rho_{i+1,j}-\rho_{i,j}|}{\max\limits_i |\rho_{i+1,j}-\rho_{i,j}|}\right)^m \tag{5.25}$$

for the x-variation of the flow parameters, and:

$$\theta^y_{i,j+\frac{1}{2}} = \chi\left(\frac{|\rho_{i,j+1}-\rho_{i,j}|}{\max\limits_j |\rho_{i,j+1}-\rho_{i,j}|}\right)^m \tag{5.26}$$

for the y-axis variation. Similarly, the second form for θ becomes for the x-axis:

$$\theta^x_{i+\frac{1}{2},j} = \max(\bar{\theta}^x_{i,j}, \bar{\theta}^x_{i+1,j}) \tag{5.27}$$

where the quantity $\bar{\theta}^x_{i,j}$ is defined as:

$$\bar{\theta}^{x}_{i,j} = \begin{cases} \left| \dfrac{|\Delta_{i+1/2,j}\rho| - |\Delta_{i-1/2,j}\rho|}{|\Delta_{i+1/2,j}\rho| + |\Delta_{i-1/2,j}\rho|} \right|^{m}, & \text{for } |\Delta_{i+1/2,j}\rho| + |\Delta_{i-1/2,j}\rho| > \epsilon_{\rho} \\ 0, & \text{for } |\Delta_{i+1/2,j}\rho| + |\Delta_{i-1/2,j}\rho| < \epsilon_{\rho} \end{cases} \tag{5.28}$$

Hence, for a two-dimensional flow, the fluxes are computed separately for each cell interface by the two methods (F^G, G^G with Godunov's method, respectively F^{MC}, G^{MC} with MacCormack's method). The switches are then computed for each interface using the values of ρ at the previous time step in (5.26); the resulting hybrid fluxes are then given by (5.23) and (5.24), and the state vector can be updated for the next time step.

The stability condition for the hybrid scheme can be evaluated using the same equation (3.44) given for MacCormack's method.

Chapter 6

NUMERICAL RESULTS

The time integration methods presented in Chapter 5 are validated through a series of test cases for internal quasi one-dimensional and two-dimensional flows, as well as an external two-dimensional flow about a symmetrical aerofoil. The results are compared with those obtained by the well-established methods in Chapter 3.

6.1 Quasi one-dimensional test cases

Test case 1. The first test has been performed for a subsonic isentropic flow, with an entrance Mach number M_{in}=0.6, in a channel with a circular arc bump on the lower wall. The channel length is L=3c, where c is the length of the bump, this one being situated between x/c=*1* and x/c=*2*. The height of the channel is c and that of the bump is h=*0.1*c.

A solution obtained by Jameson's method is displayed in Fig. 6.1; it required that the coefficients of the adaptive dissipation be set to $k^{(2)}$=*1* and $k^{(4)}$=*1/64*. Although the adaptive dissipation is relatively large, some oscillations in the numerical solution still appear near the trailing edge of the bump. Another solution, with $k^{(2)}$=*1/4* and $k^{(4)}$=*1/256*, is presented in Fig. 6.2. As can be expected, the maximum Mach number on the bump is closer to the real value, but the smaller amount of dissipation allowed odd/even point decoupling. As well as the first solution, it is still unacceptable from the point of view of the accuracy.

Results obtained by the α-method developed in Chapter 5 are displayed in Fig. 6.3. The coefficients used for the weighted average were set to $\alpha_2=0.75$, $\alpha_3=0.25$. The treatment of the boundary conditions and the Courant number were the same as in the first two cases. Dissipation terms were not needed to obtain this solution. The improvement over the precedent solutions is remarkable; the Mach number distribution on the bump is correct and the solution is almost free from oscillations. Due to the drop of dissipation terms, a greater computational efficiency is obtained (see Table 6.1). For comparison, Fig. 6.4 shows results obtained with Jameson's method after the same number of time steps, if dissipation terms are neglected (the solution fails to converge in this case).

Table 6.1

	Jameson's method, with dissipation terms, $k^{(2)}=1$	α-method, without dissipation terms
Time per iteration	100%	76.3%
Number of iterations until convergence to 10^{-4}	512	521
RMS error in Mach no. (w.r.t. the exact solution) after 500 time steps	0.009423	0.002621

Figure 6.5 shows the results obtained by MacCormack's method. As can be seen, the solution exhibits a much less pronounced oscillatory character than that obtained with Jameson's method; only very slight oscillations exist near the trailing edge. The hybrid method (Fig. 6.6) eliminates these oscillations; the behavior of the solution becomes monotonic. The switch θ has been used in the form given by (5.21). However, for this flow, the cost of the hybridization is probably not justified (Table 6.2).

Table 6.2

	α-method	MacCormack	Hybrid method
Relative computer time to convergence	100%	102.3%	121.5%
RMS error in Mach no. (w.r.t. the exact solution)	0.002621	0.008551	0.004498

Test case 2. The second test, used to verify the shock capturing properties of the methods, was the flow suggested in [36]; a flow with a stationary shock in a duct of variable cross-section $S(x) = 1.398 + 0.347\tanh(0.8x - 4)$, where $x \in [0, 10]$. The inflow conditions are supersonic, with $\rho_{in} = 0.502$, $u_{in} = 1.299$, $p_{in} = 0.3809$ and $M_{in}=1.26$ at $x=0$; at the outflow $x=10$, the pressure is specified, $p_{ex} = 0.7475$. Under these flow conditions, a shock appears in the duct at $x_s=4.8198$. The initial conditions for the numerical computation have been chosen, in this case, identical to the exact solution; due to numerical errors, the converged solution will be different. As in [36], the figures show the variation of the density with the axial position.

Fig. 6.7 represents the results obtained by MacCormack's method, with artificial viscosity terms included; the constant in the artificial viscosity term (eqs. 3.45 and 3.46) has been set to $C=0.5$. The numerically induced oscillations near the shock can be clearly seen. The number of time steps required for convergence to the accuracy 10^{-4} in all equations, with a Courant number of 0.9, was 1093.

The hybrid method developed in Chapter 5 (using the switch defined in 5.21) brings a sensible improvement in the results (Fig. 6.8). The shock is much better

solved for, and for the same precision, the number of time steps required was only 573 (see also Table 6.3). This is largely due to the dissipation contained implicitly in the fluxes computed by Godunov's method, and to the correct account for the physics of the problem.

The solution obtained by Jameson's method is shown in Fig. 6.9; the constants for the adaptive dissipation were taken to be $k^{(2)}=1.0$, $k^{(4)}=0.0156$; the oscillations, this time stronger behind the shock, are associated with a certain odd/even points decoupling before the shock. An increase of the amount of dissipation ($k^{(2)}=2.5$, $k^{(4)}=0.039$) eliminates the oscillations, but the shock is not well situated in the duct (Fig. 6.10).

The α-method offers a better solution for the shock position, with less oscillations (Fig. 6.11). A certain amount of dissipation has been added ($k^{(2)}=0.25$, $k^{(4)}=1/256$).

Table 6.3 compares the performance of the methods for this particular flow.

Table 6.3

	MacCormack	Hybrid	Jameson	α-method
Iterations to convergence*	1093	573	375	423
Relative computer cost	141.8%	100%	171.3%	193.22%
RMS error in density (w.r.t. the exact solution)	0.076	0.0241	0.0943	0.0512

* for convergence to 10^{-4} in all three equations.

Test case 3. The last one-dimensional flow used for testing was the shock-tube flow suggested by Sod [37]. The flowfield contains the two kinds of possible discontinuities: a shock and a contact discontinuity, and also a rarefaction region. Results on this case have been reported by many authors (for example, [39]). At $t=0$, a diaphragm situated at $x=0.5$ separates the two regions with $\rho_l=1.0$, $u_l=0.0$, $p_l=1.0$, respectively $\rho_r=0.125$, $u_r=0.0$, $p_r=0.1$. A discretization of the shock tube $0 \le x \le 1$ in 100 points is considered, and the results are printed when the shock wave reaches $x=0.75$, corresponding to the non-dimensional time $t=14$. The numerical procedure is exactly the same as for steady-state flows, except that the values of the boundary variables are held constant at the ends of the duct (equal to the left- and right-state values respectively) and instead of testing for convergence, the position of the shock is tracked, in order to stop the calculations when it reaches $x=0.75$. The following figures show the density distribution, since it is discontinuous both at the contact discontinuity and at the shock. MacCormack's and Jameson's methods produced an oscillatory distribution, with overshoots near the discontinuities, as can be seen in Fig. 6.12 and 6.13.

Godunov's method offers a much better result for this flow, because of its nonoscillatory character, as seen in Fig. 6.14. The contact discontinuity is however smeared over a large number of points, which was to be expected, since it is smeared at the rate $n^{1/2}$ (see [12]) for this first-order method, n being the number of time steps ($n=45$). Also the head region of the rarefaction is less accurately computed (the corner is rounded).

Because a second-order method smears the contact discontinuity at the rate $n^{1/3}$ (see again [12]), the hybrid method offers the best results in this case (Fig. 6.15). The switch was computed using (5.19).

The α-method, as well as MacCormack's and Jameson's method, had to be started with a very small value for the Courant number (0.2 in the case of MacCormack's method, 0.6 for Jameson's and α-method); this is due to the strong nonlinearities which appear in the diaphragm region, until the waves separate. After several time steps, the Courant number has been set to a convenient larger value. Godunov's method allowed a Courant number of 0.9 since the beginning, while for the hybrid method a value of 0.6 could be used. The results obtained with the α-method, using dissipation terms, are shown in Fig. 6.16.

6.2 Two-dimensional test cases

Test case 4. The subsonic flow in a circular arc bump channel, with an entrance Mach number M_{in}=0.5. The geometry is the same as for the test case 1; the grid used was uniform in the x-direction, while y-spacing varied with x, although it was kept constant for each x (see Fig. 6.17). Results for this flow have also been reported in [8] and [30].

Fig. 6.18 shows the distribution of the Mach number over the bottom and the top walls (first row of cells near the walls) obtained with Godunov's method; the grid size is 99×33. As can be seen, there is a great lack of symmetry in the results. As pointed out in [8], this is largely due to the lower accuracy of the numerical boundary conditions at the wall (in the region of the bump), as well as to the first-order accuracy of the method.

The second order methods of Jameson and MacCormack give almost identical results; a solution is shown in Fig. 6.19. It is closer to symmetry, but oscillations appear near the trailing and leading edges of the bump. The solution has been obtained on a relatively coarse grid (33x13). For MacCormack's method, the coefficient of the artificial viscosity was set to C=0.5; for Jameson's method, the

coefficients of the adaptive dissipation were $k^{(2)}=1$ and $k^{(4)}=0.0156$.

As in the one-dimensional case, the solution with the α-method could be obtained without the use of dissipation terms for the x-axis; dissipation is however computed for the y-axis, where central differences are used (see eq. 5.9). The solution, represented in Fig. 6.20, shows an improvement over the results obtained with Jameson's method - the oscillations near the leading and trailing edges have disappeared. The maximum value of the Mach number over the bump is 0.6785, which agrees better (taking into account the coarse grid) with the value of 0.68 obtained by Ni in [30] than the value 0.6735, obtained by Jameson's method. Also the value near the leading edge of the bump is better (0.381 for the α-method, 0.4317 for Jameson's method on the same grid, while the value obtained by Ni using a fine grid in this region is 0.262). The drop of the dissipation terms for the x-axis results again in an increased computer efficiency, as can be seen from Table 6.4 (results for a 33x13 grid and convergence to 10^{-4} in all four equations).

Table 6.4

	Jameson	α-method
Iterations to convergence	3127	3319
Relative time/iteration	100%	92.4%
Relative computer cost	100%	98.1%

The results obtained with the hybrid method are similar in quality to those in Fig. 6.20, but for this flow without discontinuities the use of hybridization is not justified.

A very clear picture of the performance of the methods can be built using the isoparameter diagrams. Fig. 6.21 represents the iso-Mach lines obtained with Godunov's method. The pattern is free from oscillations, but the asymmetry is clearly

visible.

Fig. 6.22 is obtained with Jameson's method. Comparing it with Fig. 6.21, one can notice the better symmetry, but also the oscillations introduced in the pattern of the lines. Finally, Fig. 6.23 represents the solution obtained by the α-method. It is clearly the best; its symmetry is remarkable, and it also lacks the oscillatory character.

Test case 5. The flow in the same channel is computed, this time with a Mach number M_{in}=0.675 at the entrance. For these flow conditions, a shock appears on the bump. A relatively precise computation with a second-order nonoscillatory method ([8]) situates the shock at 0.72%c of the bump chord-length (x/L=0.573), the maximum Mach number attained being around 1.32.

Fig. 6.24 shows a solution obtained with Godunov's method on a 99x33 grid; due to the first-order accuracy, the maximum Mach number is 1.163, the shock position being 0.65%c, not in good agreement with the more exact value in [8].

The hybrid method, using the switch (5.21), brings an improvement in the solution which can be seen in Fig. 6.25; the shock location is exact, and the maximum Mach number is 1.24. It required an average of about 25% more time per iteration than Godunov's method, which is completely justified for this flow.

The α-method (using dissipation on the x-axis), gave for this case the solution in Fig. 6.26, perfectly similar to Jameson's and MacCormack's methods. This method predicts a maximum Mach number of 1.322 before the shock, at the axial location x/L=0.570, which is in very good agreement with the previous results obtained by Eidelman, Colella and Shreeve [8].

Test case 6. The supersonic flow in a circular arc bump channel; the height of

the bump is $h=0.04$c in this case, such that the shock at the leading edge of the bump is an oblique shock, and the flow remains supersonic. The entrance Mach number is $M_{in}=1.65$. This test case very clearly shows the accuracy and the shock capturing properties of the methods.

Fig. 6.27 shows the solution for the Mach number distribution over the walls obtained with Godunov's method. The shocks are completely free from oscillations. However, the iso-Mach diagram, Fig. 6.28, clearly demonstrates the dissipative character of this first-order method: the shocks are smeared, especially the trailing edge oblique shock, which is weaker. The interactions and reflections of the different waves are almost indistinguishable.

The solution obtained using Jameson's method is shown in Fig. 6.29 and 6.30. The oscillatory behavior of the numerical solution can be clearly noticed in these figures. However, the shock structure in Fig. 6.30 is clearly superior to that in Fig 6.28, due to the second-order accuracy. The same quality of solution is obtained with both the MacCormack's and the α-method, this one having however less oscillations. It is shown in Fig. 6.31 and 6.32.

This flow, due to its more complicated shock pattern, demonstrates the advantages of using the hybrid method. The Mach number distribution over the walls, Fig. 6.33, is free from oscillations and the shocks are sharper than in the case of Godunov's method. However, the shock on the upper wall is too smeared, as can be seen from the comparison with the results in [8]; this is probably due to a too small value for ϵ_p in (5.21). The iso-Mach diagram in Fig.6.34 is better than that obtained by Godunov's method: there are no more recirculating zones before the first oblique shock as in Fig. 6.30, the lines are smooth, without oscillations, and the shock structure is clearly represented.

Table 6.5 shows the relative computational costs required by the three methods; the Courant numbers used have been 0.9 for Godunov's and hybrid methods, and 2.1 for Jameson's method. Convergence was considered to be reached when the residues in all the four equations were below 10^{-4}. The α-method was similar in terms of computer efficiency to Jameson's method for this case, since dissipation terms have been used for both directions.

Table 6.5

	Godunov	Jameson	α-method	Hybrid
Time steps to convergence	514	217	215	539
Relative time per iteration	105.3%	100%	100%	145%
Relative CPU time to convergence	249%	100%	99.1%	361%

Test case 7. To further test the accuracy of the methods, the external flow over a NACA 0012 airfoil at zero degrees incidence was also computed, for a free stream Mach number M_∞=1.2.

The first order Godunov's method produces a very smooth isobar pattern, but the fish-tail shock is almost indistinguishable (Fig. 6.35).

The hybrid method, as well as the second-order methods developed by MacCormack and Jameson and the α-method developed in Chapter 5 lead to a clear shock representation, as can be seen in Fig. 6.36, 6.37 and 6.38.

A very interesting comparison can be done using the Mach number distribution in the bottom row of cells (next to the airfoil and its symmetry axis). Godunov's method produces the result in Fig. 6.39 (the airfoil is situated between $x=1/3$ and $x=2/3$); the hybrid method (Fig. 6.40) gives an almost similar result in this respect. It can easily be noticed that the behavior of the solution is better than in the case of the second-order methods, as seen in Fig. 6.41 and Fig. 6.42, from this point of view, although the shocks are slightly sharper for the case of second-order methods. However, this can probably be further controlled by the value of the threshold ϵ_p in eq. (5.21); the value used for this case has been 0.003.

The algebraically generated grid used for these airfoil computations is partially shown in Fig. 6.43.

6.3 Figures

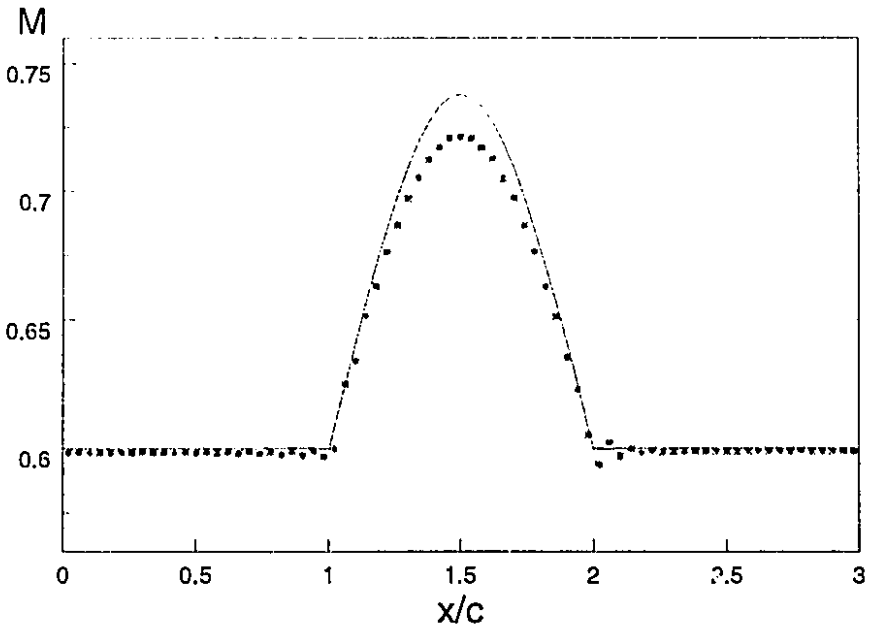

Fig. 6.1 - Subsonic quasi 1-D channel flow. Jameson's method with $k^{(2)}=1$, compared with the exact solution (solid line).

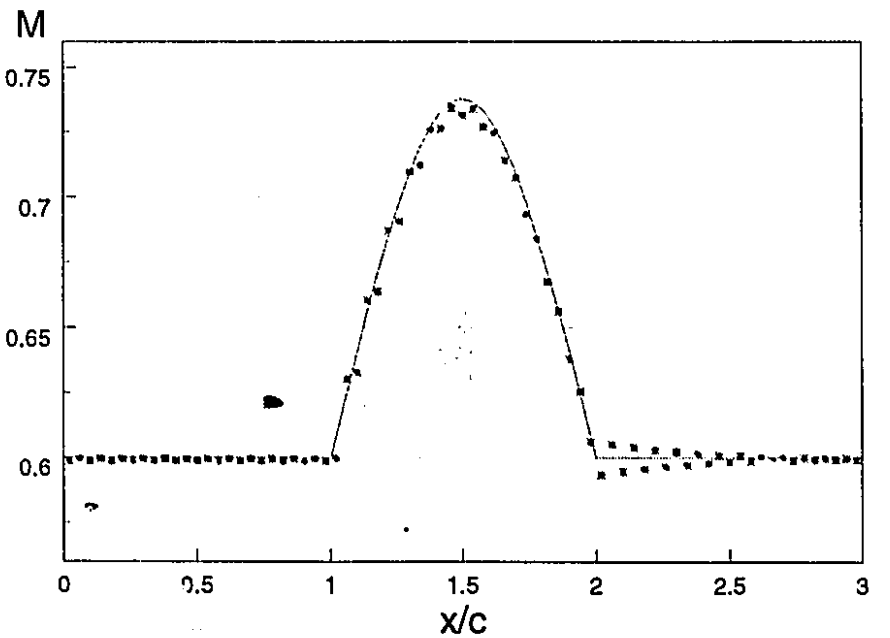

Fig. 6.2 - Subsonic quasi 1-D channel flow. Jameson's method with $k^{(2)}=0.25$, compared with the exact solution (solid line).

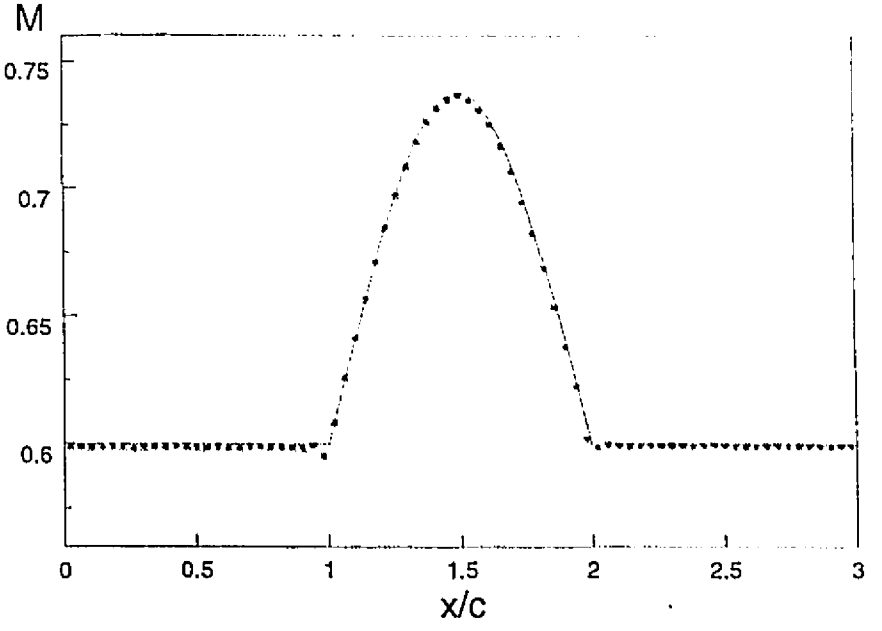

Fig. 6.3 - Subsonic quasi 1-D channel flow. The α-method, compared with the exact solution (solid line).

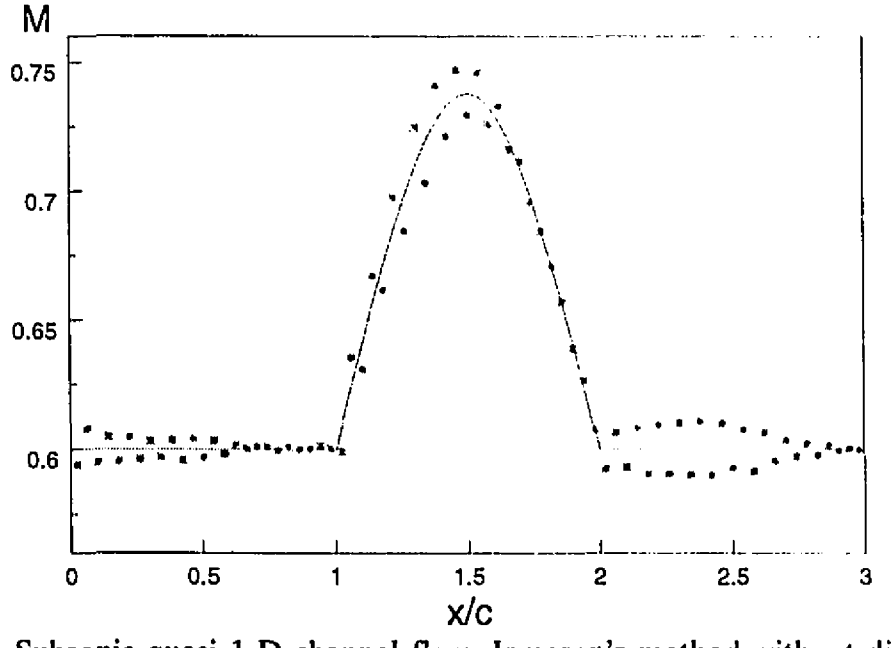

Fig. 6.4 - Subsonic quasi 1-D channel flow. Jameson's method without dissipation after 500 time steps, compared with the exact solution (solid line).

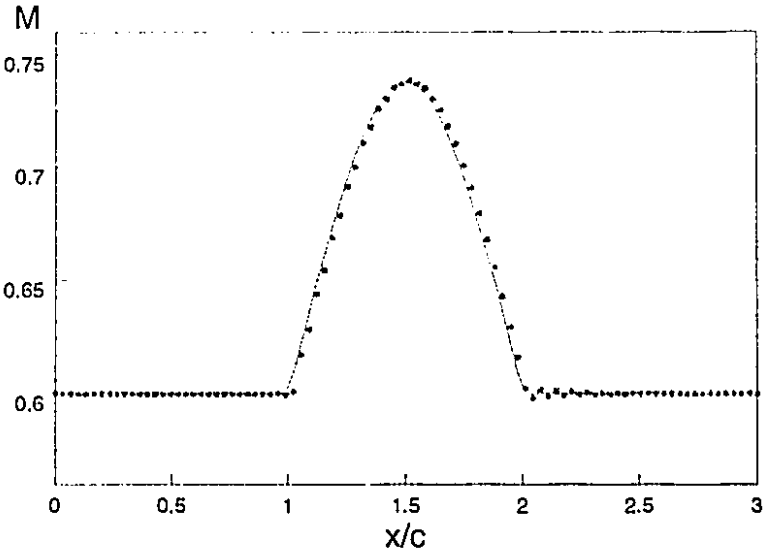

Fig. 6.5 - Subsonic quasi 1-D channel flow. MacCormack's method without artificial viscosity compared with the exact solution (solid line).

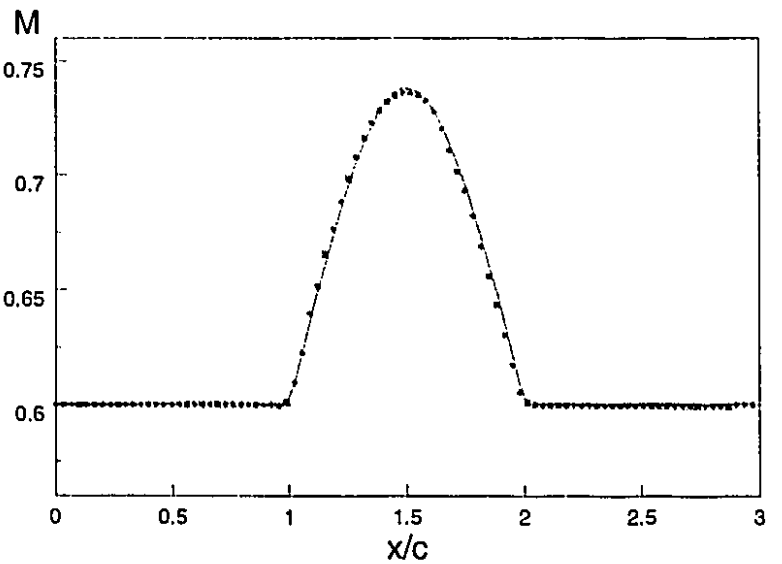

Fig. 6.6 - Subsonic quasi 1-D channel flow. Hybrid method, compared with the exact solution (solid line).

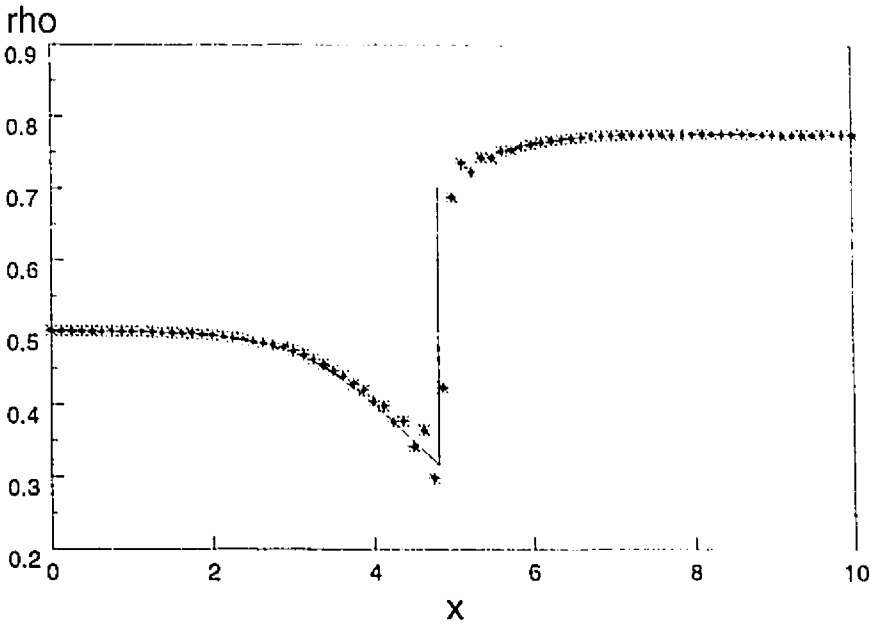

Fig. 6.7 - Duct flow with shock. MacCormack's method with artificial viscosity versus the exact solution (solid line).

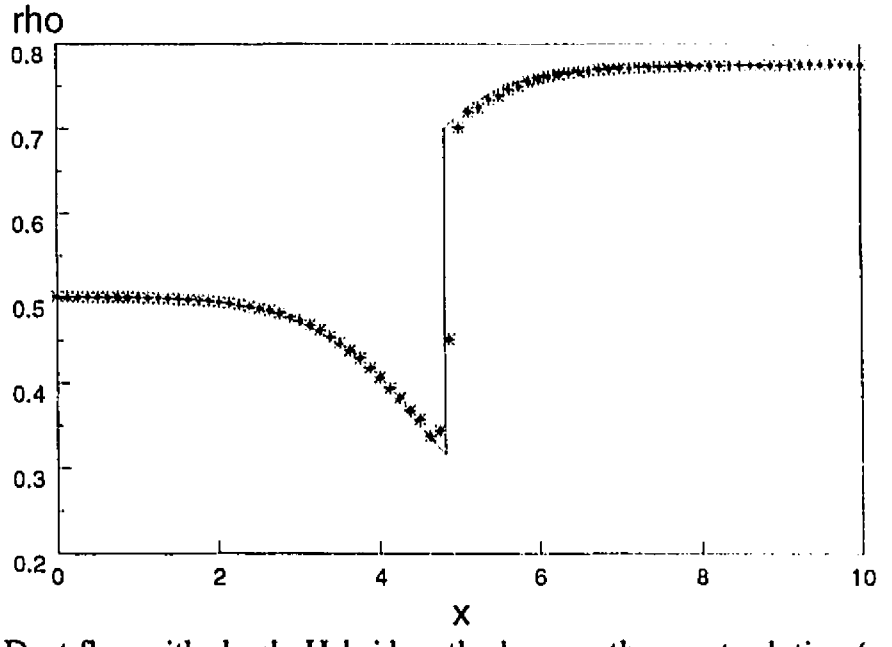

Fig. 6.8 - Duct flow with shock. Hybrid method versus the exact solution (solid line).

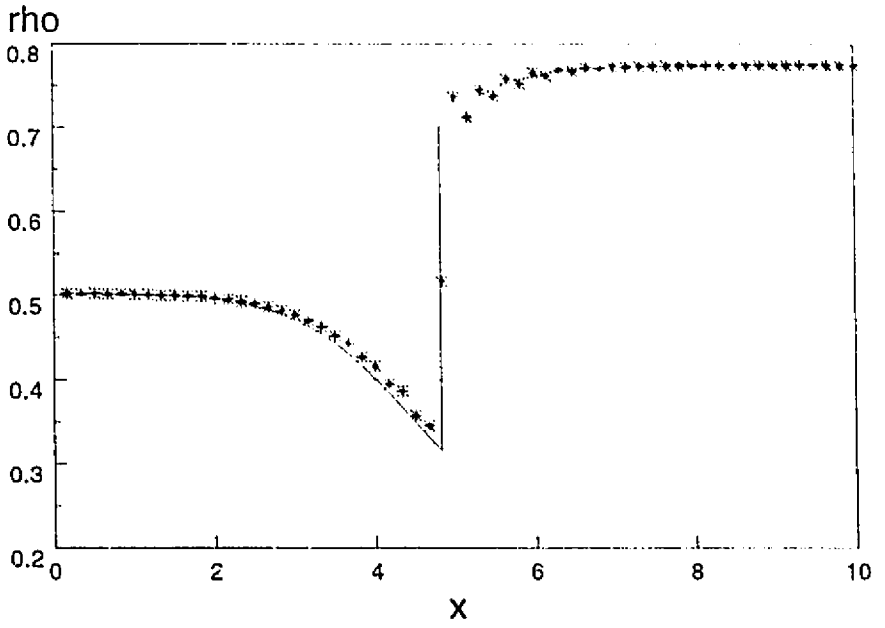

Fig. 6.9 - Duct flow with shock. Jameson's method, $k^{(2)}=1.0$, $k^{(4)}=0.0156$, versus the exact solution (solid line).

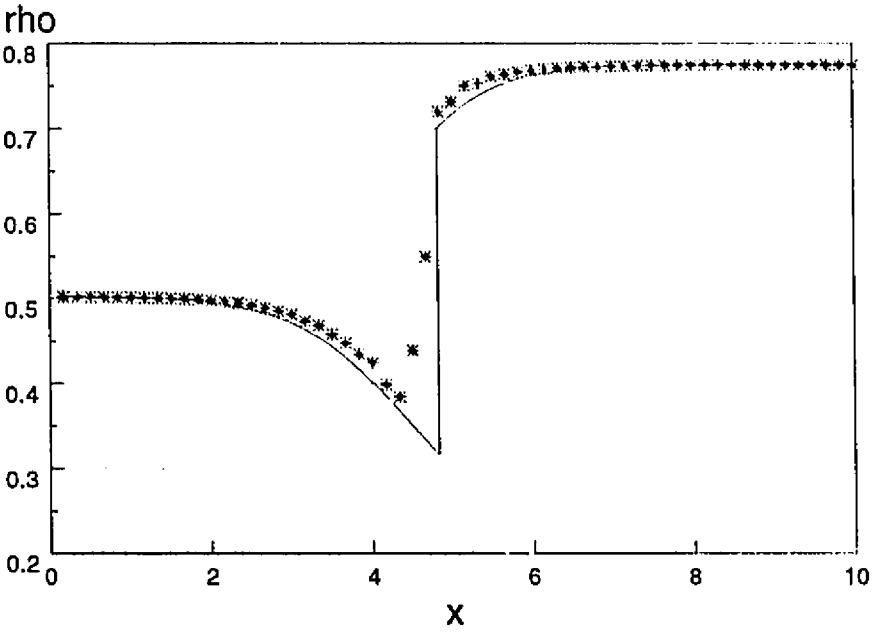

Fig. 6.10 - Duct flow with shock. Jameson's method, $k^{(2)}=2.5$, $k^{(4)}=0.039$, versus the exact solution (solid line).

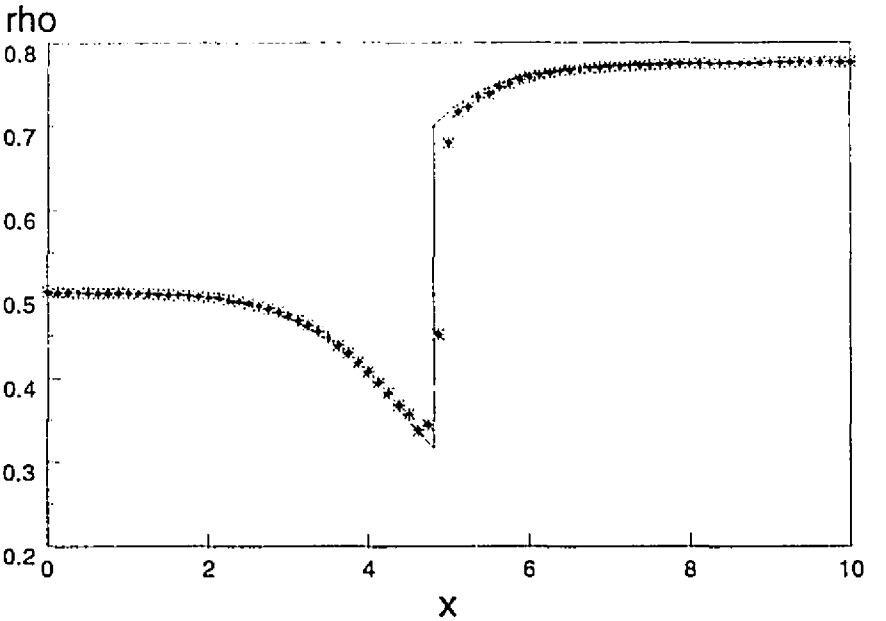

Fig. 6.11 - Duct flow with shock. The α-method, $k^{(2)}=0.25$, $k^{(4)}=0.0039$, versus the exact solution (solid line).

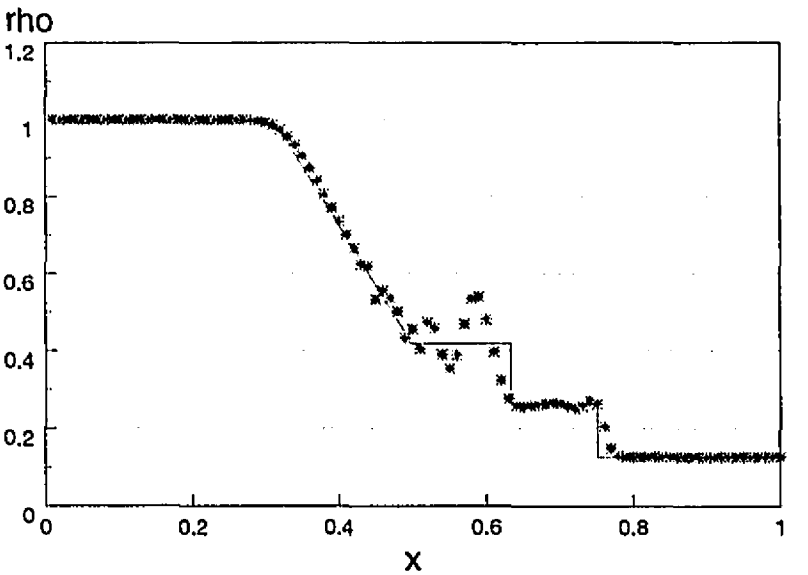

Fig. 6.12 - Shock-tube flow at $t=14$. MacCormack's method with artificial viscosity, $C=0.5$, compared with the exact solution (solid line).

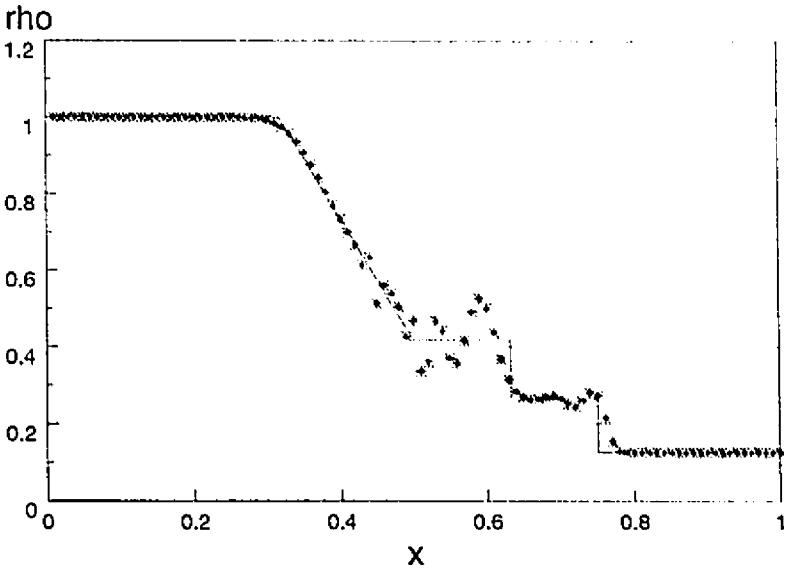

Fig. 6.13 - Shock-tube flow at $t=14$. Jameson's method, $k^{(2)}=1.0$, compared with the exact solution (solid line).

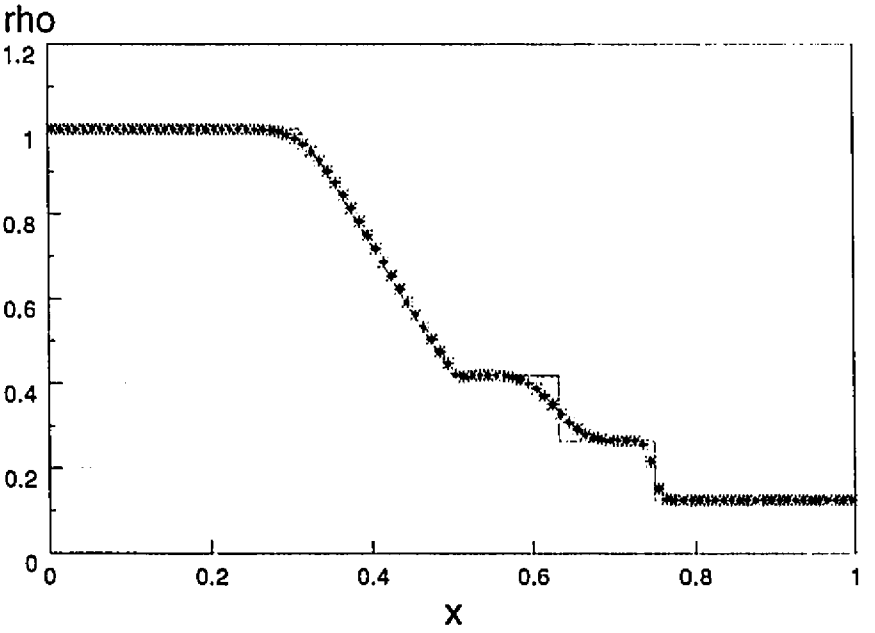

Fig. 6.14 - Shock-tube flow at $t=14$. Godunov's method compared with the exact solution (solid line).

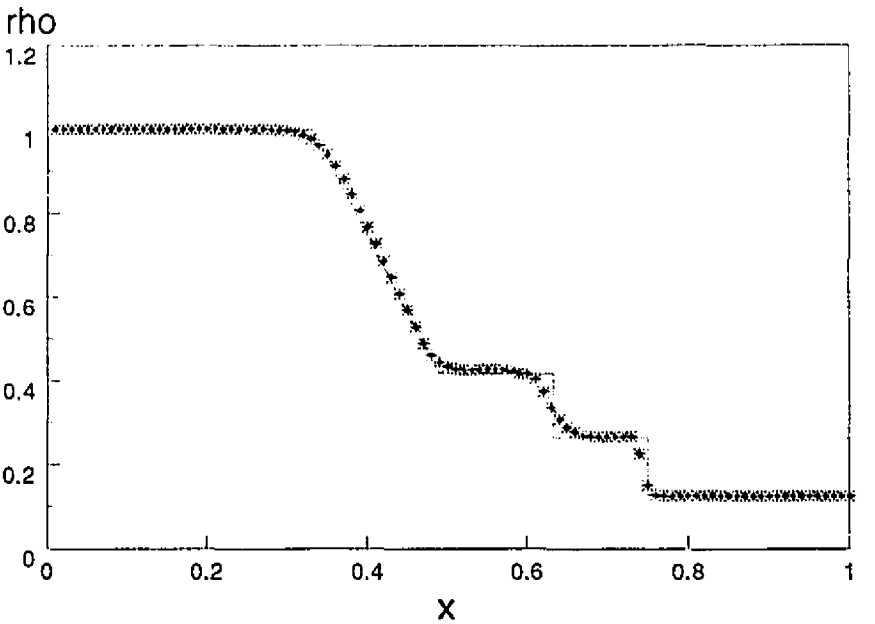

Fig. 6.15 - Shock-tube flow at t=14. Hybrid method (MacCormack-Godunov) compared with the exact solution (solid line).

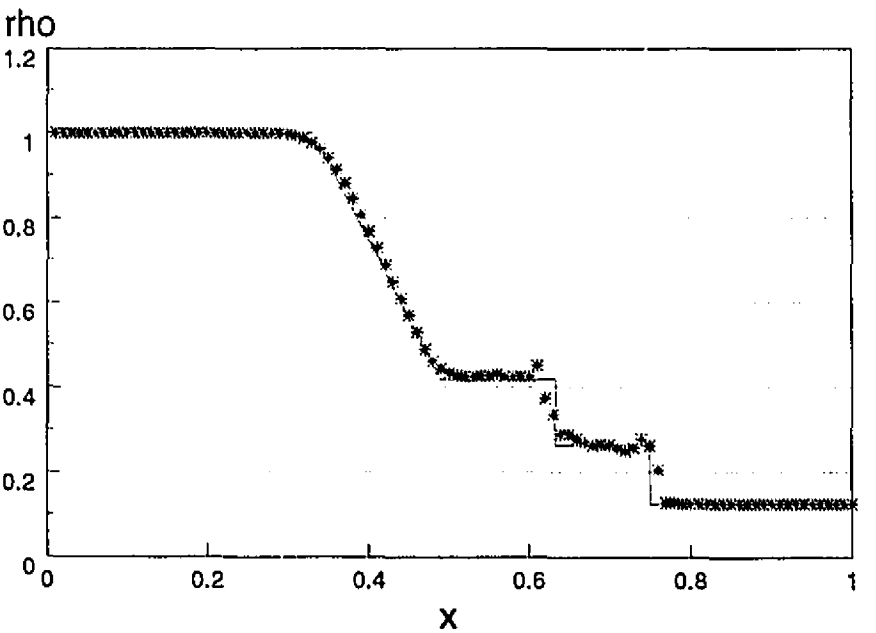

Fig. 6.16 - Shock-tube flow at t=14. The α-method with dissipation, $k^{(2)}$=0.5, compared with the exact solution (solid line).

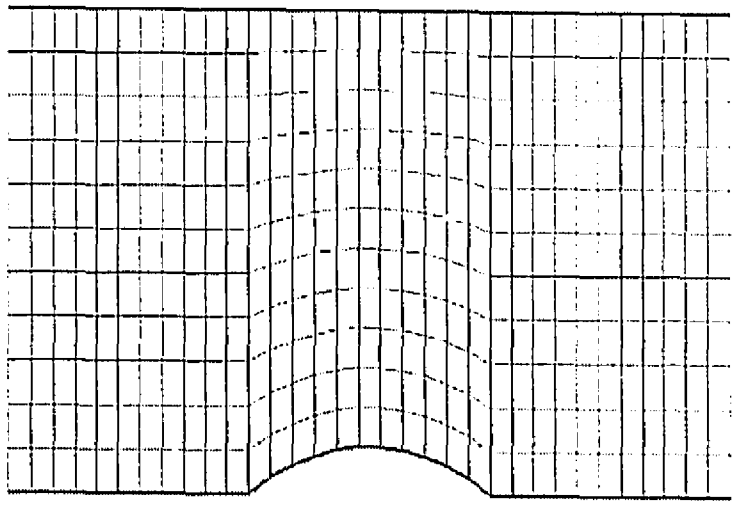

Fig. 6.17 - Typical grid (size 33x11 cells) used for 2-D circular arc bump channel.

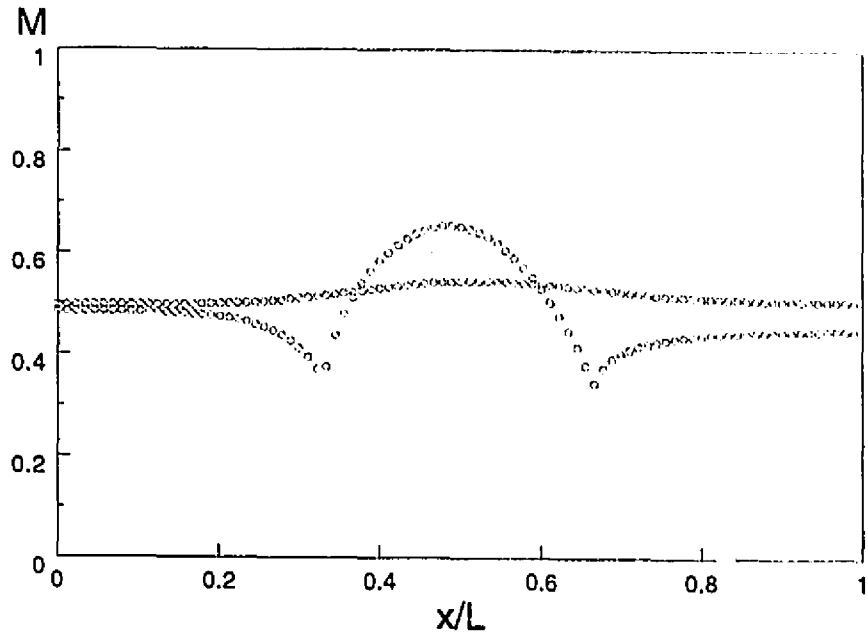

Fig. 6.18 - Subsonic 2-D bump channel flow. The Mach number distributions on the upper and lower walls by Godunov's method.

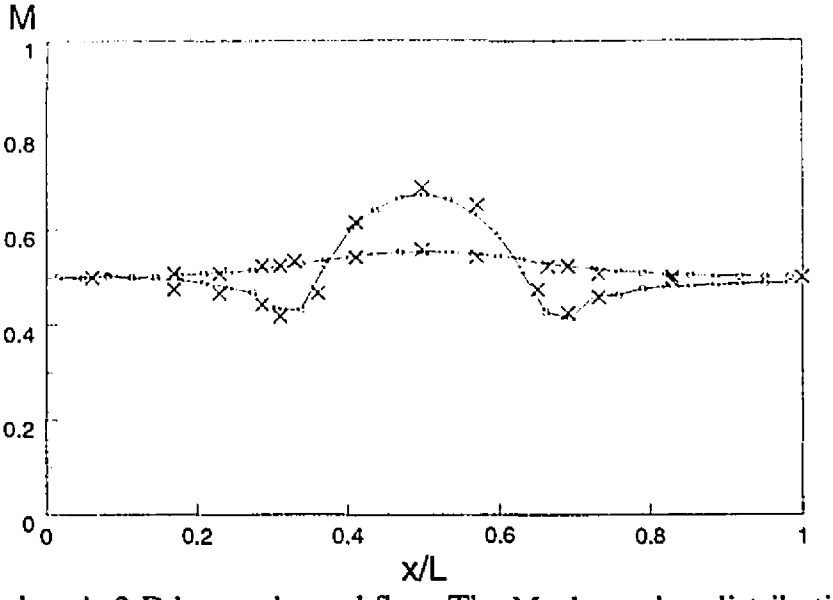

Fig. 6.19 - Subsonic 2-D bump channel flow. The Mach number distributions on the upper and lower walls by Jameson's method, compared with the results obtained by Ni in [30] (x).

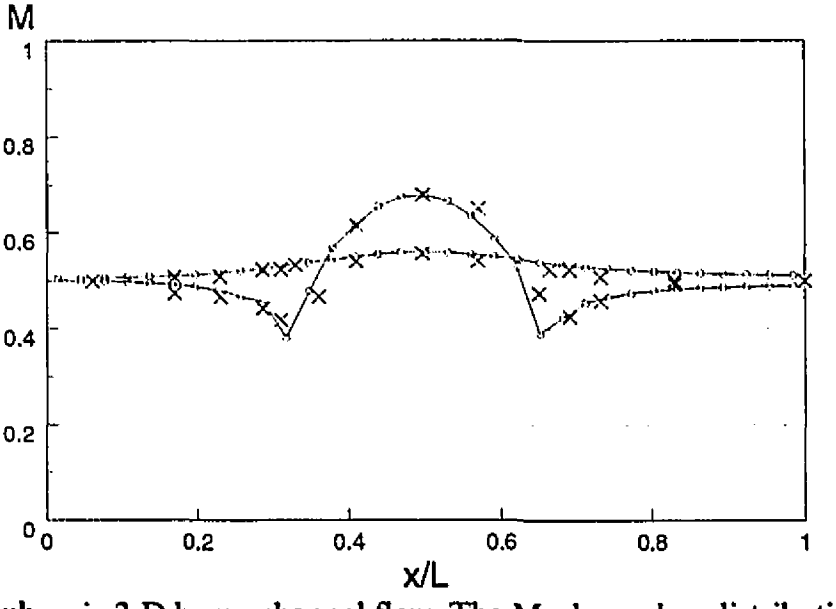

Fig. 6.20 - Subsonic 2-D bump channel flow. The Mach number distributions on the upper and lower walls by the α-method, compared with the results obtained by Ni in [30] (x).

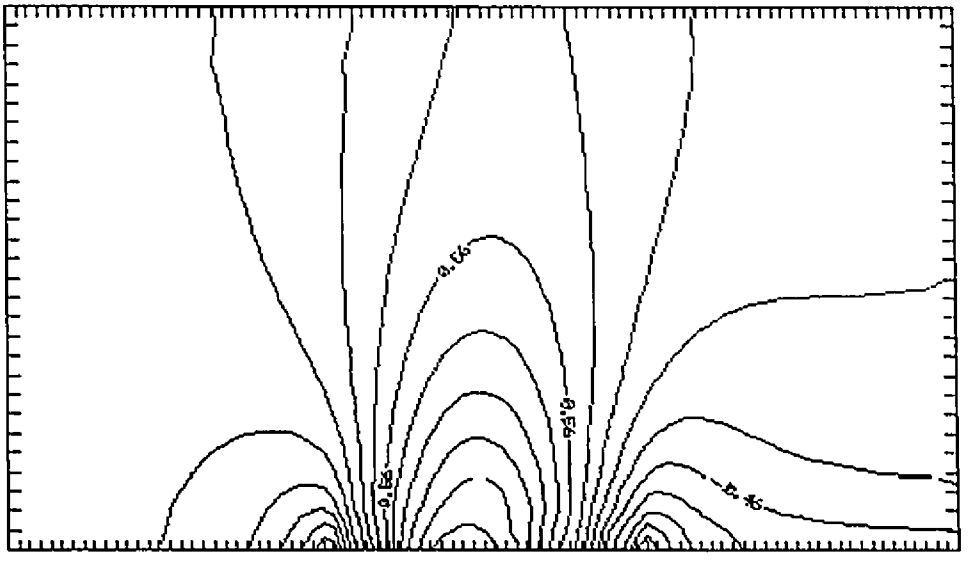

Fig. 6.21 - Subsonic 2-D bump channel flow. Iso-Mach lines by Godunov's method.

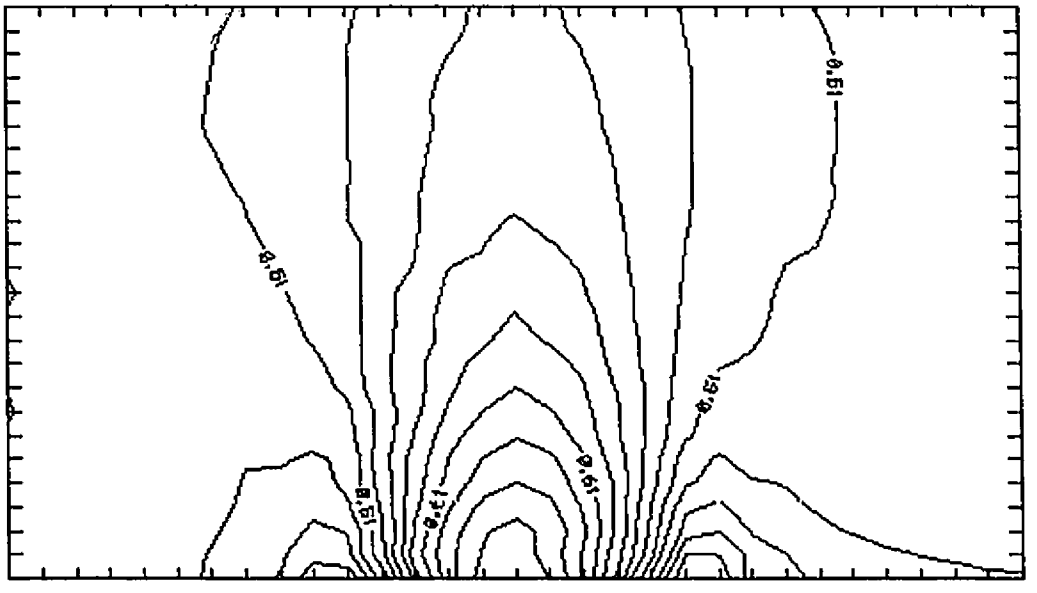

Fig. 6.22 - Subsonic 2-D bump channel flow. Iso-Mach lines by Jameson's method.

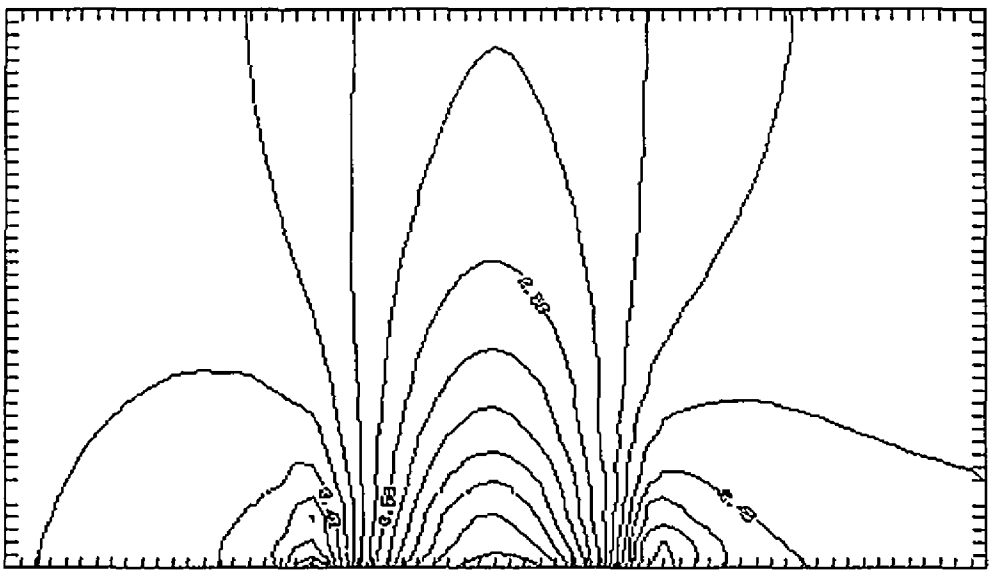

Fig. 6.23 - Subsonic 2-D bump channel flow. Iso-Mach lines by the α-method.

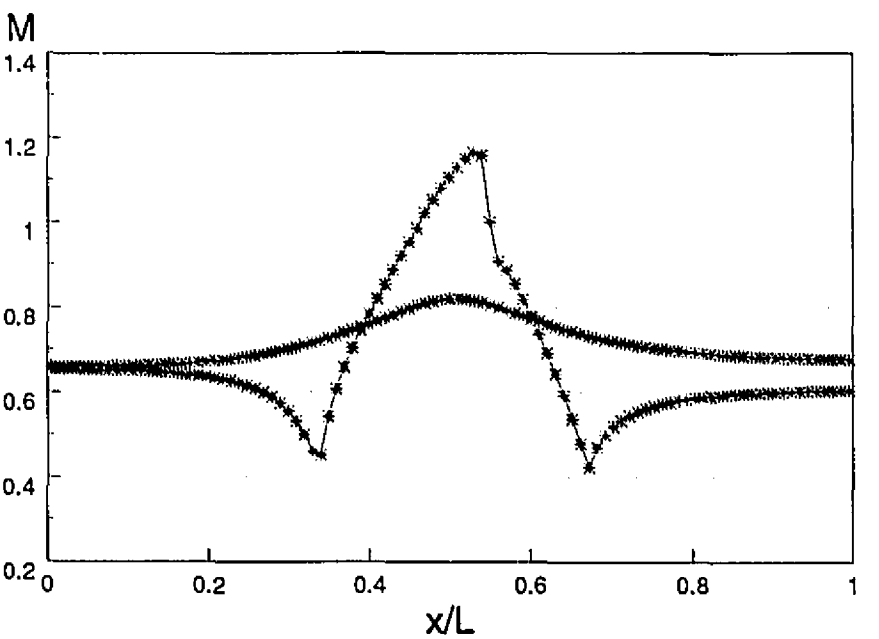

Fig. 6.24 - Transonic 2-D bump channel flow. The Mach number distributions on the upper and lower walls by Godunov's method.

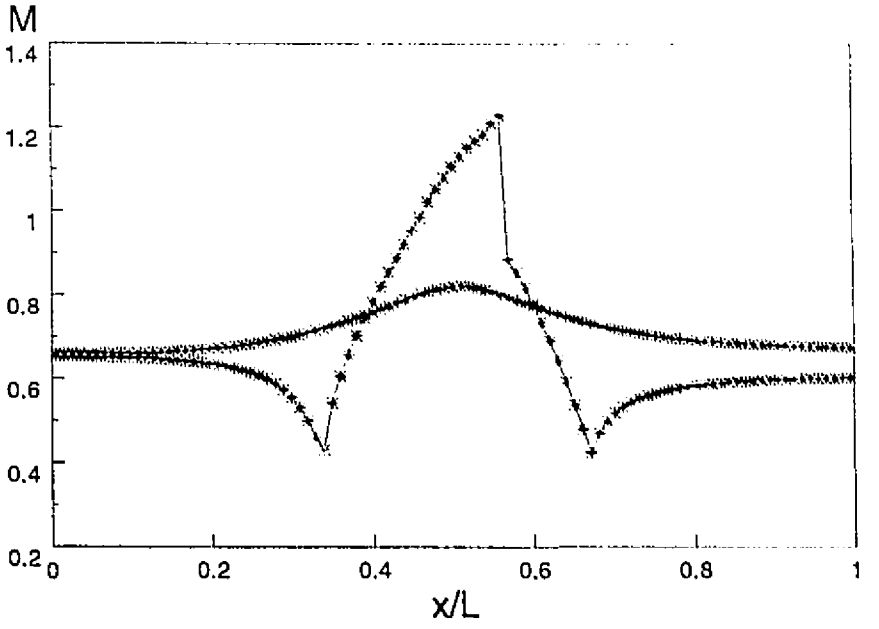

Fig. 6.25 - Transonic 2-D bump channel flow. The Mach number distributions on the upper and lower walls by the hybrid method.

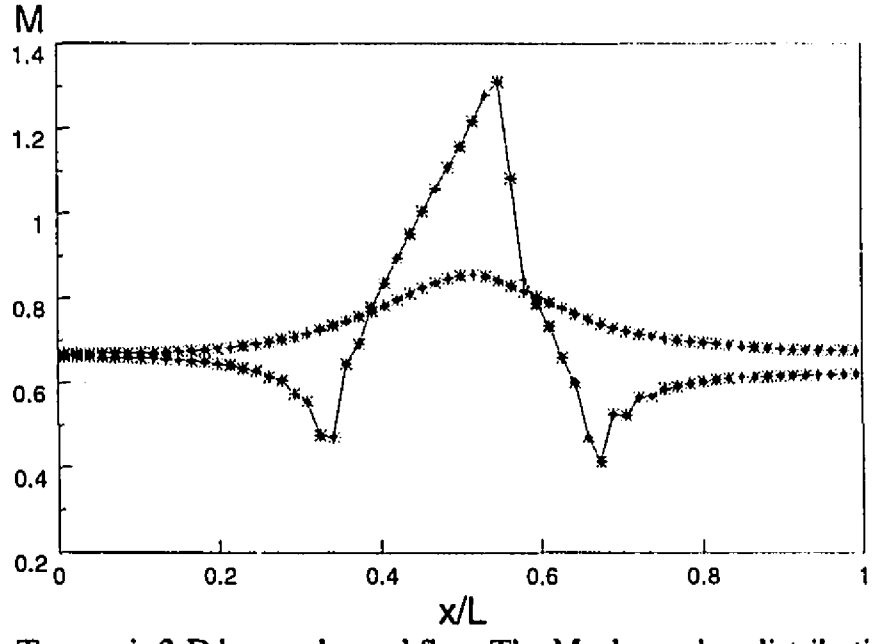

Fig. 6.26 - Transonic 2-D bump channel flow. The Mach number distributions on the upper and lower walls by the α-method.

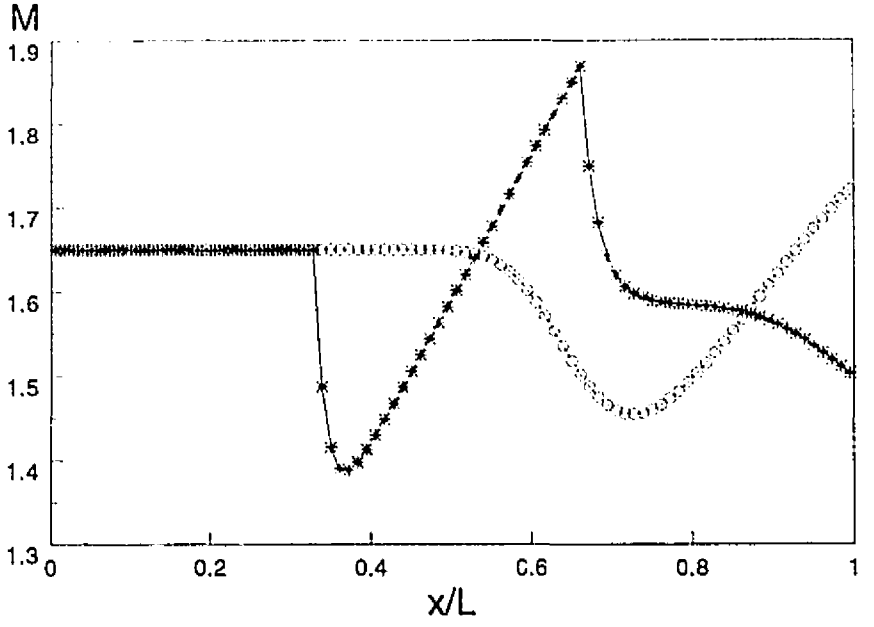

Fig. 6.27 - Supersonic 2-D bump channel flow. The Mach number distributions on the upper (circles) and lower (asterisks) walls by Godunov's method.

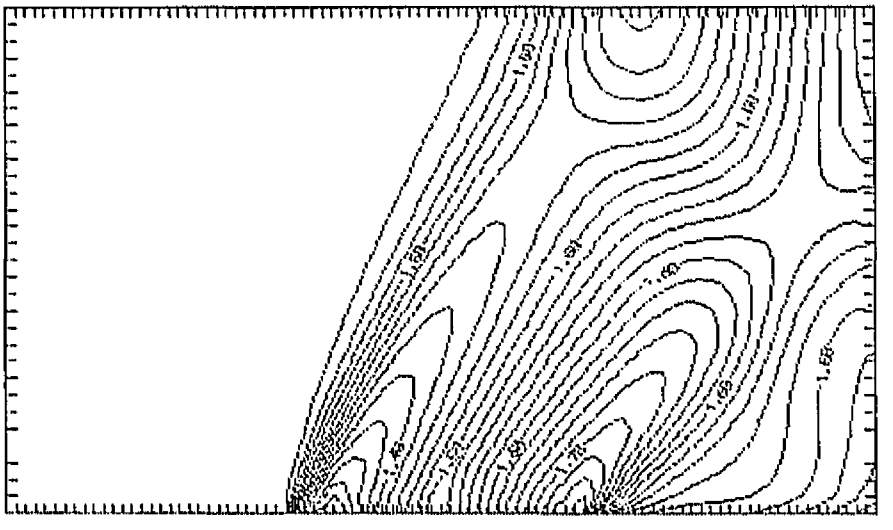

Fig. 6.28 - Supersonic 2-D bump channel flow. The iso-Mach lines by Godunov's method.

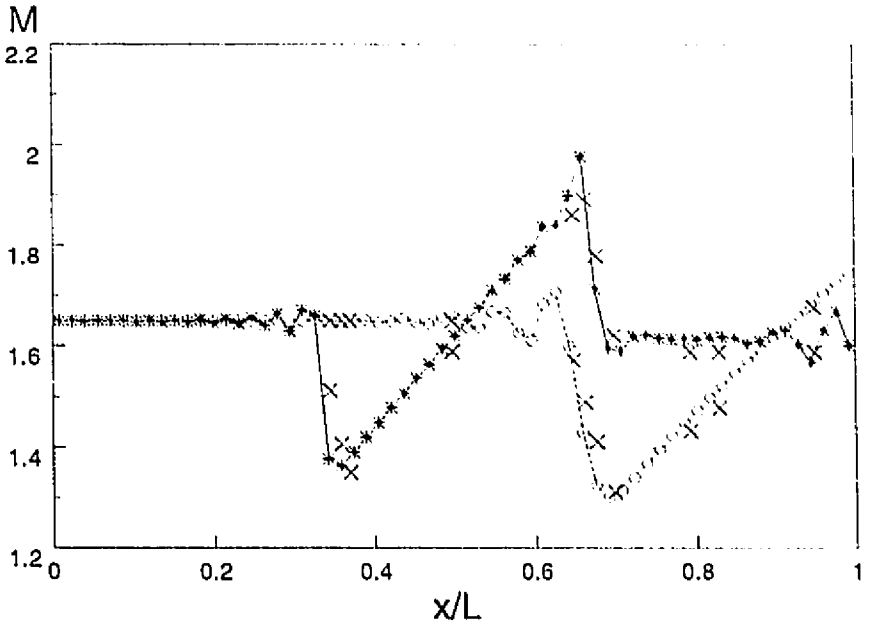

Fig. 6.29 - Supersonic 2-D bump channel flow. The Mach number distributions on the upper (circles) and lower (asterisks) walls by Jameson's method, $k^{(2)}=0.75$, compared with the solution in [8] (x).

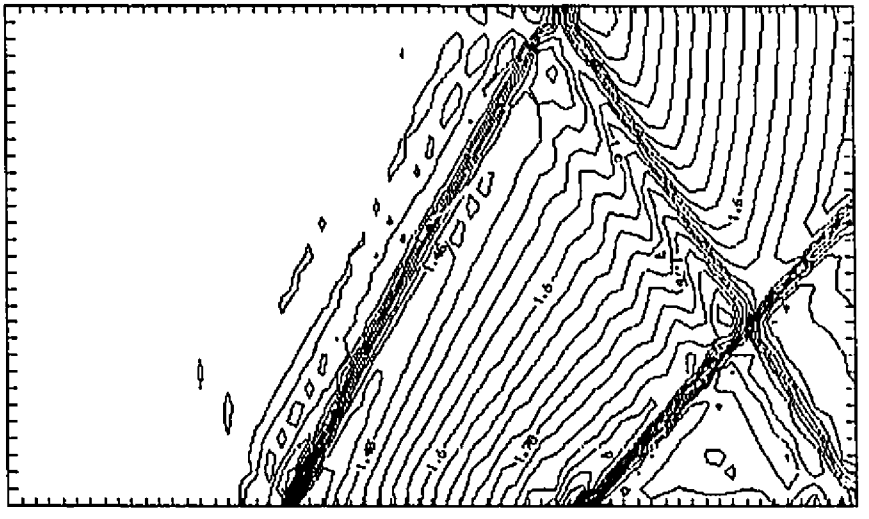

Fig. 6.30 - Supersonic 2-D bump channel flow. The iso-Mach lines by Jameson's method.

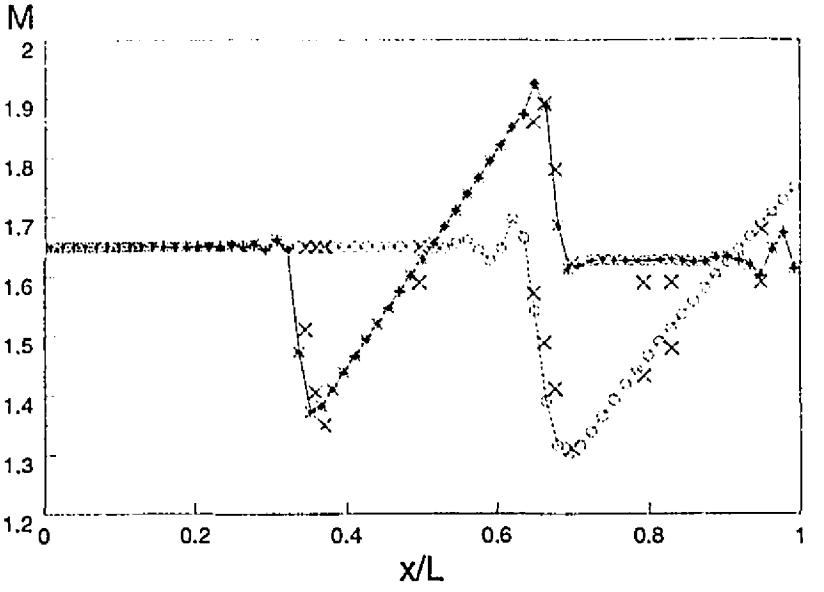

Fig. 6.31 - Supersonic 2-D bump channel flow. The Mach number distributions on the upper (circles) and lower (asterisks) walls by the α-method, compared with the solution in [8] (x).

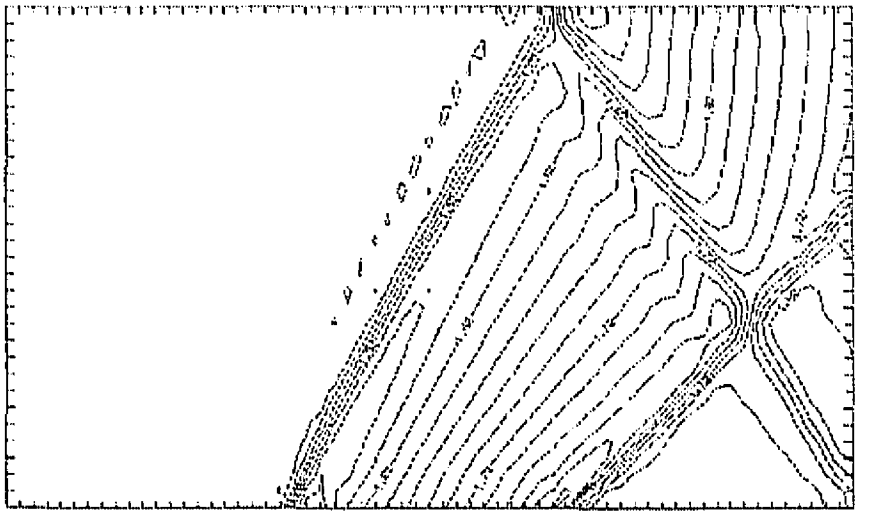

Fig. 6.32 - Supersonic 2-D bump channel flow. The iso-Mach lines by the α-method.

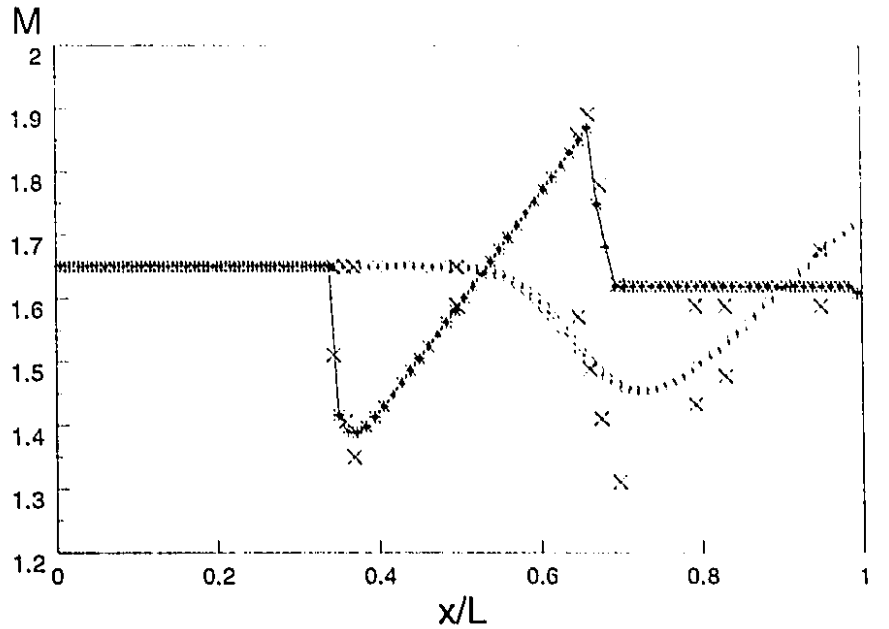

Fig. 6.33 - Supersonic 2-D bump channel flow. The Mach number distributions on the upper (circles) and lower (asterisks) walls by the hybrid method, compared with the solution in [8] (x).

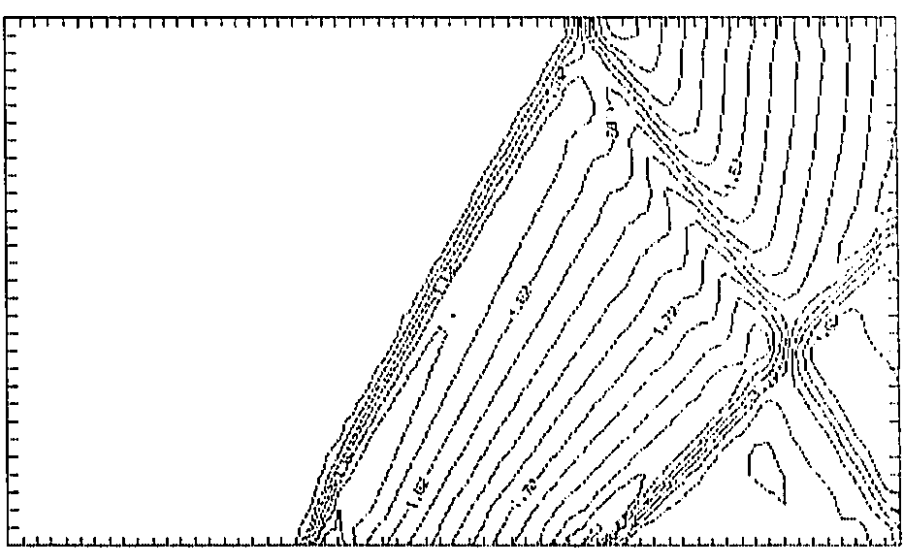

Fig. 6.34 - Supersonic 2-D bump channel flow. The iso-Mach lines by the hybrid method.

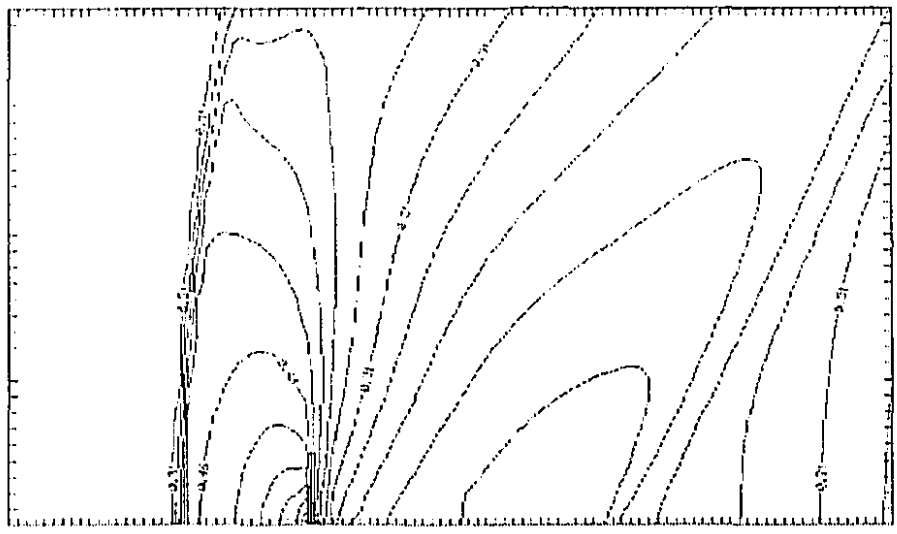

Fig. 6.35 - The isobar lines obtained with Godunov's method for the flow at M_∞=1.2 past the NACA 0012 airfoil.

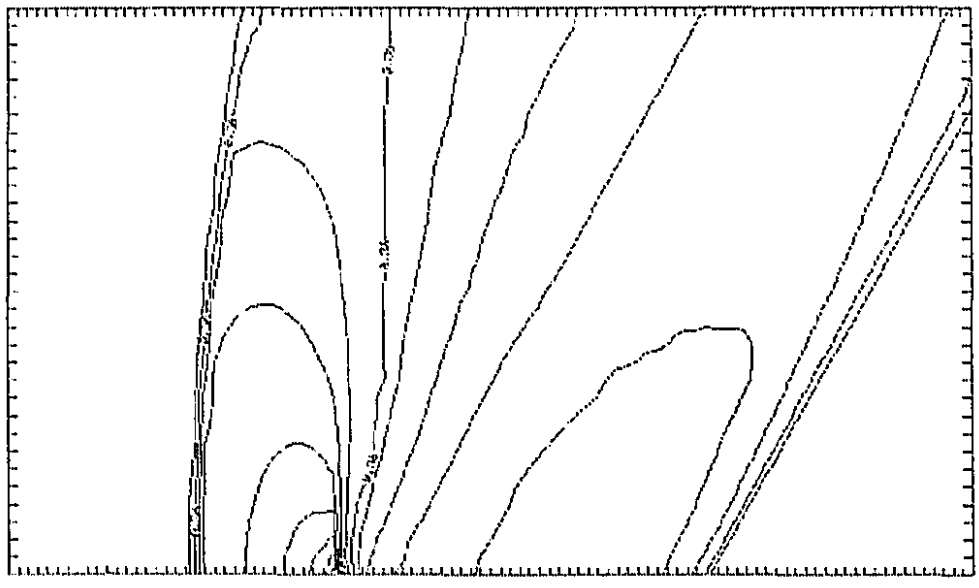

Fig. 6.36 - The isobar lines obtained with the hybrid method for the flow at M_∞=1.2 past the NACA 0012 airfoil.

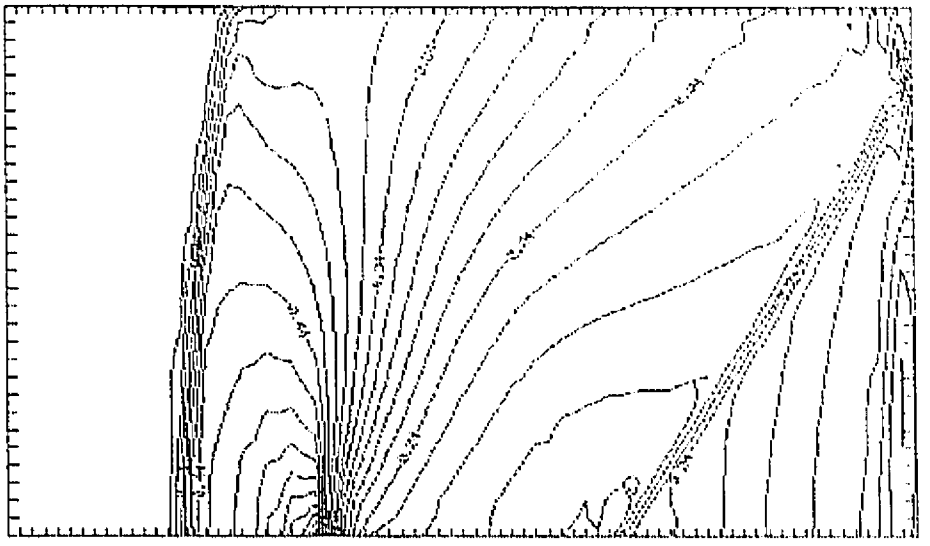

Fig. 6.37 - The isobar lines obtained with MacCormack's method for the flow at M_∞=1.2 past the NACA 0012 airfoil.

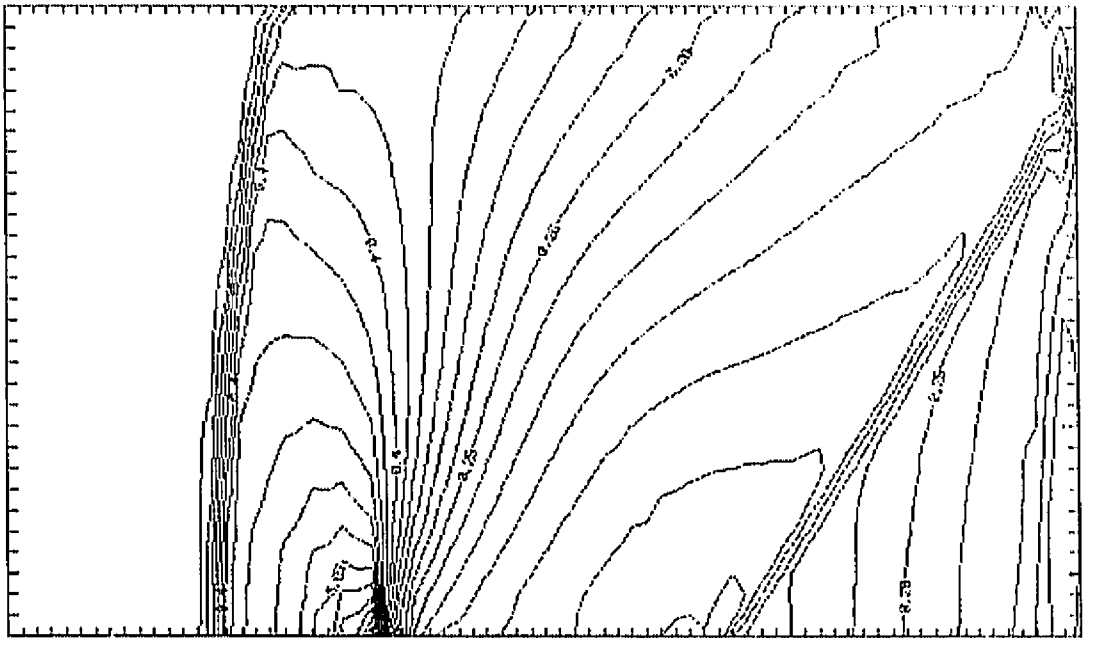

Fig. 6.38 - The isobar lines obtained with the α-method for the flow at M_∞=1.2 past the NACA 0012 airfoil.

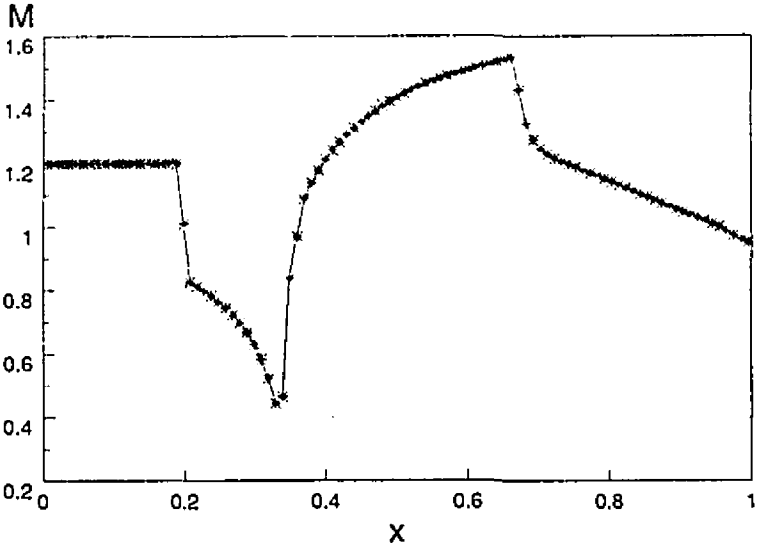

Fig. 6.39 - Mach number distribution on the airfoil and its symmetry axis by Godunov's method.

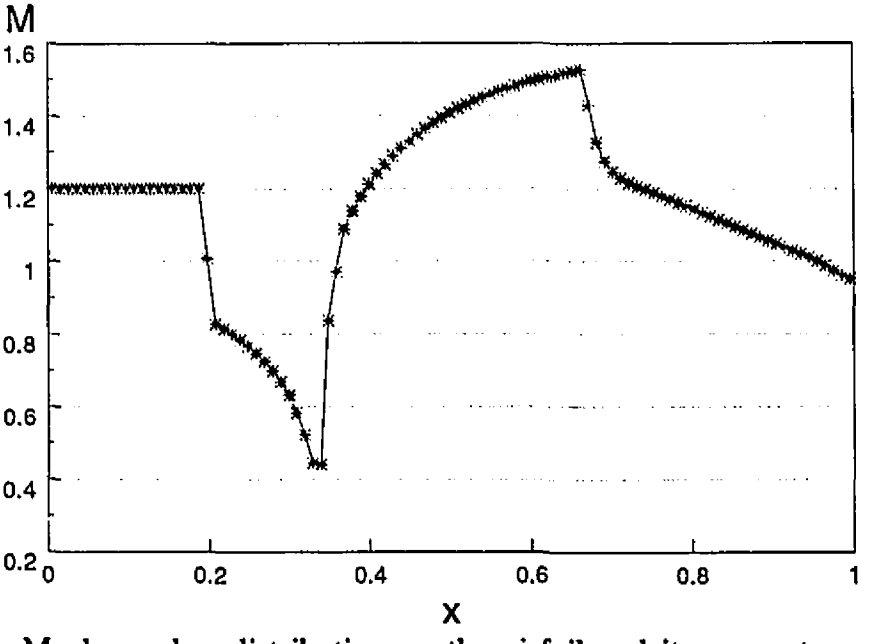

Fig. 6.40 - Mach number distribution on the airfoil and its symmetry axis by the hybrid method.

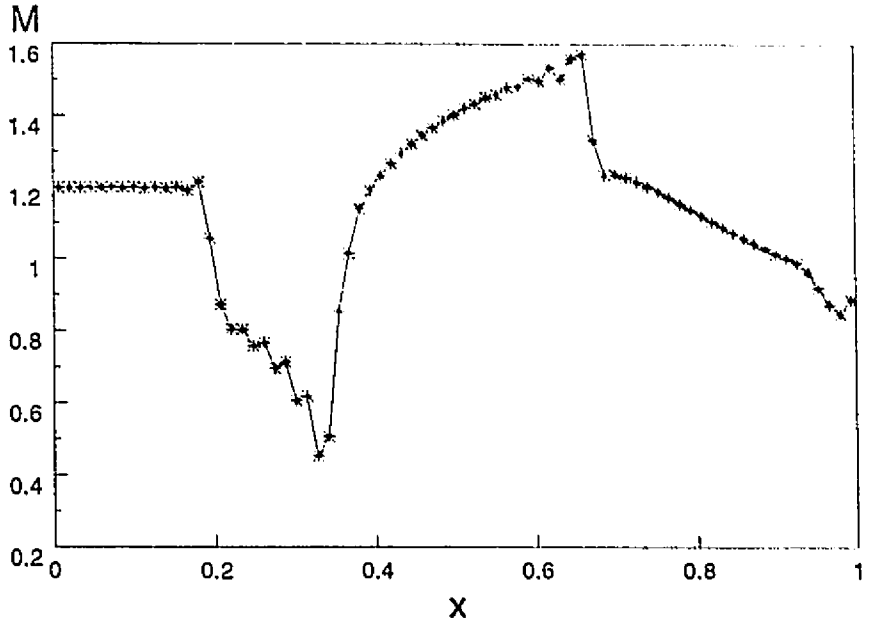

Fig. 6.41- Mach number distribution on the airfoil and its symmetry axis by MacCormack's method.

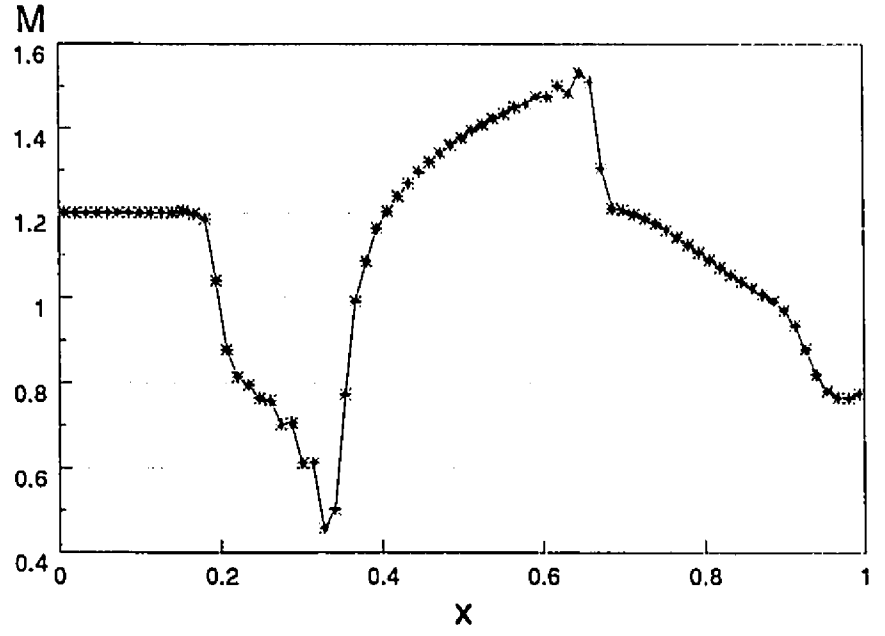

Fig. 6.42 - Mach number distribution on the airfoil and its symmetry axis by the α-method.

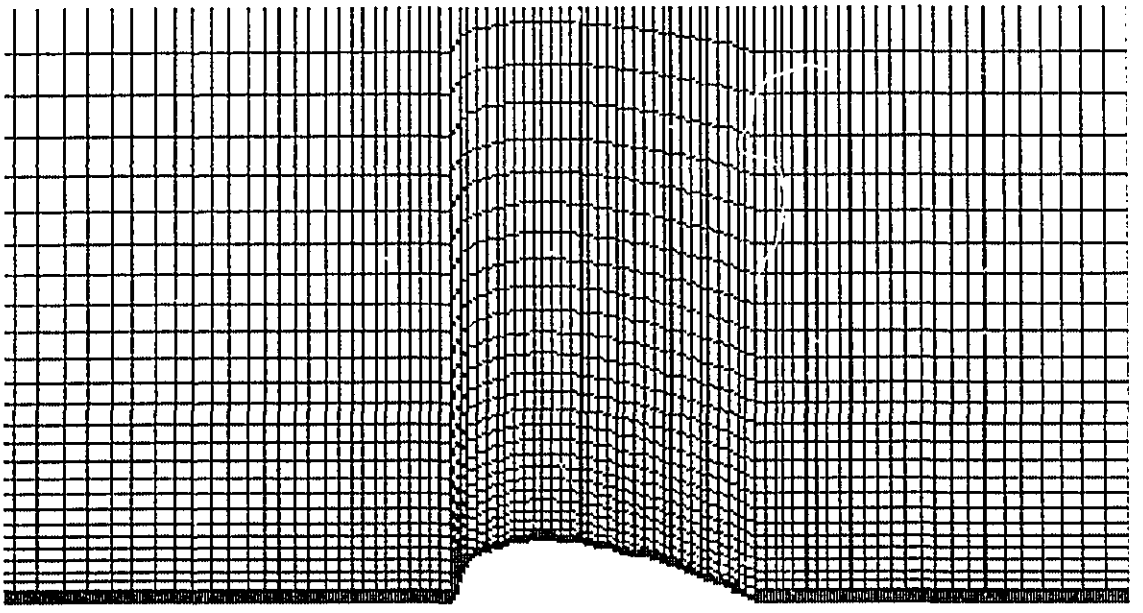

Fig. 6.43 - Partial representation (near the airfoil boundary) of the grid used for NACA 0012 airfoil calculations.

Chapter 7

Conclusions

The results presented in Chapter 6 lead to a set of conclusions about the use of the finite-volume shock capturing schemes studied herein.

First, it has been shown that the use of numerical means (artificial viscosity, adaptive dissipation) in order to control the stability and the oscillatory behavior of the second-order methods may result in a depreciation of the accuracy of the solution (e.g. Fig. 6.1). Although this effect can only be verified for quasi one-dimensional flows, where an analytical solution exists, it is to be expected that the same situation will be encountered in two-dimensional flows. The solutions in Fig. 6.19 and 6.20 show this to be the case: the α-method, which does not use dissipation on the x-axis, produces a higher (even if only slightly) maximum Mach number on the bump than Jameson's method. The use of the artificial dissipation is made more complicated by the fact that the coefficients involved must be tuned up for every flow case.

In this sense, the α-method developed in Chapter 5 can be considered an improvement over Jameson's method. It introduces a very simple and efficient bias in the estimation of the fluxes, with a more realistic model for the physics of the flow. This can be clearly seen especially for subsonic flows, where its use does not require dissipation terms. It leads to correct flow solutions in less computer time in this case. For supersonic flows without shocks, the method generally requires less time steps than Jameson's method (Table 5.1). When shocks are present, the use of

the adaptive dissipation becomes necessary; however, the amount of dissipation needed is always small, such that the discontinuities are more exacly computed.

Second, the results indicate that a nonoscillatory behavior is a very desirable feature for a numerical method applied to the Euler equations, which admit discontinuous solutions. This is especially valid when pressure/velocity distributions are needed along a certain surface in the flow: overshoots specific to second-order methods (e.g. Fig. 6.29) are eliminated.

Third, it is shown that the first-order accuracy of Godunov's method is not able to provide a clear representation of the flowfield; when wave interactions are involved, it only gives a vague picture of them (Fig. 6.28).

For these reasons, the hybrid method MacCormack-Godunov becomes a valuable tool for the analysis of flowfields containing discontinuities. It offers a clear representation of these discontinuities, void of oscillations, and the second-order accuracy in smooth regions enables the method to represent well enough the wave structures involved. Although the CPU time per iteration is greater for this method than for a common second-order method, it proves out (e.g. Table 6.3) that the total time needed for convergence to a steady state may be in some cases reduced, due to the more correct treatment of the physics of the flow.

The α-method developed in Chapter 5 can possibly be improved if the adaptive dissipation necessary in the presence of shocks will be reduced only to the second-order term; the fourth-order term, necessary in the smooth regions only, and which is in fact the most expensive, can probably be eliminated. This would bring an even higher efficiency for all flow regimes; numerical experiments are further necessary for the implementation of this feature.

Bibliography

[1] Albone, C.M., Hall, M.G., Joyce, G., Numerical solutions for transonic flows past wing-body configurations, Symposium Transsonicum II, Göttingen, ed. Springer-Verlag, 1976.

[2] Bailey, F.R., Ballhaus, W.F., Comparisons of computed and experimental pressures for transonic flows about isolated wings and wing-fuselage configurations, NASA SP-347, pp. 1213-1231, 1975.

[3] Casper, J., Finite-Volume Implementation of High-Order Essentialy Nonoscillatory Schemes in Two Dimensions, AIAA Journal, Vol. 30, No. 12, pp. 2829-2835, 1992.

[4] Casper, J., Atkins, H.L., A Finite-Volume High-Order ENO Scheme for Two-Dimensional Hyperbolic Systems, Journ. of Comp. Phys. 106, pp. 62-76, 1993.

[5] Chorin, A.J., Random Choice Solution of Hyperbolic Systems, Journ. of Comp. Phys. 22, pp. 517-533, 1976.

[6] Colella, P., Woodward, P.R., The Piecewise Parabolic Method (PPM) for Gas-Dynamical Simulations, Journ. of Comp. Phys. 54, pp. 174-201, 1984.

[7] De Neef, T., Moretti, G., Shock Fitting for Everybody, Computers and Fluids 8, pp. 327-334, 1980.

[8] Eidelman, S., Colella, P., Shreeve, R.P., Application of the Godunov Method and Its Second-Order Extension to Cascade Flow Modeling, AIAA Journal,

Vol. 22, pp. 1609-1615, 1984.

[9] Garabedian, P.R., Korn, D.G., Analysis of transonic airfoils, Comm. Pure and Appl. Maths., Vol. 24, pp. 841-851, 1971.

[10] Godunov, S.K., Finite difference method for numerical computation of discontinuous solutions of the equations of fluid dynamics, Math. Sb. 47, pp. 271-306, 1959.

[11] Godunov, S.K., Zabrodin, A.V., Prokopov, G.P., A computational scheme for two-dimensional non stationary problems of gas dynamics and calculation of the flow from a shock wave approaching a steady state, USSR Comp. Math. Math. Phys., Vol. 1, pp. 1187-1219, 1962.

[12] Harten, A., The Artificial Compression Method for Computation of Shocks and Contact Discontinuities: III. Self-Adjusting Hybrid Schemes, Math. of Comp., Vol. 32, No. 142, pp. 363-389, 1978.

[13] Harten, A., Engquist, B., Osher, S., Chakravarthy,S., Uniformly High Order Accurate Essentially Non-Oscillatory Schemes III, Journ. of Comp. Phys. 71, pp. 231-303, 1987.

[14] Harten, A., Zwas, G., Switched Numerical Shuman Filters for Shock Calculation, Journ. of Eng. Math., Vol. 6, No. 2, pp. 207-216, 1972.

[15] Jameson, A., Iterative solution of transonic flows over airfoils and wings, including flows at Mach 1, Comm. Pure and Appl. Math. 27, pp. 283-309, 1974.

[16] Jameson, A., A Multi-Grid Solution Method for the Euler Equations, Int. Multigrid Conference, Copper Mountain, Colorado, April 1983.

[17] Jameson, A., Mavriplis, D., Finite Volume Solution of the Two-Dimensional Euler Equations on a Regular Triangular Mesh, AIAA Journal, Vol. 24, No. 4, pp. 611-618, 1986.

[18] Jameson, A., Schmidt, W., Turkel, E., Numerical Solutions to the Euler Equation by Finite Volume Methods using Runge-Kutta Time Stepping, AIAA Paper 81-1259, 1981.

[19] Lapidus, A., A Detached Shock Calculation by Second-Order Finite Differences, Journ. of Comp. Phys. 2, pp. 154-177, 1967.

[20] Lax, P.D., Weak Solutions of Nonlinear Hyperbolic Equations and their Numerical Computation, Comm. Pure and Appl. Math. 7, pp. 159-193, 1954.

[21] Lax, P.D., Wendroff, B., Systems of Conservation Law, Comm. Pure and Appl. Math. 13, pp. 217-237, 1960.

[22] MacCormack, R.W., The Effect of Viscosity in Hypervelocity Impact Cratering, AIAA Paper 69-354, 1969.

[23] MacCormack, R.W., Rizzi, A.W., Inouye, M., Steady supersonic flowfields with embedded subsonic regions, Computational Methods and Problems in Aeronautical Fluid Dynamics, ed. Hewitt & al., Academic Press, pp. 424-447, 1976.

[24] Mateescu, D., Mechanics of Compressible Fluids, Course notes, McGill Univ.,

1989.

[25] Mateescu, D., Computational Aerodynamics, Course notes, McGill Univ., 1993.

[26] Mateescu, D., Private Communication, McGill Univ., December 1992.

[27] Mateescu, D., Lauzon, M., An Explicit Euler Method for Internal Flow Computation, in Computers and Experiments in Fluid Flow, ed. Carlomagno, G.M., and Brebbia, C.A., 1989.

[28] Moretti, G., The λ-scheme, Computers and Fluids 7, pp. 191-205, 1979.

[29] Murman, E.M., Cole, J.D., Calculation of plane steady transonic flows, AIAA Journal Vol. 9, No.1, pp. 114-121, 1971.

[30] Ni, R.-H., A Multiple-Grid Scheme for Solving the Euler Equations, AIAA Journal Vol.20, No. 11, pp. 1565-1570, 1982.

[31] Richtmyer, R.D., Morton, K.W., Difference Methods for Initial Value Problems, Interscience, New York, 1967.

[32] Roe, P.L., Numerical Algorithms for the Linear Wave Equation, RAE TR 81047, 1981.

[33] Roe, P.L., An Introduction to Numerical Methods Suitable for the Euler Equations, Von Karman Institute for Fluid Dynamics Lecture Series 1983-01, January 24-28, 1983.

[34] Rudy, D.H., Strikwerda, J.C., A Nonreflecting Outflow Boundary Condition for

Subsonic Navier-Stokes Calculations, Journ. of Comp. Phys. 36, pp. 55-70, 1980.

[35] Saad, M.A., Compressible Fluid Flow, Second Edition, Prentice Hall, 1993.

[36] Shubin, G.R., Stephens, A.B., Glaz, H.M., Steady Shock Tracking and Newton's method Applied to One-Dimensional Duct Flow, Journ. of Comp. Phys. 39, pp. 364-374, 1981.

[37] Sod, G.A., A Survey of Several Finite Difference Methods for Systems of Nonlinear Hyperbolic Conservation Laws, Journ. of Comp. Phys. 27, pp. 1-31, 1978.

[38] Usab, W.J., Murman, E.M., Embedded Mesh Solutions of the Euler Equations Using a Multiple-Grid Method, in Advances in Computational Transonics, ed. Habashi, W.G., 1985.

[39] Van Leer, B., Towards the Ultimate Conservative Difference Scheme. V. A Second-Order Sequel to Godunov's Method, Journ. of Comp. Phys. 32, pp. 101-136, 1979.

[40] Venkatakrishnan, V., Jameson, A., Computation of Unsteady Transonic Flows by the Solution of the Euler Equations, AIAA Journal, Vol. 26, pp. 974-981, 1988.

[41] Von Neumann, J., Richtmyer, R.D., A method for the numerical calculations of hydrodynamical shocks, Journal of Applied Physics 21, pp. 232, 1950.

[42] Zannetti, L., Colasurdo, G., Unsteady Compressible Flow: A Computational

Method Consistent with the Physical Phenomena, AIAA Journal Vol. 19, No. 7, pp. 852-856, 1981.

[43] Zhong, X.-C., Moretti, G., Comparison of different integration schemes based on the concept of characteristics as applied to the ablated blunt body problem, Computers and Fluids 10, pp. 277-294, 1982.

Appendix A

Characteristic form of the Euler equations

Several algebraical forms of the system of conservation laws known as the Euler equations are possible, depending on the choice of dependent flow variables. The density, momentum and total energy, obeying the conservation form of the equations, are called conservative variables. The variables which can be directly determined by experiment, such as density, speed and pressure, are called the primitive variables. Quantities that propagate along specific directions in a wave-like manner, known as characteristic variables, can also be defined. This appendix presents the form of the time-dependent Euler equations using these different variables, as well as the implications on the treatment of boundary conditions.

A.1 Quasi one-dimensional time-dependent Euler equations

The Euler equations in conservative variables (2.10) can be transformed by expanding the derivatives:

$$S\frac{\partial f}{\partial t} + f\frac{\partial S}{\partial t} + S\frac{\partial F}{\partial x} + F\frac{\partial S}{\partial x} = PS \qquad \text{(A.1)}$$

Since the area of the duct depends only on x, $\frac{\partial S}{\partial t} = 0$, $\frac{\partial S}{\partial x} = \frac{dS}{dx}$, and hence one obtains:

$$S\frac{\partial f}{\partial t} + S\frac{\partial F}{\partial x} = PS - F\frac{dS}{dx} \qquad \text{(A.2)}$$

which, after dividing by S and replacing F and P with their expressions in (2.8), becomes:

$$\frac{\partial f}{\partial t} + \frac{\partial F}{\partial x} = \begin{bmatrix} -\frac{\rho u}{S}\frac{dS}{dx} \\ -\frac{\rho u^2}{S}\frac{dS}{dx} \\ -\frac{\rho uH}{S}\frac{dS}{dx} \end{bmatrix} \tag{A.3}$$

Here $H = E + \frac{p}{\rho} = \frac{\gamma}{\gamma - 1}\frac{p}{\rho}$ is the stagnation enthalpy, which is constant for adiabatic flows.

Equation (A.3) can also be written in the form:

$$\frac{\partial f}{\partial t} + A\frac{\partial f}{\partial x} = Q \tag{A.4}$$

where Q denotes the source terms in the right hand side of (A.3), and

$$A = \frac{\partial F}{\partial f} = \begin{bmatrix} 0 & 1 & 0 \\ -(3-\gamma)\frac{u^2}{2} & (3-\gamma)u & \gamma - 1 \\ (\gamma - 1)u^3 - \gamma uE & \gamma E - 3\frac{\gamma - 1}{2}u^2 & \gamma u \end{bmatrix} \tag{A.5}$$

is the Jacobian matrix in terms of the conservative variables.

Introducing the state vector in terms of primitive variables,

$$f_p = \begin{bmatrix} \rho \\ u \\ p \end{bmatrix} \tag{A.6}$$

and defining the Jacobian matrix T which connects the two state vectors:

$$T = \frac{\partial f}{\partial f_p} = \begin{bmatrix} 1 & 0 & 0 \\ u & \rho & 0 \\ \frac{u^2}{2} & \rho u & \frac{1}{\gamma - 1} \end{bmatrix} \tag{A.7}$$

the equations can be written:

$$T\frac{\partial f_p}{\partial t} + AT\frac{\partial f_p}{\partial x} = Q \tag{A.8}$$

By multiplication to the left by T^{-1} results the final form of the Euler equations in primitive variables:

$$\frac{\partial f_p}{\partial t} + A_p\frac{\partial f_p}{\partial x} = Q_p \tag{A.9}$$

where A_p is the Jacobian matrix in terms of primitive variables, and Q_p is a source term. They are given by:

$$Q_p = T^{-1}Q = \begin{bmatrix} -\frac{\rho u}{S}\frac{dS}{dx} \\ 0 \\ \frac{-\rho uc^2}{S}\frac{dS}{dx} \end{bmatrix}, \quad A_p = T^{-1}AT = \begin{bmatrix} u & \rho & 0 \\ 0 & u & \frac{1}{\rho} \\ 0 & \rho c^2 & u \end{bmatrix} \tag{A.10}$$

The characteristic form of the Euler equations is obtained considering wave-like solutions of (A.9) of the form:

$$f_p(x, t) = f_p(x - \lambda t) \tag{A.11}$$

which, inserted into (A.9), leads to the eigenvalue problem:

$$\det | A_p - \lambda \mathrm{I} | = 0 \tag{A.12}$$

Hence, the eigenvalues λ of the Jacobian are the speeds of propagation of the waves.

The Jacobian matrix A_p turns out to have the eigenvalues $\lambda_1 = u$, $\lambda_2 = u + c$, and $\lambda_3 = u - c$, which can be obtained by the similarity transformation:

$$M^{-1} A_p M = \begin{bmatrix} u & 0 & 0 \\ 0 & u+c & 0 \\ 0 & 0 & u-c \end{bmatrix} = \Lambda \tag{A.13}$$

the matrix M being formed with the right eigenvectors of A_p:

$$M = \begin{bmatrix} 1 & \frac{\rho}{2c} & -\frac{\rho}{2c} \\ 0 & \frac{1}{2} & \frac{1}{2} \\ 0 & \frac{\rho c}{2} & \frac{-\rho c}{2} \end{bmatrix}, \quad M^{-1} = \begin{bmatrix} 1 & 0 & -\frac{1}{c^2} \\ 0 & 1 & \frac{1}{\rho c} \\ 0 & 1 & -\frac{1}{\rho c} \end{bmatrix} \tag{A.14}$$

Multiplying eq. (A.9) from the left by M^{-1} gives:

$$M^{-1} \frac{\partial f_p}{\partial t} + M^{-1} A_p (M M^{-1}) \frac{\partial f_p}{\partial x} = M^{-1} Q_p \tag{A.15}$$

or:

$$M^{-1} \frac{\partial f_p}{\partial t} + \Lambda M^{-1} \frac{\partial f_p}{\partial x} = M^{-1} Q_p \tag{A.16}$$

Assuming that the coefficient matrices are locally constant, (A.16) can be written:

$$\frac{\partial(\bar{M}^{-1} f_p)}{\partial t} + \Lambda \frac{\partial(\bar{M}^{-1} f_p)}{\partial x} = M^{-1} Q_p \tag{A.17}$$

where the overbar is used for locally constant values.

Denoting by:

$$W = \begin{bmatrix} w_1 \\ w_2 \\ w_3 \end{bmatrix} = \bar{M}^{-1} f_p = \begin{bmatrix} \rho - \dfrac{p}{\bar{c}^2} \\ u + \dfrac{p}{\bar{\rho}\bar{c}} \\ u - \dfrac{p}{\bar{\rho}\bar{c}} \end{bmatrix} \tag{A.18}$$

one obtains from (A.17) the characteristic form of the Euler equations:

$$\frac{\partial}{\partial t}\begin{bmatrix} w_1 \\ w_2 \\ w_3 \end{bmatrix} + \begin{bmatrix} u & 0 & 0 \\ 0 & u+c & 0 \\ 0 & 0 & u-c \end{bmatrix} \frac{\partial}{\partial x}\begin{bmatrix} w_1 \\ w_2 \\ w_3 \end{bmatrix} = \frac{1}{S}\frac{dS}{dx}\begin{bmatrix} 0 \\ -uc \\ uc \end{bmatrix} \tag{A.19}$$

The scalar equations obtained from (A.19) are all of the form:

$$\frac{\partial w_i}{\partial t} + \lambda_i \frac{\partial w_i}{\partial x} = q_i, \quad i = 1, 2, 3 \tag{A.20}$$

where $\lambda_1 = u$, $\lambda_2 = u+c$, and $\lambda_3 = u-c$ are the eigenvalues of Λ, and the source terms q_i are easily identified from (A.19). These equations can be written:

$$\left(\frac{Dw_i}{Dt}\right)_{C_i} = q_i, \quad i = 1, 2, 3 \tag{A.21}$$

where $(Dw_i/Dt)_{C_i}$ is the total time derivative of the quantity w_i along the curve C_i which is defined by the equation:

$$\left(\frac{dx}{dt}\right)_{C_i} = \lambda_i \tag{A.22}$$

Equations (A.21) describe the wave-like propagation of the quantities w_i along these curves with speeds λ_i. Hence, $w_1 = \rho - \frac{p}{\bar{c}^2}$ propagates along the characteristic curve C_1, defined by $(dx/dt)_{C_1} = u$. The quantity $w_2 = u + \frac{p}{\bar{\rho}\bar{c}}$ propagates with velocity $u+c$ along the characteristic C_2, defined by $(dx/dt)_{C_2} = u+c$. Finally, $w_3 = u - \frac{p}{\bar{\rho}\bar{c}}$ propagates with velocity u-c along C_3, defined by $(dx/dt)_{C_3} = u - c$.

The characteristic curve C_1 is the particle path, and the C_2 and C_3 characteristics are also called Mach lines. The variables w_i are the so-called Riemann variables.

Since for an isentropic flow the pressure and the density are related by:

$$\frac{dp}{\rho c} = \frac{2}{\gamma - 1} dc \tag{A.23}$$

the Riemann variables w_2 and w_3 can also be expressed in the form:

$$w_2 = u + \frac{2c}{\gamma - 1} \quad , \quad w_3 = u - \frac{2c}{\gamma - 1} \tag{A.24}$$

For the particular case of a one-dimensional flow, when $S(x)$=constant, and hence in equation (A.21) q_i=0, i=1,2,3, the characteristic relations become:

$$\left(\frac{Dw_i}{Dt}\right)_{C_i} = 0 \iff w_i = \text{constant along } C_i \tag{A.25}$$

In this case the Riemann variables w_i are also called Riemann invariants.

A.2 Two-dimensional time-dependent Euler equations

The two-dimensional Euler equations in conservative variables (2.9) can also be written:

$$\frac{\partial f}{\partial t} + A\frac{\partial f}{\partial x} + B\frac{\partial f}{\partial y} = 0 \tag{A.26}$$

where A and B are the two (conservative) Jacobians:

$$A = \frac{\partial F}{\partial f}, \quad B = \frac{\partial G}{\partial f} \tag{A.27}$$

Defining the Jacobian matrix:

$$T = \frac{\partial f}{\partial f_p} = \begin{bmatrix} 1 & 0 & 0 & 0 \\ u & \rho & 0 & 0 \\ v & 0 & \rho & 0 \\ \frac{u^2+v^2}{2} & \rho u & \rho v & \frac{1}{\gamma - 1} \end{bmatrix} \tag{A.28}$$

where f is the state vector in terms of conservative variables, given by (2.6), and f_p is the state vector in terms of primitive variables:

$$f_p = \begin{bmatrix} \rho \\ u \\ v \\ p \end{bmatrix} \tag{A.29}$$

the Euler equations can successively be written as:

$$T\frac{\partial f_p}{\partial t} + AT\frac{\partial f_p}{\partial x} + BT\frac{\partial f_p}{\partial y} = 0$$

$$T^{-1}T\frac{\partial f_p}{\partial t} + T^{-1}AT\frac{\partial f_p}{\partial x} + T^{-1}BT\frac{\partial f_p}{\partial y} = \frac{\partial f_p}{\partial t} + A_p\frac{\partial f_p}{\partial x} + B_p\frac{\partial f_p}{\partial y} = 0 \qquad \text{(A.30)}$$

The new Jacobians in terms of primitive variables are:

$$A_p = T^{-1}AT = \begin{bmatrix} u & \rho & 0 & 0 \\ 0 & u & 0 & \frac{1}{\rho} \\ 0 & 0 & u & 0 \\ 0 & \rho c^2 & 0 & u \end{bmatrix}, \quad B_p = T^{-1}BT = \begin{bmatrix} v & 0 & \rho & 0 \\ 0 & v & 0 & 0 \\ 0 & 0 & v & \frac{1}{\rho} \\ 0 & 0 & \rho c^2 & v \end{bmatrix} \qquad \text{(A.31)}$$

The problem of finding the characteristic form of the equations reduces to looking for wave-like solutions of eq. (A.30) of the form:

$$f_p(x, y, t) = f_p(xk_x + yk_y - \lambda t) \qquad \text{(A.32)}$$

where $\vec{k} = k_x\vec{i} + k_y\vec{j}$ is a unit vector in the direction of propagation of the wave. After substitution in (A.30), this leads to the eigenvalue problem:

$$\det|\bar{A}_p - \lambda I| = 0 \qquad \text{(A.33)}$$

where I is the fourth order identity matrix, and $\bar{A}_p = A_p k_x + B_p k_y$.

The eigenvalues have a simple form; they are:

$$\lambda_1 = \lambda_2 = uk_x + vk_y = \vec{V}\cdot\vec{k}$$
$$\lambda_3 = uk_x + vk_y + c = \vec{V}\cdot\vec{k} + c \qquad \text{(A.34)}$$
$$\lambda_4 = uk_x + vk_y - c = \vec{V}\cdot\vec{k} - c$$

Similar to the one-dimensional case, the characteristic variables for a given value of (k_x,k_y) can be obtained by multiplying the primitive variables with $\bar{M}^{-1}$, where $\bar{M}$ is the matrix formed with the right eigenvectors of $\tilde{A}_p$. The overbar denotes that the matrix is considered locally constant. It is given by:

$$\bar{M} = \begin{bmatrix} 1 & 0 & \frac{\bar{\rho}}{2\bar{c}} & \frac{\bar{\rho}}{2\bar{c}} \\ 0 & k_y & \frac{k_x}{2} & -\frac{k_x}{2} \\ 0 & -k_x & \frac{k_y}{2} & -\frac{k_y}{2} \\ 0 & 0 & \frac{\bar{\rho}\bar{c}}{2} & \frac{\bar{\rho}\bar{c}}{2} \end{bmatrix}, \quad \bar{M}^{-1} = \begin{bmatrix} 1 & 0 & 0 & -\frac{1}{\bar{c}^2} \\ 0 & k_y & -k_x & 0 \\ 0 & k_x & k_y & \frac{1}{\bar{\rho}\bar{c}} \\ 0 & -k_x & -k_y & \frac{1}{\bar{\rho}\bar{c}} \end{bmatrix} \qquad \text{(A.35)}$$

and the coresponding form of the characteristic variables is:

$$W = \bar{M}^{-1} f_p = \begin{bmatrix} W_1 \\ W_2 \\ W_3 \\ W_4 \end{bmatrix} = \begin{bmatrix} \rho - \frac{p}{\bar{c}^2} \\ k_y u - k_x v \\ k_x u + k_y v + \frac{p}{\bar{\rho}\bar{c}} \\ -k_x u - k_y v + \frac{p}{\bar{\rho}\bar{c}} \end{bmatrix} \qquad \text{(A.36)}$$

The two-dimensional case is thus much more complex than the one-dimensional case because the wave-like solutions can travel along an infinity of

directions determined by the vector $\vec{k}$, the characteristic variables themselves being also a function of $\vec{k}$.

The compatibility relations along the characteristic surfaces are of the form:

$$\frac{\partial W}{\partial t} + (\bar{M}^{-1}\bar{A}_p\bar{M})\nabla W = 0 \qquad \text{(A.37)}$$

where $\bar{A}_p = A_p k_x \vec{i} + B_p k_y \vec{j}$.

A.3 Implications on boundary conditions treatment

A.3.1 Quasi one-dimensional case

Consider a quasi one-dimensional flow, with the inflow boundary at $x=x_{in}$ and outflow at $x=x_{ex}$, and P_{in} and P_{ex} two points on these boundaries, at a given time (Fig. A.1).

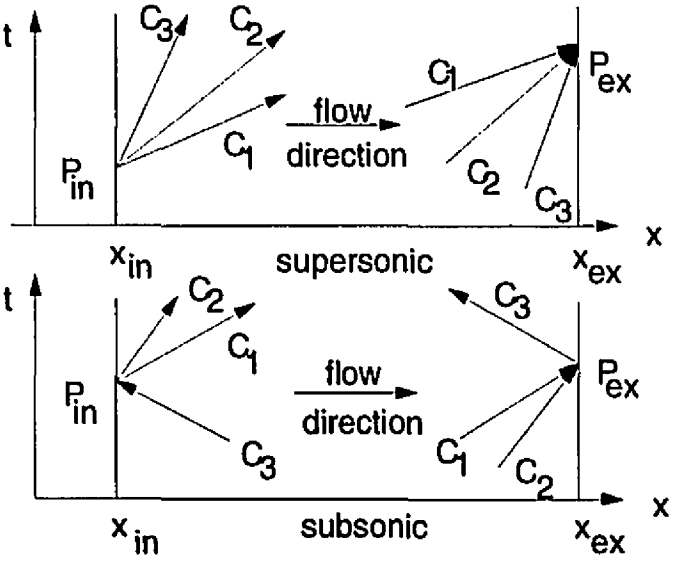

Fig. A.1

At the inflow, the characteristics C_1 and C_2 have slopes u and $u+c$, which are positive if the flow is in the positive x direction. Hence, these two characteristics will always carry information from the inlet boundary towards the interior of the domain; this means that the values of the transported quantities must be known at P_{in}. The third characteristic C_3 has the slope $u-c$, which is negative for subsonic inflow conditions, and positive if the inflow is supersonic. Therefore, in the subsonic case, information comes from the interior towards the boundary along C_3, and no boundary condition associated with C_3 can be fixed. In the supersonic case, the information enters the domain along C_3, and hence a corresponding boundary condition has to be imposed.

Similar considerations at the outflow lead to the following table:

Table A.1

	Subsonic	Supersonic
Inflow	-two conditions specified (corresponding to w_1 and w_2) -one information from the interior (w_3)	-three conditions specified (corresponding to w_1, w_2 and w_3)
Outflow	-one condition imposed (corresponding to w_3) -information from the interior corresponding to w_1 and w_2	-all information comes from the interior (w_1, w_2 and w_3)

A.3.2 Two-dimensional case

The treatment of the two-dimensional case can be done under the assumption that waves travel in a direction normal to the boundary. Then, the number of

boundary conditions to be imposed will correspond to the number of characteristic directions associated with $\vec{k} = \vec{n}$ (the unit vector normal to the boundary surface) that enter the computational domain.

If $\vec{k} = \vec{n}$ is introduced in (A.34) and (A.36), the eigenvalues and the characteristic variables become:

$$\lambda_1 = \lambda_2 = \vec{V}\cdot\vec{n} = V_n\,, \quad \lambda_3 = V_n + c\,, \quad \lambda_4 = V_n - c$$

$$W = \begin{bmatrix} W_1 \\ W_2 \\ W_3 \\ W_4 \end{bmatrix} = \begin{bmatrix} \rho - \dfrac{p}{\bar{c}^2} \\ V_t \\ V_n + \dfrac{p}{\bar{\rho}\,\bar{c}} \\ -V_n + \dfrac{p}{\bar{\rho}\,\bar{c}} \end{bmatrix} \tag{A.38}$$

Hence, for a locally supersonic flow on the direction normal to the boundary, all information comes from upstream, while for a locally subsonic flow, three characteristics propagate from upstream, and one from downstream.

The following table summarizes the appropriate treatment of the boundary conditions:

Table A.2

	Subsonic	Supersonic
Inflow	-three conditions specified (corresponding to w_1, w_2, and w_3) -one information from the interior (corresponding to w_4)	-four conditions specified (corresponding to w_1, w_2, w_3 and w_4)
Outflow	-one condition imposed (corresponding to w_4) -information from the interior corresponding to w_1, w_2, and w_3	-all information comes from the interior (w_1, w_2, w_3 and w_4)

Appendix B

CONTINUITY RELATIONS ACROSS PLANAR WAVES

In this appendix the basic relations required for the implementation of Godunov's method are developed.

B.1 The Euler equations for a discontinuity

Consider a discontinuity surface Σ defined by the equation $\Sigma(x, y, z, t)=0$, moving with the velocity $\vec{U}_\Sigma$.

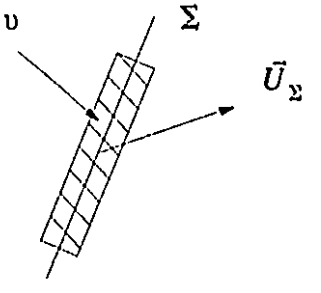

Fig. B.1

The integral form of the Euler equations (2.1) applied to the infinitesimally small volume υ attached to it, as seen in Fig. B.1, can be written ([25]) as:

$$\frac{\partial}{\partial t}\int_{\upsilon} f d\upsilon + \int_{\partial\upsilon} \vec{\mathrm{F}}\cdot\vec{n}\, dA = 0 \qquad \text{(B.1)}$$

where $\vec{F}$ is the total flux term, $\vec{F}\cdot\vec{n} = f(\vec{r},t)\vec{n}\cdot\vec{V} + g(\vec{r},t)$.

The time derivative must account for the motion of the surface Σ, and hence of the control volume υ:

$$\frac{\partial}{\partial t}\int_{\upsilon} f d\upsilon = \int_{\upsilon}\frac{\partial f}{\partial t}d\upsilon + \int_{\upsilon} f\frac{\partial}{\partial t}(d\upsilon) = \int_{\upsilon}\frac{\partial f}{\partial t}d\upsilon + \int_{\partial\upsilon} f\vec{U}_{\Sigma}\cdot\vec{n}\,dA \tag{B.2}$$

The second integral in (B.1) can be written, in the limit $\upsilon\rightarrow 0$, as:

$$\int_{\partial\upsilon}\vec{F}\cdot\vec{n}\,dA = \int_{\Sigma}\vec{F}\cdot\vec{n}\,dA \tag{B.3}$$

Inserting equations (B.2) and (B.3) into (B.1), one obtains, for $\upsilon\rightarrow 0$, that:

$$\int_{\Sigma}\left(\vec{F}\cdot\vec{n} - f\vec{U}_{\Sigma}\cdot\vec{n}\right)dA = 0 \tag{B.4}$$

Integrating over an infinitesimally small element of the discontinuity surface and taking into account the different values of the flux and state vectors on the two sides of the discontinuity, the Euler equations become:

$$[\vec{F}]\cdot\vec{n} - [f]\,\vec{U}_{\Sigma}\cdot\vec{n} = 0 \tag{B.5}$$

where the notation:

$$[A] = A_R - A_L \tag{B.6}$$

denotes the jump in the variable A across the discontinuity.

Because the total time derivative expressing the change of the surface Σ is:

$$\frac{d\Sigma}{dt} = \frac{\partial\Sigma}{\partial t} + \vec{U}_{\Sigma}\cdot\nabla\Sigma \tag{B.7}$$

using also the definition of the normal unit vector:

$$\vec{n} = \frac{\nabla\Sigma}{|\nabla\Sigma|} \tag{B.8}$$

equation (B.5) takes the form:

$$[\vec{F}]\cdot\nabla\Sigma + \frac{\partial\Sigma}{\partial t}[f] = 0 \tag{B.9}$$

Equation (B.5), or its equivalent (B.9), expressed for each component of the vectors f and $\vec{F}$, leads to a system of scalar equalities. These relations, in the case the discontinuity is a shock, are known as the Rankine-Hugoniot relations.

B.2 Case of a planar shock wave

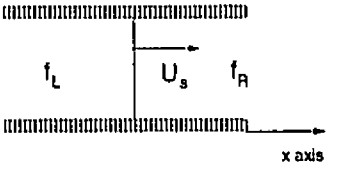

Fig. B.2

Consider the one-dimensional unsteady shock moving with a constant positive velocity U_s along the x axis, as shown in Fig. B.2. The position of the shock is described by the equation:

$$\Sigma(x,t) = x - U_s t = 0 \tag{B.10}$$

Because in this case the total flux vector is $\vec{F} = \vec{i}F$, using the form (B.9), the Euler equations can be written:

$$(f_R - f_L)\frac{\partial \Sigma}{\partial t} + (F_R - F_L)\frac{\partial \Sigma}{\partial x} = 0 \qquad \text{(B.11)}$$

where f and F are the one-dimensional state and flux vectors given by (2.8).

From (B.11) one can obtain the jump relation connecting the variables on the two sides of the shock:

$$U_s[f] = [F] \qquad \text{(B.12)}$$

Expressing the jump relation (B.12) for each of the three components of the state and flux vectors results in:

- the continuity equation:

$$U_s(\rho_R - \rho_L) = \rho_R u_R - \rho_L u_L \qquad \text{(B.13)}$$

- the momentum equation:

$$U_s(\rho_R u_R - \rho_L u_L) = (\rho_R u_R^2 + p_R) - (\rho_L u_L^2 + p_L) \qquad \text{(B.14)}$$

- the energy equation:

$$U_s(\rho_R E_R - \rho_L E_L) = (\rho_R E_R + p_R) u_R - (\rho_L E_L + p_L) u_L \qquad \text{(B.15)}$$

The continuity equation can be written

$$\rho_R(U_s - u_R) = \rho_L(U_s - u_L) \qquad \text{(B.16)}$$

Define the mass flux which is swept over by the shock in unit time per unit area:

$$\dot{m} = \rho_R(U_s - u_R) = \rho_L(U_s - u_L) \qquad \text{(B.17)}$$

The same mass flux can be obtained from the momentum equation written as:

$$\rho_R u_R(u_R - U_s) - \rho_L u_L(u_L - U_s) = -\dot{m}u_R + \dot{m}u_L = p_L - p_R \tag{B.18}$$

which leads to:

$$\dot{m} = \frac{p_R - p_L}{u_R - u_L} \tag{B.19}$$

Similarly, the energy equation can be written as:

$$\dot{m}(E_L - E_R) = p_L u_L - p_R u_R \tag{B.20}$$

An useful set of relations can be obtained by combining equations (B.17), (B.19) and (B.20). From (B.17), eliminating U_s between the two equalities, the mass flux can be expressed as:

$$\dot{m} = \frac{(u_R - u_L)\rho_R\rho_L}{\rho_R - \rho_L} \tag{B.21}$$

which, combined to (B.19), gives:

$$\dot{m} = \sqrt{\frac{(p_L - p_R)\rho_L\rho_R}{\rho_L - \rho_R}} = \sqrt{\frac{p_L - p_R}{\vartheta_R - \vartheta_L}} \tag{B.22}$$

where $\vartheta = \frac{1}{\rho}$ is the specific volume.

Inserting this expression in equation (B.19), the difference in velocities across the shock results to be:

$$u_R - u_L = \sqrt{\frac{(p_R - p_L)(\rho_R - \rho_L)}{\rho_R\rho_L}} = \sqrt{(p_L - p_R)(\vartheta_R - \vartheta_L)} \tag{B.23}$$

If the internal specific energy, e, defined by:

$$e = \frac{1}{\gamma - 1}\frac{p}{\rho} = \frac{1}{\gamma - 1} p\vartheta = E - \frac{u^2}{2} \tag{B.24}$$

is used instead of the total specific energy E, its discontinuity at the shock results from (B.20):

$$e_L - e_R = \frac{p_L u_L - p_R u_R + \frac{\dot{m}}{2}(u_R^2 - u_L^2)}{\dot{m}} \tag{B.25}$$

Equations (B.22), (B.23) and (B.25) are one of the forms of the Rankine-Hugoniot relations.

In terms of the specific volume, the continuity equation can be written:

$$\dot{m} = -\frac{1}{\vartheta_R}(u_R - U_s) = -\frac{1}{\vartheta_L}(u_L - U_s) \tag{B.26}$$

or, expressing the shock speed:

$$\dot{m}\vartheta_R + u_R = \dot{m}\vartheta_L + u_L = U_s \tag{B.27}$$

This leads to:

$$u_L = \dot{m}\vartheta_R + u_R - \dot{m}\vartheta_L \tag{B.28}$$

which, inserted into (B.25), allows one to write:

$$
\begin{aligned}
e_L - e_R &= \frac{p_L(\dot{m}\vartheta_R + u_R - \dot{m}\vartheta_L) - p_R u_R}{\dot{m}} + \frac{1}{2}\left[u_R^2 - (\dot{m}\vartheta_R + u_R - \dot{m}\vartheta_L)^2\right] \\
&= p_L(\vartheta_R - \vartheta_L) - \frac{1}{2}\dot{m}^2(\vartheta_R - \vartheta_L)^2 + u_R\left[\frac{p_L - p_R}{\dot{m}} - \frac{p_L - p_R}{\dot{m}}\right] \\
&= \frac{(p_L + p_R)}{2}(\vartheta_R - \vartheta_L)
\end{aligned}
\tag{B.29}
$$

Writing equation (B.29) as:

$$
\frac{1}{\gamma - 1}p_L\vartheta_L - \frac{1}{\gamma - 1}p_R\vartheta_R = \frac{(p_L + p_R)}{2}(\vartheta_R - \vartheta_L) \tag{B.30}
$$

gives for the specific volume ϑ_L the expression:

$$
\vartheta_L = \frac{(\gamma + 1)p_R\vartheta_R + (\gamma - 1)p_L\vartheta_L}{(\gamma + 1)p_L + (\gamma - 1)p_R} \tag{B.31}
$$

This expression can be inserted into (B.22) in order to express the mass flux in a form easy to use in Godunov's method:

$$
\begin{aligned}
\dot{m} &= \sqrt{\frac{(p_L - p_R)[(\gamma + 1)p_L + (\gamma - 1)p_R]}{2(p_L - p_R)\vartheta_R}} \\
&= \sqrt{\frac{(\gamma + 1)p_L + (\gamma - 1)p_R}{2\vartheta_R}} \\
&= \sqrt{\frac{\gamma + 1}{2}p_L\rho_R + \frac{\gamma - 1}{2}p_R\rho_R}
\end{aligned}
\tag{B.32}
$$

Since the mass flux has a positive value in the case of a shock, it can be written in the more concise form:

$$|\dot{m}| = \dot{m} = \sqrt{p_R \rho_R} \cdot \Phi\left(\frac{p_L}{p_R}\right) \tag{B.33}$$

where for the shock case $p_L \geq p_R$, and the function Φ has the form:

$$\Phi(w) = \sqrt{\frac{\gamma+1}{2} w + \frac{\gamma-1}{2}}, \quad \text{if} \quad w \geq 1 \tag{B.34}$$

B.3 Case of a planar rarefaction fan

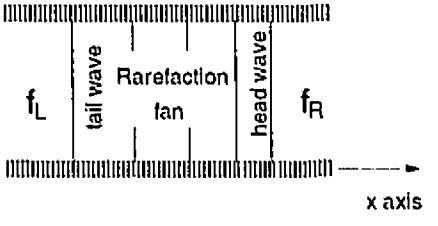

Fig. B.3

Unlike flow across shock waves, across the rarefaction fan the flow is isentropic. The sudden increase in density across an infinitesimally small element dx in the rarefaction fan (Fig. B.3) can be related to the variation of the velocity (see [24]) through the equation:

$$\frac{d\rho}{\rho} = -\frac{du}{c} \tag{B.35}$$

Because the flow is isentropic, the local speed of sound is given by the isentropic law:

$$\frac{c}{c_R} = \left(\frac{\rho}{\rho_R}\right)^{\frac{\gamma-1}{2}} \tag{B.36}$$

The velocity differential becomes:

$$du = -c\frac{d\rho}{\rho} = -c_R\left(\frac{\rho}{\rho_R}\right)^{\frac{\gamma-1}{2}}\frac{d\rho}{\rho} \tag{B.37}$$

By integration:

$$\int_{u_R}^{u_L} du = -\int_{p_R}^{p_L} c_R\left(\frac{\rho}{\rho_R}\right)^{\frac{\gamma-1}{2}}\frac{d\rho}{\rho} \tag{B.38}$$

one can obtain the difference between the velocities on the two sides of the rarefaction:

$$u_L - u_R = \frac{2c_R}{\gamma-1}\left[1-\left(\frac{\rho_L}{\rho_R}\right)^{\frac{\gamma-1}{2}}\right] = \frac{2c_R}{\gamma-1}\left[1-\left(\frac{p_L}{p_R}\right)^{\frac{\gamma-1}{2\gamma}}\right] \tag{B.39}$$

The mass flux swept over in unit time per unit area by the rarefaction fan, expressed from the momentum equation in a form similar to (B.19), will therefore be:

$$\dot{m} = \frac{p_L - p_R}{u_L - u_R} = \frac{(\gamma-1)(p_L - p_R)}{2c_R\left[1-\left(\frac{p_L}{p_R}\right)^{\frac{\gamma-1}{2\gamma}}\right]} =$$

$$= \frac{(1-\gamma)p_R\left(1-\frac{p_L}{p_R}\right)}{2\sqrt{\gamma\frac{p_R}{\rho_R}\left[1-\left(\frac{p_L}{p_R}\right)^{\frac{\gamma-1}{2\gamma}}\right]}} \tag{B.40}$$

Taking into account the fact that for an expansion the mass flux is negative, its absolute value can be written in the same condensed form as (B.33):

$$|\dot{m}| = \dot{m} = \sqrt{p_R \rho_R} \cdot \Phi\left(\frac{p_L}{p_R}\right) \tag{B.41}$$

where for this case of an expansion $p_L < p_R$ and:

$$\Phi(w) = \frac{\gamma - 1}{2\sqrt{\gamma}} \cdot \frac{1 - w}{1 - w^{\frac{\gamma - 1}{2\gamma}}}, \quad \text{if } w < 1 \tag{B.42}$$

B.4 General form of the mass flux

The function Φ defined by (B.34) and (B.42) is continuous at $w=1$ and takes the value $\Phi(1) = \sqrt{\gamma}$, corresponding to the case of a sonic wave, $\dot{m} = \rho c = \sqrt{\gamma \rho p}$. Combining the two expressions for this function gives a general relation for the mass flux, valid for both cases of a shock and an expansion,

$$|\dot{m}| = \sqrt{p_R \rho_R} \cdot \Phi\left(\frac{p_L}{p_R}\right) \tag{B.43}$$

where:

$$\Phi(w) = \begin{cases} \sqrt{\frac{\gamma + 1}{2} w + \frac{\gamma - 1}{2}}, & w \geq 1 \\ \frac{\gamma - 1}{2\sqrt{\gamma}} \cdot \frac{1 - w}{1 - w^{\frac{\gamma - 1}{2\gamma}}}, & w \leq 1 \end{cases} \tag{B.44}$$